STRUCTURAL STUDIES OF SOL-GEL AND CONVENTIONAL GLASSES USING OPTICAL PROBES.

KEVIN B. DEVLIN.

SCHOOL OF PHYSICAL SCIENCES
DUBLIN CITY UNIVERSITY.

THESIS SUBMITTED FOR DEGREE OF DOCTOR OF PHILOSOPHY.

SUPERVISOR : Dr C Mc Donagh.

SEPTEMBER 1991.

ABSTRACT.

The optical spectroscopy of the europium ion has been used as a probe of the structure of sol-gel glasses. The fluorescence and optical decay times of the Eu^{3+} ion were monitored during the different stages of the sol-gel process and changes in these optical properties were interpreted in terms of the constantly changing environment of the Eu^{3+} ion. Eu^{3+} doped high temperature fusion glasses were also investigated for comparison purposes. The technique of Fluorescence Line Narrowing was used to investigate both the high temperature and sol-gel glasses. While the high temperature glasses narrowed significantly, the sol-gel glasses did not show any evidence of narrowing. This is interpreted as being due to residual OH^- still within the glass structure and also clumping of the dopant ions.

A study of Cr^{3+} in sol-gel glasses was also made. It is found that most of the Cr^{3+} is oxidised to the Cr^{6+} state even when produced in a reducing atmosphere. High temperature borate an silicate glasses were also investigated in the case of Cr^{3+} for comparison purposes.

DECLARATION.

THIS THESIS IS BASED ON MY OWN WORK.

CHAPTER 1. INTERACTION OF RADIATION WITH OPTICALLY ACTIVE MATERIALS.

CHAPTER 2. GLASS.

CHAPTER 1.

1. INTERACTION OF RADIATION WITH OPTICALLY ACTIVE MATERIALS.

1.1 INTRODUCTION.

Optically active materials are of great importance and play a part in many of the high technology instruments and devices now available. Research interest has been fuelled by a demand for solid state lasers of all wavelengths and powers. In this chapter the idea of luminescence between electronic energy levels of a solid and how the emission is characteristic of the material will be introduced.

In general, luminescence involves the excitation of electrons to higher electronic states and when they return to their ground state, emission of electromagnetic radiation. There are several ways this can be achieved. If the excitation is caused by a photon, the process is called photoluminescence, if it is an electron it is called electroluminescence. Chemiluminescence is luminescence resulting from a chemical reaction.

The concept of the excitation and emission processes can be explained more easily by reference to Fig 1.1. The ground state has zero energy E_o, and E_1, E_2 and E_3 represent excited energy levels. Excitation of the material from E_o to E_3 is achieved with the absorption of electromagnetic radiation. It is found that if the gap between some excited state and another state lower in energy is small, the excited state decays non-radiatively to the lower state. Non-radiative decay takes the form of phonon vibrations through the material. In Fig 1.1 the emission is described by,

$$h\nu_1 = E_2 - E_1 \qquad (1.1)$$

$$h\nu_2 = E_2 - E_0 \qquad (1.2)$$

where h is Planck's constant and ν is the frequency in Hertz.

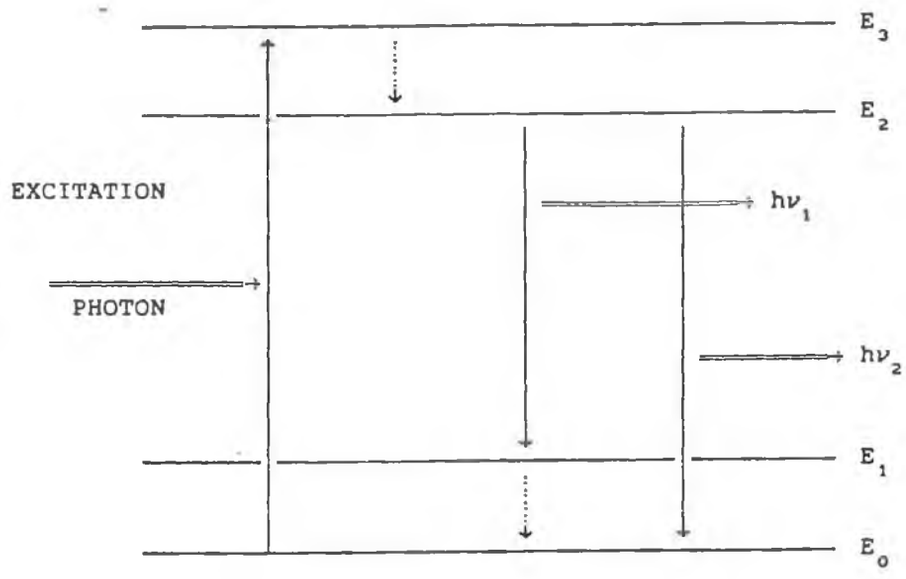

Fig 1.1 Excitation and Emission processes. Broken lines indicate non-radiative decay and double lines indicate emission of photons.

1.2 THE FREE ION.

When an ion is within a crystal lattice it takes part in the vibrational motion of the lattice. As a result of the vibrational motion the energy levels are modulated, yielding a broadened output. Initially we will look at the free ion and then consider the effects of the vibrational motion of the ion in the solid.

The free ion Hamiltonian is [1,2],

$$H_{FI} = H_0 + H_{EL} + H_{SO} \qquad (1.1)$$

$$H_0 = \sum_i (p_i^2/2m + V_i(r_i)) \qquad (1.2)$$

$$H_{EL} = \sum_{i>j} (e^2/4\pi\varepsilon_0 r_{ij}) \qquad (1.3)$$

$$H_{SO} = \sum_{i} \zeta (r_i)\, \mathbf{l}_i \mathbf{s}_i \qquad (1.4)$$

In the above case H_0 is a summation of the kinetic and potential energies of the electrons, H_{EL} is the electrostatic coulomb interaction energy between the electrons in the outer shells and H_{SO} is the spin orbit interaction energy.

Using the method of perturbation theory, H_0 is taken as the unperturbed Hamiltonian. As H_0 is the sum of the single electron terms, the eigenfunctions of H_0 are products of single electron eigenfunctions and are described by the quantum numbers n,ℓ,m_ℓ,m_s. When H_{EL} and H_{SO} are included the quantum numbers of orbital angular momentum $\mathbf{L} = \sum \mathbf{l}_i$, total spin angular momentum $\mathbf{S} = \sum \mathbf{s}_i$, and total angular momentum $\mathbf{J} = \mathbf{L} + \mathbf{S}$ are used to describe the eigenfunctions. The energy levels are labelled by the notation $^{2S+1}L_J$, where L = 0,1,2,3,4,5,6... for S,P,D,F,G,H,I...etc.

1.3 OPTICALLY ACTIVE IONS.

1.3.1 TRANSITION METAL IONS.

The feature that unifies the transition metal ions into a distinguishable group is the existence of an incomplete shell of d-electrons. The electronic configurations of transition metal ions are,

$$1s^2\ 2s^2\ 2p^6\ 3s^2 3p^6\ 3d^n \qquad (1.5)$$

where n is less than ten. A table of some of the common valence states is given. The incomplete shell electron

configuration can have a number of states close together in energy and the gaps between the ground state and some other electron states correspond to the energies of visible photons. The fact that the 3d electrons are optically active and are also the outermost means that they interact strongly with the electric fields from nearby ions and the associated crystal fields are stronger than those experienced by the rare-earth ions.

ION	n Value
Ti^{3+}, V^{4+}	1
V^{3+}	2
V^{2+}, Cr^{3+}, Mn^{4+}	3
Mn^{3+}	4
Mn^{2+}, Fe^{3+}	5
Fe^{2+}, Co^{3+}	6
Co^{2+}	7
Ni^{2+}	8
Cu^{2+}	9

Table 1.1 Values of n for valence states of transition metals.

1.3.2 RARE EARTH IONS.

The electronic configurations of the rare earth atoms are given by

$$1s^2\ 2s^2\ 2p^6\ 3s^2\ 3p^6\ 3d^{10}\ 4s^2\ 4p^6\ 4d^{10}\ 4f^n\ 5s^2\ 5p^6\ 5d^m\ 6s^2,$$

$$= (\ \text{Pd core}\ )^{46}\ 4f^n\ 5s^2\ 5p^6\ 5d^m\ 6s^2 \qquad (1.6)$$

where m = 1,2 and n = 2,3,.....,13 and their atomic numbers range from Z = 58 (Ce) and Z = 70 (Yb). When in the trivalent ionic state the unfilled 4f shell is screened by

the 5s and 5p shells. The rare earths are mainly in the doubly or triply ionised states when in solids. The electronic configuration of the triply ionised rare earth ion is

$$1s^2\ 2s^2\ 2p^6\ 3s^2\ 3p^6\ 3d^{10}\ 4s^2\ 4p^6\ 4d^{10}\ 5s^2\ 5p^6\ 4f^n \qquad (1.7)$$

where n varies from 1 to 13.

The incomplete 4f shell is optically active and as a result of the shielding by the complete $5s^2$ $5p^6$ shells the 4f electrons are effected to a lesser extent by surrounding fields. The energy levels in this case are sharp compared to the transition metal ions. A list of the number of electrons in the unfilled 4f shell for each triply charged rare earth ion is given in table 1.2.

ION	n VALUE
Ce^{3+}	1
Pr^{3+}	2
Nd^{3+}	3
Pm^{3+}	4
Sm^{3+}	5
Eu^{3+}	6
Gd^{3+}	7
Tb^{3+}	8
Dy^{3+}	9
Ho^{3+}	10
Er^{3+}	11
Tm^{3+}	12
Yb^{3+}	13

Table 1.2 The values of n for triply ionised rare earths.

1.4 INTERACTION OF RADIATION WITH AN OPTICALLY ACTIVE ION.

When an optically active ion is within a solid,

electromagnetic radiation can interact with this ion through two different processes (1) the electric field of the radiation, called an electric dipole process, or, (2) the magnetic field of the radiation, called a magnetic dipole process. If *a* is the initial state before absorption and *b* is the final state after absorption of light, and the energy difference between states *a* and *b* is equal to the energy of a photon $\hbar\omega$, the probability of a transition from *a* to *b* with a photon of energy $\hbar\omega$ being absorbed is [3],

$$P_{ab} = (2\pi/\hbar) \; |V_{ba}|^2 \; \delta(E_b - E_a - \hbar\omega) \qquad (1.8)$$

where V_{ba} is the matrix element, $\langle b|V|a\rangle$, of the transition, and **V** is the operator denoting the energy of interaction of the ion with the radiation. For an electric dipole transition **V** = **p**.**E** , where **p** is the electric dipole moment operator and **E** is the electric field intensity of the radiation field. The value of **p** , the electric dipole moment is $\mathbf{p} = \sum_i e\mathbf{r}_i$. For a magnetic dipole transition **V** = μ.**B** , where μ is the magnetic dipole operator and **B** is the magnetic field strength of the radiation field. The value of μ is given by $\mu = \sum_i e/2m \; (\mathbf{l}_i + 2\mathbf{s}_i)$. To determine whether or not an optical transition can or cannot occur, and if it does how strong it will be depends on the value of the matrix element. Laportes selection rule [4] says that electric dipole radiation is always associated with a change of parity. Electric dipole transitions are forbidden between states of the same configuration, because such states all have the same parity. For an allowed magnetic dipole transition the initial state *a* and final state *b* must have the same parity.

For a rare earth ion, all of the free ion levels are formed by the same $(4f)^n$ configuration so transitions between these levels should occur only by magnetic dipole transitions. Mixing of the $(4f)^{n-1}$ 5d configuration into

the $(4f)^n$ configuration relaxes the Laporte selection rule and makes the transition more allowed by an electric dipole process. The mixing occurs if the rare earth ion experiences a crystal field that lacks inversion symmetry.

In the case of the transition metal ion it is the mixing of the $(3d)^{n-1}$ 4p configuration into the $(3d)^n$ which allows electric dipole transitions to occur.

1.5 SPONTANEOUS TRANSITION PROBABILITY.

The spontaneous transition probability (A_{ba}) is a measure of the probability that an excited ion will spontaneously decay with the emission of a photon from an excited state *b* to a lower state *a*.

For an electric dipole process [3],

$$A_{ba} = \frac{1}{4\pi\varepsilon_0} \frac{4e^2\omega^3}{3\hbar c^3} n \left(\frac{E_{loc}}{E_{mac}} \right)^2 \frac{1}{g_b} \sum_{ab} |\langle a|\mathbf{V}|b\rangle|^2 \qquad (1.9)$$

where g_b is the final state degeneracy and n is the refractive index of the material.

If the atom or ion that is undergoing the transition is within a dielectric material, then the electric field that acts locally on the atom or ion will not be the same as the field that acts macroscopically. If $\mathbf{E}_{mac}$ is the macroscopic field and $\mathbf{E}_{loc}$ is the local field acting at the same time, then the transition probability formulas are multiplied by the local field correction factor. For an ion in a high field octahedral crystal site this is [3],

$$\left(\frac{E_{loc}}{E_{mac}} \right)^2 = \left(\frac{n+2}{3} \right)^2 \qquad (1.10)$$

where n is the refractive index of the material.

For a magnetic dipole process [3],

$$A_{ba} = \frac{\mu_0}{4\pi} \frac{4\omega^3}{3\hbar c^3} n^3 \frac{1}{g_b} \sum |\langle a|V|b\rangle|^2 \qquad (1.11)$$

There is no local field correction to be made for magnetic fields in non-magnetic materials.

1.6 OPTICAL ABSORPTION.

Optical absorption occurs when an electron is optically excited from the ground state *a* to some excited state *b*. Fig 1.2 shows a parallel beam of light I_o incident on a sample of thickness d. Let the flux of photons be N per meter square and let *k* be the probability of absorption of a photon per meter length of material.

This gives

$$dN = -N\,k\,dx \qquad (1.12)$$

$$\int_{N_0}^{N_1} dN/N = -k \int dx$$

$$= -k\,d$$

$$\text{Ln } N_0/N_1 = -k\,d$$

$$N_1 = N_0 \exp^{-kd}$$

The intensity of the light I_0 is proportional to N_0, so

$$I_1 = I_0 \exp^{-kd} \qquad (1.13)$$

k is called the absorption coefficient. The absorption of the radiation will vary with frequency so this is written,

$$I_1(\nu) = I_0(\nu) \exp^{-k(\nu)d} \qquad (1.14)$$

where ν represents the frequency of interest.

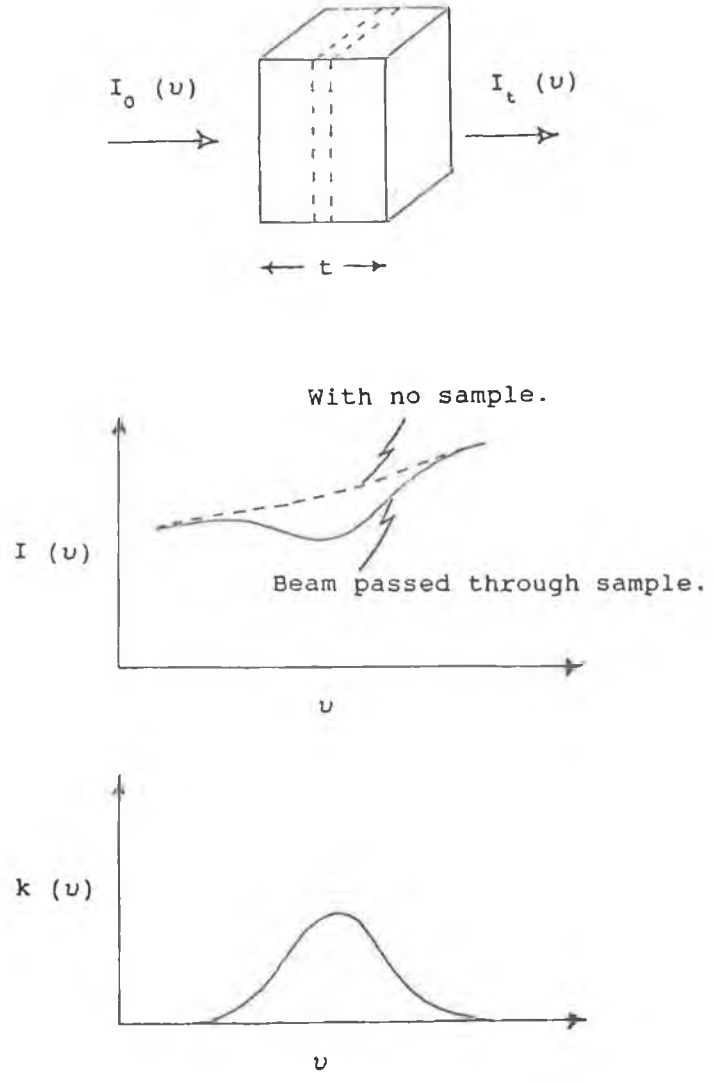

Fig 1.2 Optical Absorbtion.

1.7 IONS IN A STATIC CRYSTALLINE ENVIRONMENT.

It is easier initially to look at the case of an ion in a static environment and later to take account of the vibrational motion of the solid. In the case of the ion in a static crystalline environment the Hamiltonian operator which is used to describe the electronic centre takes account of the fact that the optical transitions take place at the outer electrons. The electrons which occupy closed shells or subshells are normally not affected by the transitions and they are regarded as creating a constant electrostatic central field. The outer electrons which are optically active, interact with this central field.

For the static crystalline environment,

$$H = H_{FI} + H_C \qquad (1.15)$$

$$= H_O + H_{EL} + H_{SO} + H_C \qquad (1.16)$$

H_C is the interaction energy of the optically active outer electrons with the electrostatic crystal field and this can be written as [1],

$$H = \sum_i \sum_l H_C (r_i, R_l) \qquad (1.17)$$

where r_i = electronic coordinates and R_l = ionic coordinates.

For the transition metal ions the optically active 3d electrons are on the outside of the ion and they are very sensitive to the crystalline environment, in this case H_C is comparable with H_{EL} the coulomb interaction of the 3d electrons with each other.

It is useful to look at three different cases [5], weak, intermediate and strong crystal field and to show how the methods of determining the eigenstates and eigenvalues of the Hamiltonian depend upon the relative sizes of the various terms.

1. Weak Crystal Field. $H_C << H_{EL}, H_{SO}$

In the weak field case we can initially neglect the crystal field term H_C . The terms remaining make up the free ion Hamiltonian and this is calculated as in the case of the free ion. At this point H_C is taken into account using perturbation theory. An example of the weak crystal field case, is when trivalent rare-earth ions are the dopant ions. In this case the 4f electrons are screened from the lattice ions by the outer $5s^2$, $5p^6$ subshells. The result of this is that the spectra of dopant rare earth ions have narrower line widths than the spectra produced from transition metal ions.

2. Intermediate Crystal Field. $H_{EL} > H_C > H_{SO}$

For the intermediate crystal field case the spin orbit

interaction H_{SO} is neglected. As H_C is an orbital operator the free ion L functions are used as basis functions to calculate matrix elements of H_C from which new crystal field orbital states are formed. These are multiplied by spin S functions and the effect of H_{SO} is then calculated.

3. Strong Crystal Field. $H_C > H_{EL} > H_{SO}$

In the strong field case we firstly calculate the single electron orbitals in the presence of the crystal field. Then we take account of how the H_{EL} term couples the single electron orbitals together. H_{SO} is then added as a perturbation. The strong field case is used for the $(3d)^n$ ions in solids.

1.8 TRANSITION METAL IONS IN A SOLID.

When an ion is part of a solid the crystal field experienced by the ion is related to the symmetry of the crystalline environment of which it is part. Three types of crystalline environment are shown in Fig 1.3. [6]

In the first case (a) the transition metal ion is at the centre of eight point charges of size -Ze at the corners of a regular cube. The crystal field produced at the central ion is of cubic symmetry.

In the second case (b) the transition metal ion is at the centre of four point charges of size -Ze at the corners of a tetrahedron. The crystal field produced at the central ion by this arrangement is said to have tetrahedral symmetry. The group theoretical notation for tetrahedral symmetry is T_d.

In the third case (c) the transition metal ion is at the centre of six point charges of size -Ze in the ±x, ±y, and ±z directions. The combination of electric fields produced by the six neighbouring ions produces a field of octahedral symmetry at the ion in the central position. The

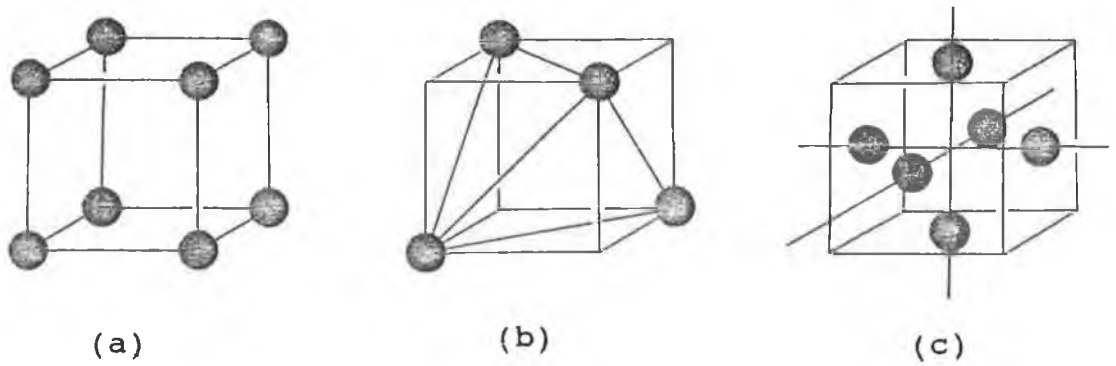

Fig 1.3 Three types of crystalline environment.

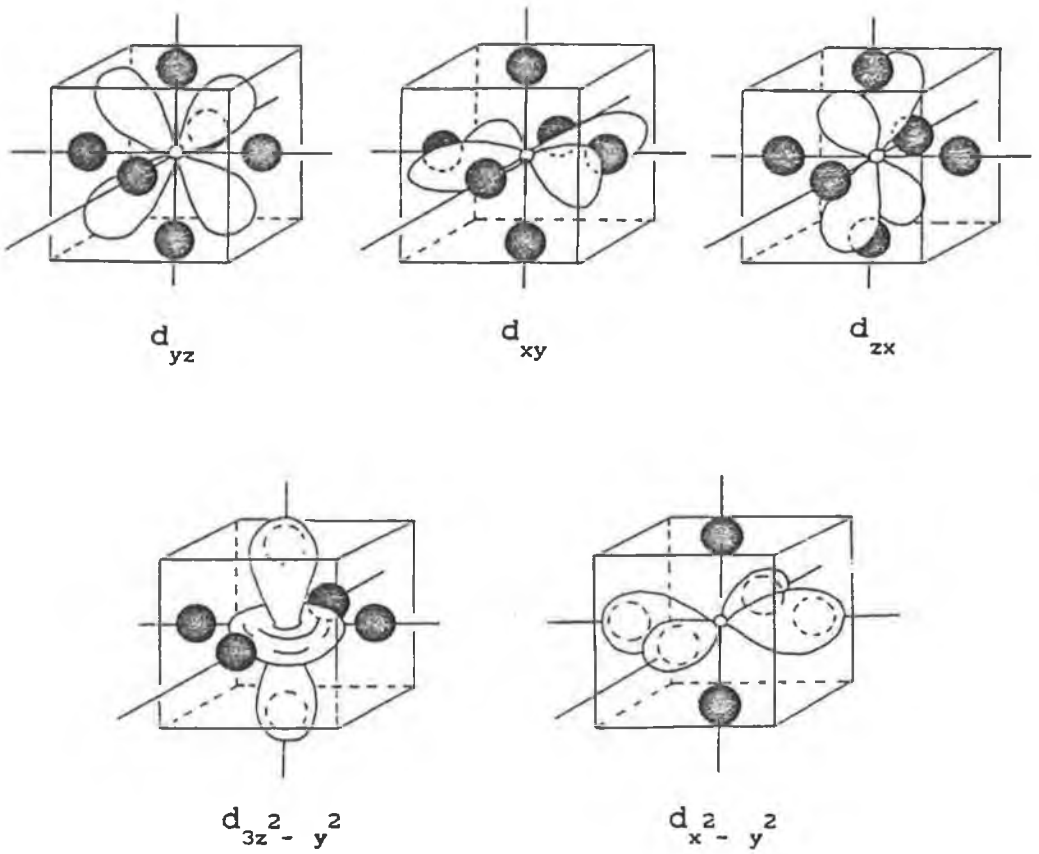

Fig 1.4 The octahedral crystal field orbitals.

group theoretical notation for octahedral symmetry is O_h.

The arrangement in Fig 1.3 (c) is most often found but it may have a slight distortion from exact octahedral symmetry, O_h. The main crystal field component is due to octahedral symmetry and the other components are much smaller. In this case the best method of analysis is to calculate the wavefunctions in the high symmetry field and then to consider the weak lower symmetry fields using perturbation theory.

As Ti^{3+} has only one 3d electron it is the easiest example to look at initially, so we assume the Ti^{3+} ion finds itself in a position of octahedral symmetry. The 3d state will have five-fold orbital degeneracy as there are five orbitals with the same energy. The octahedral crystal field orbitals formed are shown in Fig 1.4. Three of the orbitals have their lobes pointing between negatively charged ions, d_{yz},d_{xy},d_{zx} and the crystal field will effect each of these orbitals to the same extent. The three orbitals are called the t_{2g} orbitals. The two remaining orbitals the $d_{3z^2-r^2}$ and the $d_{x^2-y^2}$ have exactly the same energy and these are called the e_g orbitals. The e_g orbitals are higher in energy than the t_{2g} orbitals and the overall effect of the octahedral crystal field is to split the 3d level into two, Fig 1.5. The energy separation between e_g and t_{2g} is labelled 10 Dq, where Dq is a parameter which measures the strength of the octahedral field.

If the number of 3d electrons is increased the electrostatic interactions among the 3d electrons as well as the crystal field must be taken into account. Fig 1.6 is called a Tanabe Sugano diagram [7] and it shows how the free ion levels are split as the ratio of the crystal field to the inter-electron interaction (Dq/B) increases. The dependence of E/B on Dq/B will vary slightly for different values of B and C. These are called Racah parameters and their values vary from ion to ion and host to host. The split lines are labelled A_2,E,T_1,T_2 and these are group theoretical labels [8] that relate to the symmetry of the

orbital wavefunctions in the octahedral crystal field.

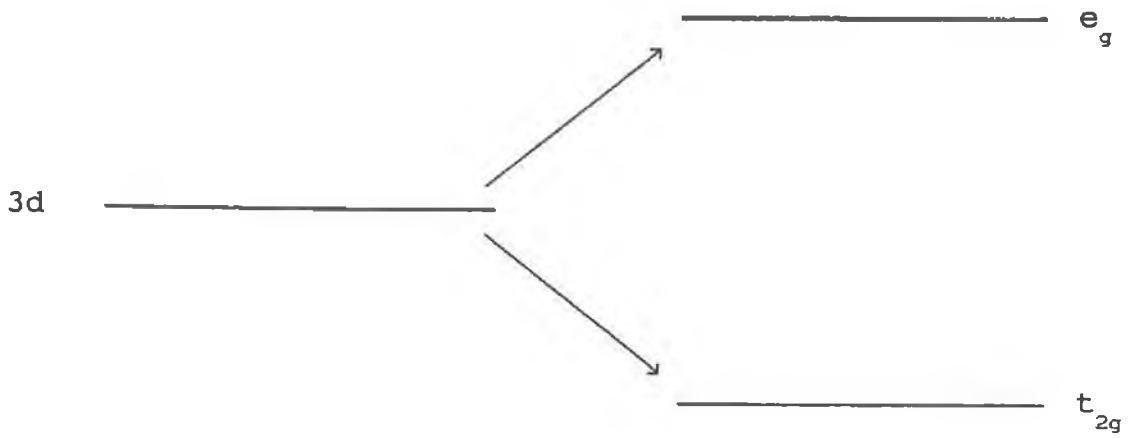

Fig 1.5 Splitting of the 3d level due to octahedral field.

1.9 RARE EARTH IONS IN SOLIDS.

As has been described earlier, rare ions in glass fall into the category of the weak field case. For the weak field case $H_C << H_{EL}$, H_{SO} , and for this reason H_C can be treated as a small perturbation on the free-ion energies. The local field at the dopant rare earth ion in a solid can be described by expanding the crystal field potential V in terms of tensor operators $C^{(k)}_{-q}$ that transform as spherical harmonics. This yields,

$$V = \sum_{k,q,i} B^k_q \left(C^{(k)}_{-q} \right)_i \qquad (1.18)$$

where B_q^k are the crystal field parameters and the summation i is over all electrons of interest. For example as the site symmetry in glass is C_1, [9] all the terms in eqn 1.18 are allowed. For f electrons k is limited to values ≤ 6. The crystal field splitting is caused by the even-k terms which remove the degeneracy of the free ion J states. The odd-k terms admix states of different parity and make normally parity forbidden electric dipole transitions between states of $4f^n$ configuration possible.

An example of the energy levels for trivalent rare earth ions in lanthanum chloride as determined by Dieke [10] is given in Fig 1.7. The small semicircle under the level indicates that luminescence occurs from this level of the ion when it is in lanthanum chloride. The states are indicated by their $^{2S+1}L_J$ free ion values. As the ions are in a solid the crystal field causes the levels to split, but as the splitting is small in the rare earths, this is indicated in the diagram by broadened lines. If the rare earth ions are dopant ions in other host materials the position of the levels are essentially the same, but the splitting is different due to different crystal field strengths and symmetries. As the optical transitions in rare earth ions occur between the same $4f^n$ configuration the only transitions that should occur between these states should be magnetic dipole transitions ($\Delta L=0$, $\Delta S=0$, $\Delta J=0$, ± 1). When the rare earth ion is in a site that lacks inversion symmetry the parity selection rule is lifted and weak electric dipole transitions can occur.

1.10 ION IN A VIBRATING LATTICE.

How the static crystalline environment effects the dopant optically active ion has already been examined. In this section the effect on the absorption and luminescence of an optically active ion which is part of a crystal lattice that undergoes static and dynamic distortions is examined. When an optically active ion is part of a crystal lattice, its neighbouring ions vibrate about some average

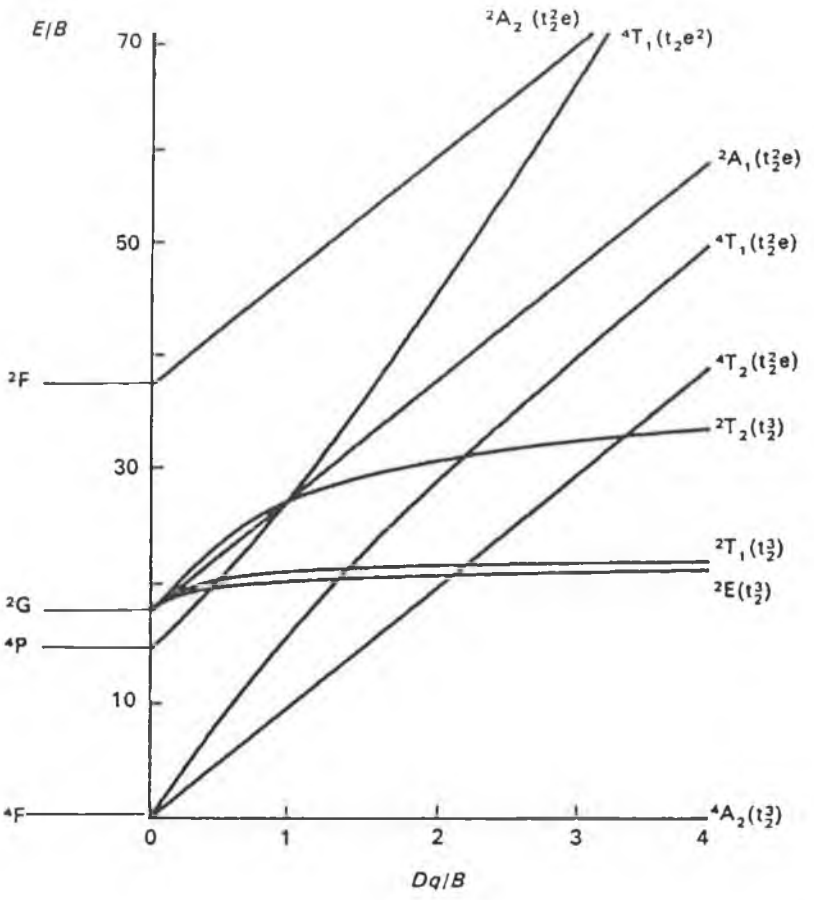

Fig 1.6. Tanabe Sugano diagram. Energy levels of a $3d^3$ system in an octahedral field. In this case the values have been calculated for γ = 4.8, which is for Cr^{3+} in aluminium oxide. [7]

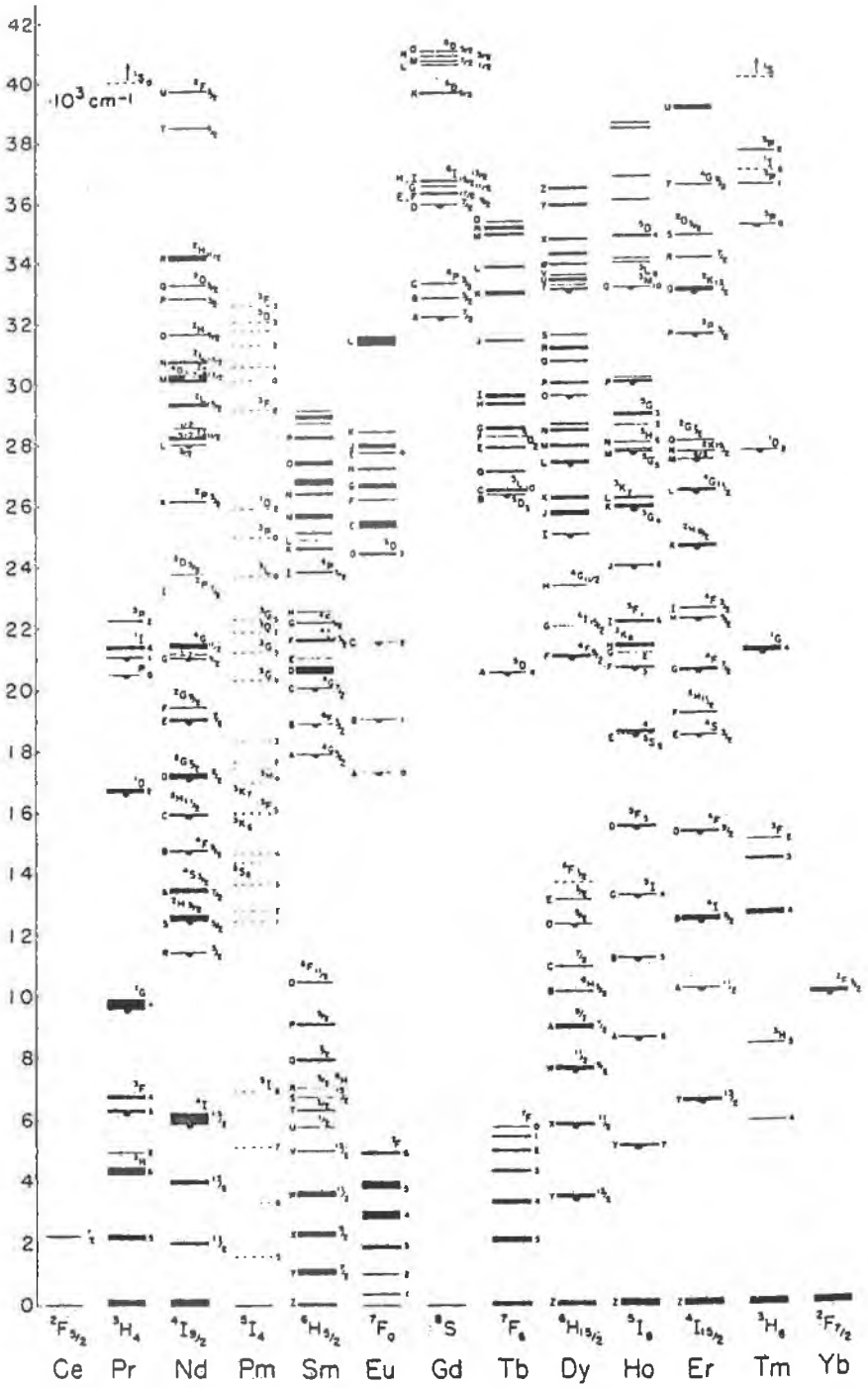

Fig 1.7 Dieke diagram showing energy levels of trivalent rare earth ions. [10]

position. The resultant dynamic crystal field effects the electronic states of the dopant ion.

The vibrational states of the lattice are described in terms of phonons. The state of vibration is described by listing the number of phonons of each frequency that are present. This is written as follows, $|n_1,n_2,n_3,n_4, ...>$, where n_i is the number of phonons in the ith vibrational mode. This is usually written $|n>$ for simplicity. The Hamiltonian in this case that describes the ion plus lattice system is [2],

$$H = H_{FI} + V_C + H_L \qquad (1.19)$$

H_{FI} is the free ion Hamiltonian of the dopant ion, H_L is the Hamiltonian that descrides the lattice and V_C is the interaction energy of the ion in the crystal field of the lattice. The Hamiltonian of the vibrating lattice can be expressed as [2],

$$H_L = \sum_k \frac{\hbar\omega}{2} \quad (a_k^+ a_k + a_k a_k^+) \qquad (1.20)$$

where a_k and a_k^+ are the annihilation and creation operators for phonons of wave vector k.

The term that describes the crystal field V_C can be split into two terms V_C^O , which is the interaction energy with the ions in their average positions and V_C^V , which describes the interaction energy with the time varying crystal field, (the electron phonon interaction.)

If we firstly consider the case were $V_C^V = 0$. The lattice is not affected by electronic changes in the dopant ion, so the H_{FI} and H_L terms are independent of each other. H_L is the dynamic lattice Hamiltonian whose eigenstates are $|n>$. If the $|\imath>$ states are the free ion wavefunctions then the eigenstates of the full Hamiltonian $H_{FI} + H_L$ are the product state $|\imath>|n>$ which can be written as $|\imath,n>$. The probability of an electronic transition from an initial

state $|i,n\rangle$ to a final state $|i,m\rangle$ depends on the square of the matrix element $\langle i,m|d|i,n\rangle$, were d is the appropriate electronic operator. As the electronic operator does not act on the lattice states, the matrix elements look like this $\langle i|d|i\rangle \langle m|n\rangle$. Due to orthogonality $\langle m|n\rangle=0$ unless m=n. In this case transitions do not effect lattice states and we get sharp transitions.

For the second case if we consider that V_c^v is not equal to zero. The crystalline field is due to the charges of the ligand ion surrounding the optically active ion, and if there is distortion of the ligand ions, this affects the crystal field. This is viewed in terms of a local strain ε due to the lattice vibrations; ε is given by, [2]

$$\varepsilon = \sum_q \left(\frac{\hbar\omega}{2M\nu^2} \right)^{1/2} (b_q - b_q^+) \qquad (1.21)$$

where M is the mass of the crystal, b_q and b_q^+ are the annihilation and creation operators for the qth vibrational oscillator respectively, ν is the average velocity of sound waves in the crystal. The dynamic crystal field potential can be expressed as,

$$V_c^v = V_1\varepsilon + V_2\varepsilon^2 + \ldots\ldots \qquad (1.22)$$

V_1 and V_2 are coupling parameters which are functions of the electronic coordinates of the dopant ion.

1.11 CONFIGURATION COORDINATE MODEL.

The broadbands that are found in the spectra of dopant ions in crystals are due to the electron phonon interaction. The simplest way of explaining the spectra produced is by means of the configurational coordinate diagram [11]. The configurational coordinate Q is the average separation of the dopant ion and its nearest

neighbours. In this model the mode of vibration is the breathing mode, in which the ions pulsate in and out about the optically active dopant ion. A harmonic oscillator function is used to describe these pulsations. Q the configurational coordinate oscillates about its equilibrium Q_0^1.

Figure 1.8 shows an example of a configurational coordinate diagram in which each state of the ion lattice system is shown as a harmonic oscillator parabola. The lower parabola represents the ground state while the higher represents some excited state.

The configuration coordinate model relies on the application of the Franck Condon principle [12], which states that, because nuclei are so much more massive than electrons, the electronic redistribution occurs while the nuclei stay at their initial separations. This allows us to say that the value of Q is the same just before and just after a transition, or that a transition can be represented by a vertical arrow. For an ion in the electronic ground state A the most likely value of Q is Q_0^1. The most likely absorption transition to take place would be from A to B in Fig 1.8. Transitions from other values of Q also take place with less probability, yielding a broadened spectrum. When an ion is in an excited electronic state B and it is also in some high vibrational level, it will decay non-radiatively to the zero-vibrational level of the state. This is indicated in the diagram by the arrow from B to C.

Like the absorption transition the most probable luminescence transition is from the zero-vibrational level of the state. It should also be noted that transitions also occur from different vibrational levels, yielding a broadened output. Due to the differing effect of the crystal field on the ground state and excited states, the peak of the luminescence output is shifted to lower energies in relation to the peak of the absorption band. The energy separation of the two peaks is known as the Stoke's shift.

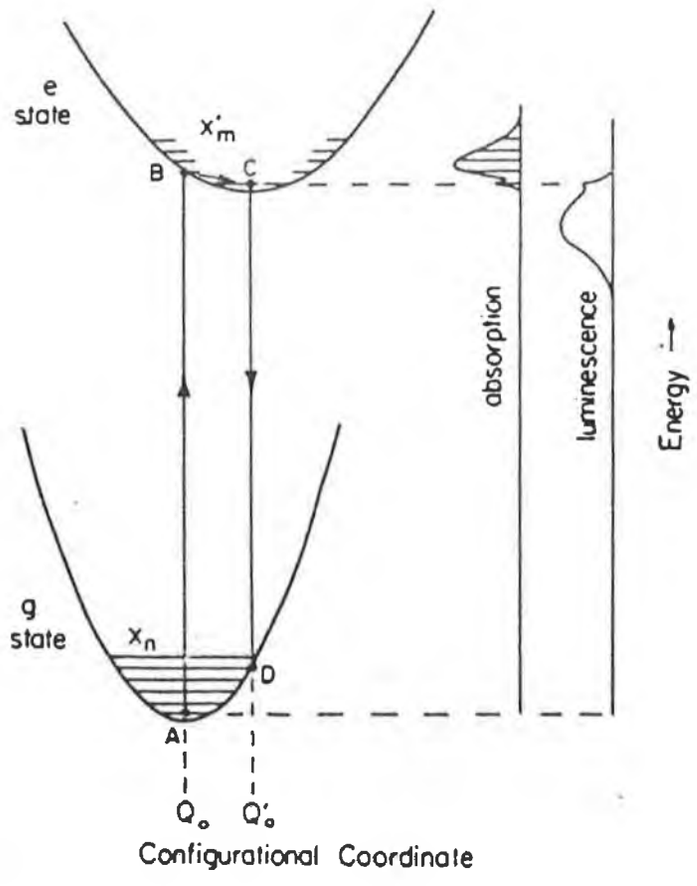

Fig 1.8 Configurational Coordinate diagram showing optical transitions between e and g.

1.12 LINE BROADENING.

The two types of line broadening that can contribute to the width of a no-phonon line are the homogeneous and inhomogeneous broadening mechanisms. For example when applied to glass, the environment of each dopant ion is not identical and we get a range of transition frequencies. The line observed from ions in a glass host is inhomogeneously broadened as it is a mix of contributions from ions in slightly different sites. If all the ions were in identical sites i.e., as in a pure crystal, we would get a sharp line which would have the homogeneous width of the transition.

When a broadband excitation source is used, ions in different sites have an equal probability of being excited and the luminescence output displays the inhomogeneous broadening of the material. If a narrow band laser is used, this will excite only a small number of ions were the absorption frequencies are within the laser linewidth. The luminescence emitted from these ions will have a much narrower frequency band than the inhomogeneous linewidth of the material. The use of a narrow band laser to give a narrowed line luminescence output is called fluorescence line narrowing (FLN) and this will be described in more detail later.

The homogeneous broadening of a line is as a result of the lifetime of the initial and final states of a transition. If each state has a lifetime τ then there will be an uncertainty in the energy of the state ΔE.

$$\Delta E \, \tau = \hbar \qquad (1.23)$$

The uncertainty in the energy results in a broadening of the transition. There are a number of relaxation processes that can be involved and the broadening is given by [11],

$$B = \hbar \sum_i W_i \qquad (1.24)$$

where W_i are the relaxation rates of the processes that contribute to the lifetime.

The relaxation mechanisms that lead to homogeneous line broadening are shown in Fig 1.9, in which two states *a* and *b* are separated by δ which is within the range of phonon energies. The first process (1) illustrates the direct relaxation process between *a* and *b*. The second process (2) is a two phonon Orbach [13] process from *b* to *a* involving a real electronic state *c* and the third process (3) is a two phonon Raman process from *b* to *a* via a virtual intermediate state *d*.

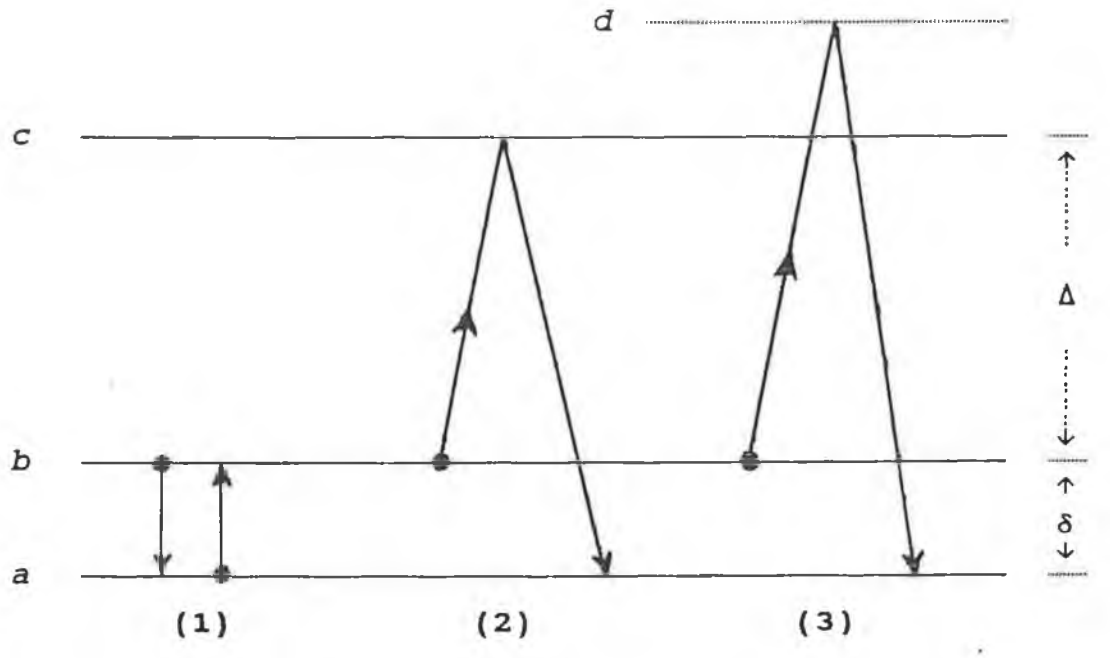

Fig 1.9 Schematic diagram showing the relaxation mechanisms that lead to homogeneous broadening.

Process (1) is the process of direct relaxation as illustrated in Fig 1.9. For this process we can write

$$W_{ab}^{(1)} = W_o^{(1)} (n) \qquad (1.25)$$

$$W_{ba}^{(1)} = W_o^{(1)} (1+n) \qquad (1.26)$$

where n is the thermal occupancy of phonons of energy $\hbar\omega=\delta$. $W_o^{(1)}$ is the rate of relaxation between *b* and *a* at a temperature of absolute zero. For electric and magnetic dipole radiative processes the transition probability increases as ω^3, where $\hbar\omega$ is the energy of the photon involved. When an ion is raised to an excited state, the probability that it will decay radiatively to a lower state varies as the cube of the energy gap between the two states. The probability of nonradiative decay will decrease as the energy gap between the two states increases. If the energy gap between the states *a* and *b* is greater than the range of phonon energies, a direct process can still occur by a multiphonon process. There is a point when the gap becomes too large for the multiphonon process to be efficient enough to stop luminescence from occuring. The process of non radiative decay will be dealt with in the following section.

Process (2) is known as an Orbach [**] process. As can be seen in Fig 1.9, this is a two phonon process which involves the absorption of a phonon that raises the ion to an excited state *c*, and then the subsequent emission of another phonon. This process will occur if the electronic state c lies within the range of phonon energies. This process depends upon the availability of thermal phonons for the initial excitation and it is assummed that $\Delta\gg\delta$. In this case the relaxation rate varies as, [11]

$$W_{ba}^{(2)} = W_{ab}^{(2)} = W_o^{(2)}\, n \cong W_o^{(2)}\, \exp(-\Delta/kT) \qquad (1.27)$$

where $\Delta\gg kT$ and n is the thermal occupancy of phonons. $W_o^{(2)}$ is related to the sensitivities of levels *a*,*b* and *c* to lattice distortions.

Process (3) is called a Raman relaxation process and this is again a two phonon process. In this case the process involves a virtual state and this is represented in Fig 1.9 by a broken line. In the Debye approximation and

if δ is less than the maximum phonon energy, then the Raman relaxation rate is given by [2]

$$W^{(3)} = A\left(\frac{kT}{h}\right)^7 \int_{x}^{x_0} x^6 \, e^x \, (e^x - 1)^{-2} \, dx \qquad (1.28)$$

where A is the coupling coefficient between the energy levels of the ion and the lattice vibrations. $x_0=\hbar\omega_0/kT$, where ω_0 is the Debye cut off frequency.

1.13 NONRADIATIVE RELAXATIONS.

The fact that most luminescent ions have a quantum efficiency of less than one can be explained by assuming that a mechanism exists whereby an ion in an excited state can return to its ground state without the emission of radiation. The reason that this occurs is due to the coupling of the excited ion with the host lattice and the excited ion energy is converted to vibrational energy of the lattice (phonons). Nonradiative transitions occur when the total energy of the phonons created in a transition equals the energy gap between the initial and final states. This process is illustrated in Fig 1.10,

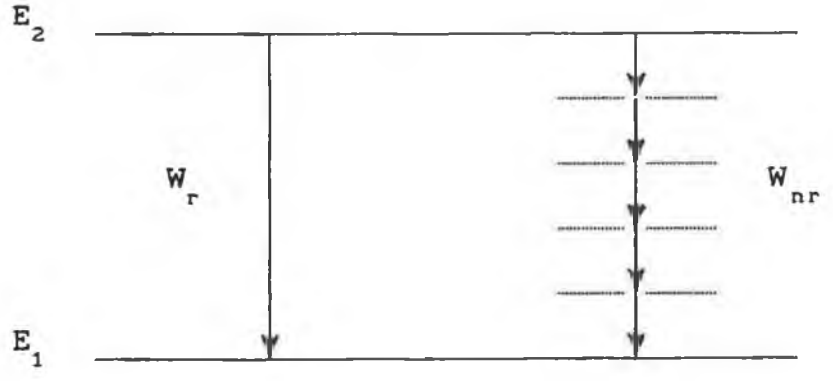

Fig 1.10 Radiative and nonradiative processes between two energy levels E_2 and E_1. W_r is the radiative probability and W_{nr} is the nonradiative probability.

The decay time of the transition τ can be expressed as

follows,

$$\frac{1}{\tau} = \frac{1}{\tau_r} + \frac{1}{\tau_{nr}} \qquad (1.29)$$

$$= W_r + W_{nr} \qquad (1.30)$$

where W_r and W_{nr} are the radiative and nonradiative transition probabilities respectively.

1.14 ENERGY TRANSFER.

As the concentration of optically active ions within a solid increases it becomes possible for two ions to become close enough for them to interact with each other. The interaction may be such that excitation can be transferred from one ion to another. This energy transfer between optically active ions can have a great effect on the fluorescence properties of the material. When the concentration is increased, clustering can occur. This is when two or more ions are close enough to interact strongly and form a resolvable center (dimer). Also individual ions may be close enough so that a weak interaction can occur between them. This weak interaction may be such that excitation on one of the ions can be transferred non-radiatively to the other ion. If this energy transfer is efficient enough, energy can migrate through the material and it can decay non-radiatively upon reaching a sink (defect or impurity etc). For these reasons the fluorescence efficiency of a material can decrease when the optically active ion concentration is increased significantly and this is called concentration quenching.

The basic theoretical background for the energy transfer process in inorganic materials was developed by Förster [14] and Dexter [15]. This work formed the basis of much of the later work on energy transfer.

In general, the energy transfer process involves the

initial excitation, by light, of a group of ions called donors (D) and the transfer of energy to another group of ions called acceptors (A). There are a number of different processes by which this can occur (a) resonant transfer, (b) non-resonant transfer, (c) cross relaxation and (d) up-conversion. A diagram representing each of the above processes is shown in Fig 1.11. [16]

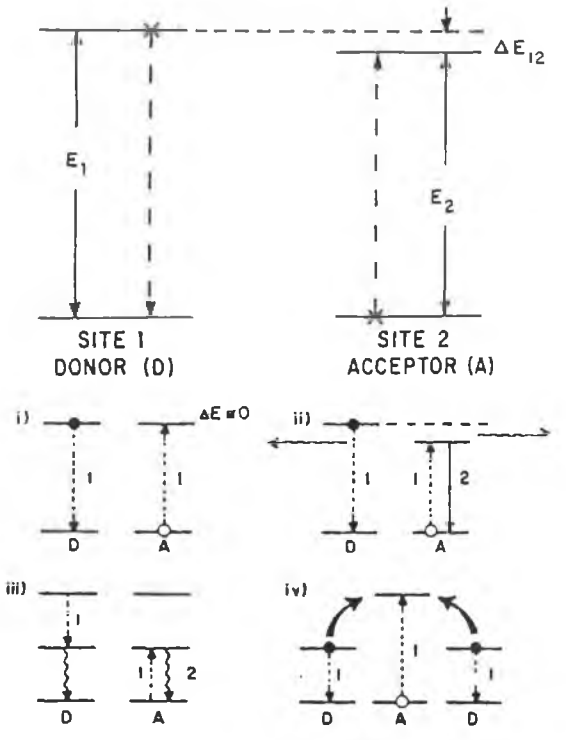

Fig 1.11 Schematic illustration of energy transfer between donor and acceptor ions. (1) resonant D-A transfer, (2) non-resonant transfer, (3) cross relaxation and (4) upconversion.

Förster and Dexter showed that multipolar interactions and exchange can cause transfer, the transfer rate varying as R^{-n}, where R is the separation of the donor and acceptor, and n = 6,8,10, for dipole-dipole, dipole-quadropole, and quadropole-quadropole interactions

respectively. The transfer rate due to exchange falls off exponentially with increasing R. These processes were considered resonant and therefore depended on the overlap of the emission and absorption spectra of the donor and acceptor ions respectively. If there is no acceptor-donor back transfer, the transfer probability can be written as [16],

$$W_{12} = \frac{2\pi J^2}{\hbar^2} \int g_1(\omega)\, g_1(\omega)\, d\omega \qquad (1.31)$$

where $J = \langle 1^*,2 \mid H_{INT} \mid 1,2^* \rangle$, and the asterisk denotes an excited ion, H_{INT} is the interaction Hamiltonian for the appropriate multipolar interaction which couples 1 and 2, J depends on the nature of the optical excitation and includes any parametric dependencies, such as interionic separation.

The Förster and Dexter model was used to describe systems where the absorption and emission lines were broad and overlap occurred. This is the case with transition metal ions. In the case of narrow lines from rare-earth ions (see section 1.9), the simple process involving resonant energy transfer is inadequate. A number of different models have been presented, Inokuti and Hirayama [17], Yakota and Tanimoto [18], and a review of all the models presented is given in Holstein et al [19]. Fluorescence line narrowing which is described in chapter 6 is an ideal tool for investigating energy transfer, as a small subset of ions can be probed and viewed at various delays after excitation. [20]

CHAPTER 2.

2. GLASS.

2.1 INTRODUCTION.

Glass is one of the oldest and still one of the most technologically important materials used by man. It was first used during the bronze age period 5000 - 6000 years B.C. to make coloured beads for decorative purposes and by the start of the Christian period was used for the production of vessels of all shapes and sizes. The development of glass production techniques was a gradual process and by the 15^{th} and 16^{th} centuries exquisite glass pieces were being produced in Venice. The blowpipe production technique used has not changed in hundreds of years and is still followed today for ornate "crystal" glass. Research into the properties of glass took an upturn in the 1950's and 60's with glass being used as fibers for optical communication purposes and also the development of glass lasers. It is an indication of the versatility of glass that it is still technologically an extremely important material.

In this chapter details of the properties and general theories of glass will be given. The background behind the production of glasses by the high temperature and sol-gel processes will also be given.

2.2 PROPERTIES.

Glasses are defined by properties which are common to them all but which are different to those of liquids and crystalline solids. It can be shown using X-ray and electron diffraction studies that unlike crystals, glasses lack long range periodic order of the constituent atoms. It can be seen in Fig 2.1 that they resemble liquids and not crystalline solids in their atomic distribution.

Like crystalline solids they have excellent elastic properties, and under a shear stress they flow. It can be seen that glasses possess some of the properties of

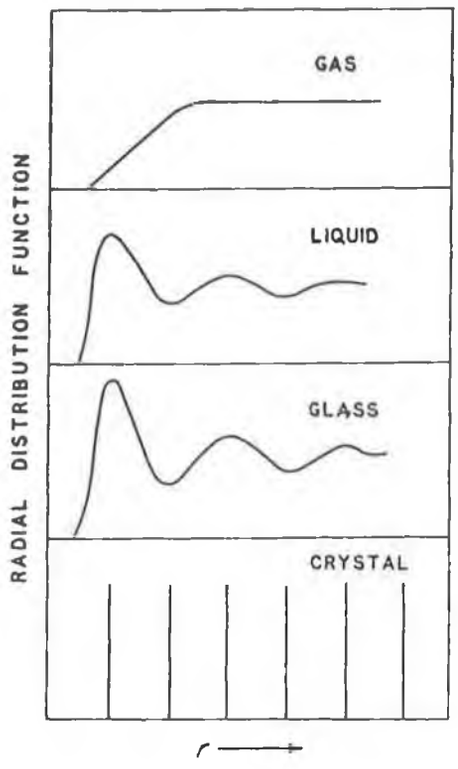

Fig 2.1 Atomic distribution diagram.

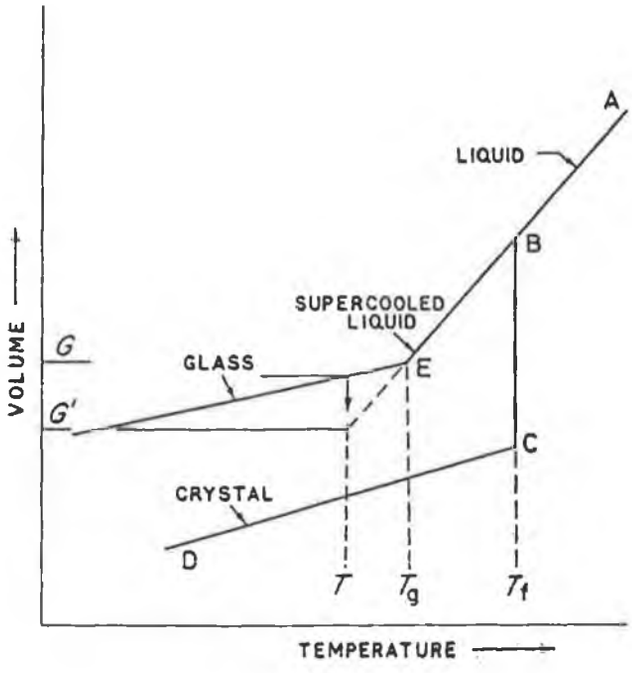

Fig 2.2 Temperature volume diagram.

crystals and some of the properties of liquids.

A glass can be obtained by cooling a liquid below its freezing point under certain conditions. When a liquid is cooled its fluidity decreases, and, at a certain temperature below the freezing point, becomes nearly zero.

The liquid becomes rigid. How the glass comes about with relation to its liquid and crystalline phase can be explained by Fig 2.2, a temperature - volume diagram.

When a liquid is cooled from its initial state A, the volume will decrease along a constant slope. If the liquid is cooled slowly enough, crystallisation will take place at T_f , the freezing temperature. On crystallisation the volume will decrease sharply from B to C and upon further reduction of temperature will fall along the slope C to D.

If the rate of cooling is fast, crystallisation will not take place at the freezing temperature T_f , but the volume of the "supercooled" liquid will decrease along the slope B to E which is the same as A to B. When the temperature reaches T_g , the glass transition temperature, the volume temperature line undergoes a change in slope and continues along a line parallel to CD. At temperatures below T_g the material is said to be a glass.

The point E does not have an exact position as its position varies with the rate of cooling. This is known as the transformation range. It is also found that if the temperature of the glass is held constant at a temperature T, that the volume G will continue to decrease at a slow rate until it reaches G^1.

The glass forming oxides B_2O_3, SiO_2, GeO_2, and P_2O_5 are known as "glass formers" as they easily form glasses on their own and form many of the mixed oxide glasses.

2.3 DEFINITION OF A GLASS.

The exact definition of what constitutes a glass has long been a subject of debate amongst glass technologists. In 1945 the American Society for Testing Materials [A.S.T.M.] gave the definition "Glass is an inorganic

product of fusion which has cooled to a rigid condition without crystallising". This definition is applicable to the more familiar glasses, however, it does not cover non-crystalline solids prepared by deposition from the vapour phase, or by sputtering in a low pressure system or materials produced through the Sol Gel route. To try to overcome these problems the U.S. National Research Council proposed the general definition, "Glass is an X-ray amorphous material which exhibits the glass transformation", this being defined as that phenomenon in which a solid amorphous phase exhibits with changing temperature a more or less sudden change in the derivative thermodynamic properties, such as heat capacity and expansion coefficient from crystal-like to liquid-like values.

2.4 ZACHARIASEN'S THEORY.

As the density and mechanical properties of an oxide glass are very similar to those of the corresponding crystal, the interatomic forces and distances must also be similar. Zachariasen's theory [21] states that the atoms must form extended three dimensional networks as is the case with crystals. X-ray diffraction experiments show that the network in glass is not symmetrical and periodic as is the case with crystals. If we take SiO_2 as an example, the only difference between the crystalline and the glassy forms is that in the glassy form the orientation of the silicon oxygen tetrahedra is variable while in the crystalline form it is constant. Zachariasen suggested a set of rules that an oxide must follow for it to be a glass former.

(1) No oxygen may be linked to more than two atoms of A.

(2) The number of oxygen atoms surrounding A must be small (3 or 4).

(3) The oxygen polyhedra share corners with each other not edges or faces.

(4) At least three corners of each polyhedra must be

shared.

The X-ray investigations of vitreous silica by Warren [22] in 1941 verified Zachariasen's theory, and this model is illustrated in Fig 2.3. There are many other theories that try to explain the properties of glass [23], but the random network theory by Zachariasen is the most widely accepted.

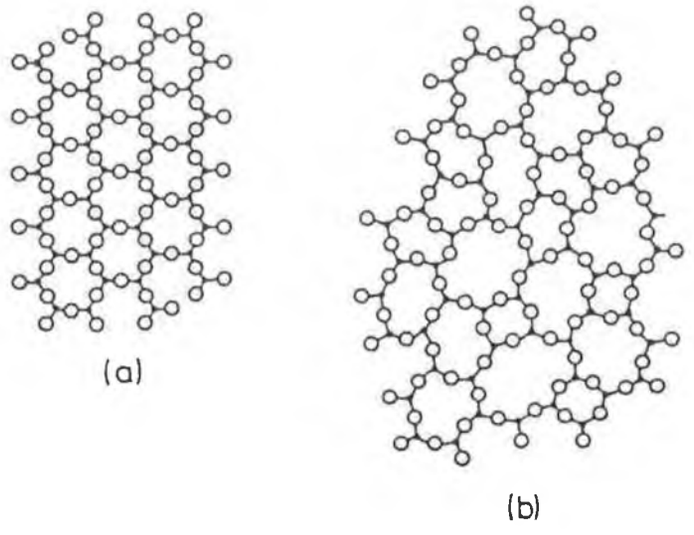

Fig 2.3 Schematic two-dimensional representation of the structure of (a) a hypothetical crystalline compound A_2O_3 and (b) the glassey form of the same compound.

Glass forming substances have been classified in terms of chemical bonding. Dietzel [24] proposed that these substances can be classified into (a) glass forming oxides (glass formers), (b) intermediate oxides (intermediates), and (c) modifier oxides (network modifiers). The substances were classified by z/a^2, where z is the electric charge and a is the interionic distance between the cation and oxygen ions.

Glass forming oxides	P^{5+}, B^{3+}, Si^{4+}, Ge^{4+} etc.
Intermediate oxides	Al^{3+}, Be^{4+} etc.
Modifier oxides	Mg^{2+}, Ca^{2+}, Na^{+} etc

The values of z/a^2 as well as the single bond strengths are shown in table 2.1.

	ION	COORDINATION NUMBER	$2z/a^2$	SINGLE BOND STRENGTH kcal
Glass Formers	P^{5+}	4	4.3	88 to 111
	B^{3+}	3	3.22	119
	Si^{4+}	4	3.14	106
	Ge^{4+}	4	2.65	108
Inter-mediates	Al^{3+}	(4)	1.69	53 to 67
	Be^{4+}	4	1.51	63
Network modifiers	Mg^{2+}	6	0.95	37
	Ca^{2+}	8	0.69	32
	Na^{2+}	6	0.35	20

Table 2.1 Glass-forming substances and their classification into revelant groups.

Silica glass represents the simplest case to understand as only SiO_4 tetrahedra form its network. An example of the structure of silica glass with network modifier added is shown in Fig 2.4. It was the X-ray diffraction work of Warren that elucidated what happened to the glass structure with the introduction of network modifier ions. The network modifier ions introduced in the form of Na_2O for example, causes a breakage of some of the Si—O—Si bonds present in the silica glass. For every two Na^+ ions added to the glass there is a break in one bond between two tetrahedra. The bridging oxygen is replaced by two non bridging oxygens bonded to the sodium ion (see Fig 2.4). The extra negative charge is compensated for by the positive charges of the alkali ion. The consequent effect of introducing network modifier ions into the structure is to loosen the structure which lowers the melting temperature and yields a glass with a lower density.

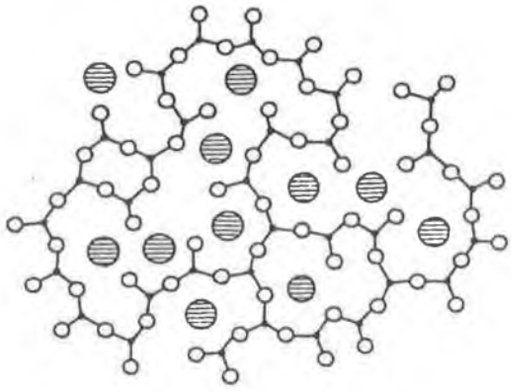

Fig 2.4 (a) Structure of silica glass with Na added.

2.5 THE SOL-GEL PROCESS.

As interest in glass has been fueled in recent years with the development of optical fibers and glass lasers. A technique that has attracted attention is the production of glass by the sol-gel process. Basically the sol-gel process means the synthesis of an inorganic network by a chemical reaction in a solution at low temperature.

In this process the starting material is a solution of the relevant materials known as the "sol". A chemical reaction takes place within the solution and a rigid jelly like substance is formed known as a "gel". When the gel is formed it can be subjected to various furnace regimes. It is possible to obtain a glass with similar properties to a conventional fusion glass, without using temperatures above the melting temperature.

There are two standard methods of producing a gel, the first relies on the gelation of colloidal silica, the second is based on the polymerization reaction of alkoxysilane.

2.5.1 GELATION OF COLLOIDAL SILICA.

The term colloidal silica refers to stable dispersions or sols of discrete particles of amorphous silica. This definition excludes the solutions of alkoxides as the polymer molecules or particles are so small that they are not stable. In the case of the gelation of colloidal silica the following route is adopted. Metal compounds are dispersed into their elementary units in an aqueous solvent. This stage is called the "sol". The "sol" is then converted into a rigid jelly-like substance known as a "gel" by a destabilization process. A complete explanation of the colloid route can be found in Iler. [25]

2.5.2 POLYMERIZATION OF ALKOXYSILANE.

The second and more commonly used method of producing "gels" is based on the hydrolysis and polycondensation of organometallic compounds (i.e. alkoxides), which are dissolved in alcohols and water.

Any precursor that can form reactive "inorganic" monomers or oligomers can be used for the sol-gel process. In general, alkoxides are normally used as precursors, as they are soluble in most common solvents and they provide "inorganic" monomers. Also by using alkoxides the rates of hydrolysis and condensation can be controlled by chemical means. The most widely used monomeric alkoxide of silicon is tetraethoxyorthosilane $Si(OC_2H_5)_4$ which is usually written as "TEOS".

The gelling process consists of three stages.

(1) The polymerization of monomer to form particles.

(2) Growth of particles and linking of particles together into branched chains.

(3) Networks extending throughout the liquid medium and forming a rigid gel.

The gel can be subjected to heat treatments, and after the removal of volatiles left within the porous structure,

densification will take place and a glass will be formed. The methods of densification can vary and this will be dealt with in a later section.

Equation 2.1 represents the hydrolysis reaction and equations 2.2 and 2.3 show the condensation reactions that take place and lead to the formation of a gel, when the alkoxide route is used.

$$\equiv M\text{–}X + H_2O \longrightarrow \equiv M\text{–}OH + HX \qquad (2.1)$$

$$\equiv M\text{–}OH + X\text{–}M \longrightarrow \equiv M\text{–}O\text{–}M\equiv + HX \qquad (2.2)$$

$$\equiv M\text{–}OH + HO\text{–}M\equiv \longrightarrow \equiv M\text{–}O\text{–}M\equiv + H_2O \qquad (2.3)$$

In the above equations M is metal or Si and X is a reactive ligand like halogen, OR, NR_2, or acylate. The starting solution "sol" becomes increasingly viscous as polymerisation proceeds until a gel is formed. The gel is composed of interconnected oxide phases and pores which contain alcohol, water and unreacted TEOS. The main reason this route is chosen over the route described earlier, is that the chemistry of this process is more easily controlled than the colloid route.

2.6 DENSIFICATION.

The process of densification is essentially a process in which a gel upon heating is transformed into a solid glass. The densification is very much dependent on the ageing and drying conditions under which it was produced [26,27]. It is also found that major differences in the gel structure result depending on whether processing is carried out under acid or base conditions [27]. It is possible to obtain a wide range of gel structures as the pH is varied. The gels differ in their pore size distribution, surface area, skeletal density and particle size, and all these characteristics determine the final structure [28].

A gel can be converted to a glass in one of the following ways.

(1) At temperatures below the glass transition temperature T_g.

As a gel is a highly porous amorphous solid that contains unreacted starting material in the porous network, when the sample is heated the polycondensation reaction speeds up and there is a substantial shrinkage.

(2) At temperatures above T_g but below the melting temperature. This technique is normally performed under pressure by a technique known as "hot pressing" [29].

(3) At temperatures above the melting temperature. When the organics and water have been removed the gel can be used as a starting material for glass production by the standard high temperature fusion process. The advantage gained by using a gel as the starting material is mainly the excellent purity that can be obtained.

2.7 ADVANTAGES AND DISADVANTAGES OF USING SOL-GEL PROCESS FOR PRODUCTION OF GLASSES.

2.7.1 ADVANTAGES.

(1). Monolithic pieces of glass can be formed without melting, avoiding many of the problems associated with working at high temperature.

(2) The process can be used to make ultra-pure glasses, as many alkoxides can be purified by distillation.

(3) The macroscopic homogeneity and the submicroscopic homogeneity of glass made by the sol gel process is much better than glasses made by conventional processes.

(4) The process is extremely well suited to coating a substrate with a glass coating. Optical fibers can be coated by dipping the fiber into the sol. An important point for this application [33] is that despite large shrinkages during drying, if the surface preparations are

good, the gel will shrink in the thickness direction rather than laterally.

(5) If the gel is used to produce a glass by going above the melting temperature, then homogeneous glass can be obtained at lower melting temperatures and shorter melting times. [30,31,32,33]

2.7.2. DISADVANTAGES.

(1) There is a very large shrinkage of the material associated with the gelation process and the drying of the gel.

(2) The precursors can be expensive.

(3) There is a tendency during drying for many of the gels to bloat and fracture, making it difficult to produce monolithic pieces.

(4) There is a lack of knowledge about many of the complexities associated with the process.

2.8 IONS IN GLASSES.

When optically active ions enter an ideal crystalline environment they are in identical sites. The luminescence from a crystal containing these dopant ions will have the resolution of an individual ion (i.e there will be no broadening). In reality, most crystals have strains and defects that can result in small variations in energy levels of some of the ions. This results in an inhomogeneous broadening of the luminescence from the crystal sample. The broadening associated with good quality crystals is very small and the resultant spectra consist of sharp lines. The case of optically active ions in glasses is quite different as each ion can be in an environment that is significantly different form another ion.

SiO_2 glass is built up from oxygen tetrahedra around Si^{4+} ions, with the tetrahedra being linked together to form a random network possessing interstices of various shapes and sizes as shown in Fig 2.3. Due to the lack of

any long range periodicity in the structure, any luminescent ions that are introduced into this network will be in a range of different local environments. This in turn means that the local fields that each of the ions see can be quite different. This results in different energy levels and different radiative and non-radiative transition probabilities for ions in different sites.

If these "doped" glasses are excited with a broadband light source, such as a xenon arc lamp, the absorption and emission spectra and excited state decays consist of a superposition of contributions from individual ions among the complete collection of local sites. Fig 2.5 shows how an inhomogeneous profile is made up from the homogeneous contributions of ions in different sites.

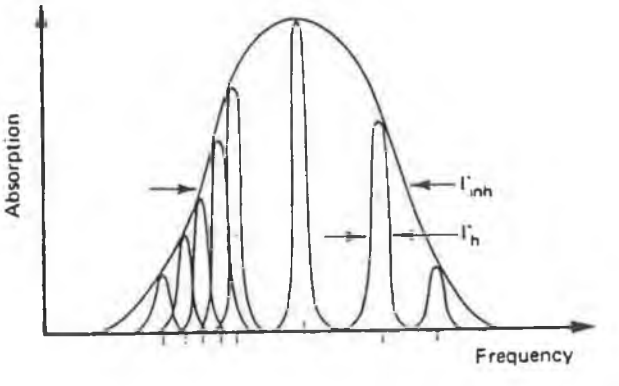

Fig 2.5 Inhomogeneous broadened profile showing homogeneous components.

The incorporation of optically active ions in the trivalent state would require the simultaneous creation of three extra negative charges in most cases. Three non bridging oxygens would be expected to neutralise each optically active ion. In single component glasses, all the O^{2-} ions are bridging oxygens, whereas in two component glasses involving alkalis or alkaline earth oxides there

are also non bridging oxygens. Equation 2.4 illustrates the breaking of oxygen bonds by Na^+ ions,

$$\equiv Si-O-Si\equiv + Na_2O \longrightarrow \equiv Si-O-Na + Na-O-Si\equiv \qquad (2.4)$$

The incorporation of Na_2O into the glass structure produces non bridging oxygens and makes the introduction of optically active ions into the glass structure easier. Ions such as Na^+ and Ca^{2+} that modify the glass network are called network modifiers. A table of the groups of network forming and modifying ions etc, is given in table 2.1.

2.9 DOPED SOL-GEL GLASSES.

Despite the large number of publications appearing in journals regarding the sol-gel process for producing glasses, surprisingly few involve the use of dopant optically active ions introduced into the glass matrix.

It has been pointed out by Pope and Mackenzie [34] that silica glass containg neodymium is potentially a very important laser material as it has a low thermal expansion coefficient and high temperature stability. The problem involved with producing silica glass from the melt is that the maximum neodymium solubility in silica is approximately 0.5 weight percent, and this is lower than required for a laser glass. It has been reported [34] that dense silica glass monoliths containing as much as 5 weight percent neodymium have been prepared using the sol-gel process. There are still problems involved with this route as clumping of the Nd_2O_3 has been found to occur [35], also, non-radiative decay through residual OH^- ions reduces the fluorescence effeciency. The use of a network modifier such as Al has been shown to prevent clumping from occuring, and with the improvement of drying techniques it should be possible to remove the OH^- from the glass and yield a Nd

doped silica glass suitable for laser action.

As well as the obvious uses for doped sol-gel glasses as laser materials, dopant ions can be used as structural probes of the sol-gel to glass route and can provide us with information about the process. Trivalent europium is an ideal ion for use as a probe of symmetry and chemical bonding in glass [36,37]. Trivalent europium is chosen because of its intense (Laporte forbidden) f-f transitions, also, the small homogeneous linewidths of the $^5D_0 \longrightarrow {}^7F_J$ transitions and the relatively simple Stark structure of the ^7F_J and ^5D_J states for J = 0,1,2. The use of trivalent europium as a probe of the sol-gel glass environment will form the basis of much of the work contained in this thesis.

CHAPTER 3.

3. EXPERIMENTAL DETAILS.

3.1 INTRODUCTION.

In this chapter a review of each of the production techniques used for the production of glasses will be given. A description of the experimental arrangements used for the various optical spectroscopic experiments will also be given.

3.2 PRODUCTION OF "HIGH TEMPERATURE" GLASSES.

The following apparatus was used during the making of high temperature glasses, a "Pyreco" chamber box furnace, platinum crucible, platinum tipped tongs, platinum/gold casting dish and a "Glen Creston" shaker. Platinum implements were used due to its high melting point (1769°C) and its high resistance to chemical attack.

3.2.1 BORATE GLASSES.

Table 3.1 shows the standard composition of the glasses that were developed at D.C.U. [38] to produce good quality stable borate glasses.

BATCH COMPOSITION	PERCENTAGE (by mass)
Spectroflux	73 - 83 approx.
Silica (SiO_2)	8.3
Alumina (Al_2O_3)	8.3
Lanthanide or Transition metal.	0.1 - 10

Table 3.1 shows the composition of borate glasses.

The glass former "Spectroflux" which is manufactured by Johnson Matthey was used. This consists of a eutectic mixture of 80% lithium metaborate and 20% dilithium tetraborate which have a low melting point (840°C) and a

low viscosity.

The starting materials were placed in a plastic container with three glass beads, to assist mixing, and sealed. The container was then agitated on a "Glen Creston" shaker for ten minutes. The homogenised powder was then transferred to the platinum crucible and placed in the pre-heated furnace (1200°C). After ten minutes the crucible was removed and swirled to assist in homogenisation of the molten glass. Using the platinum tipped tongs the crucible was removed from the furnace and poured into the platinum/gold casting dish, which was pre-heated in the furnace. When the casting dish cooled to below red hot it was placed over a jet of air from a small compressor. The cooling stopped the glass from sticking to the casting dish and allowed it to be removed more easily.

The glass samples were treated to a simple annealing process to relieve stresses in the glass. The glasses were placed in a furnace preheated to 700°C and allowed to cool to room temperature over a 24 hour period.

3.2.2 SILICATE GLASSES.

The preparation of silicate glasses requires higher temperatures and a different melting procedure than borate glasses.

BATCH COMPOSITION	PERCENTAGE (by mass)
Silica. (SiO_2)	74
Sodium Oxide. (Na_2O)	13
Calcium Oxide. (CaO)	11
Lanthanide or Transition metal.	2

Table 3.2 shows the composition of the silicate glasses.

All the starting materials were of analytical grade (100μm powder). The starting materials were mixed as

before. The homogenised powders were transferred to a platinum crucible in a preheated furnace (1400°C). After 3-4 hours the molten mixture was swirled in the container. The mixture was left for a further 22 hours in the furnace.

The casting process is much more difficult for the silicates due to the high viscosity of the melt. The process of pouring the melt into the casting dish was done in the furnace to help overcome this problem. The silicate glass was treated in a similar manner to the borate.

3.3 PREPARATION OF SOL - GEL GLASSES.

Europium - doped silicate glasses made by the sol-gel route were prepared as follows [39]. The starting mixture which consists of Tetraethoxyorthosilane (TEOS), water at a preselected pH, ethanol and europium nitrate pentahydrate in the molar ratio 1 : 4.4 : 1 : 0.003 was stirred magnetically. The solution was then cured in a furnace at 72°C - 74°C which yielded a rigid Gel. The cured gels were then calcined at various temperatures up to 800°C.

A series of samples was prepared by the same technique using deuterium oxide instead of water, in this instance the samples were carefully sealed after the appropriate heat treatment. The europium concentration in all samples was 2% of the silicon concentration.

3.4 STEADY STATE FLUORESCENCE MEASUREMENTS.

For recording steady state fluorescence spectra, the experimental arrangement shown in Fig 3.1 was used. The samples which were placed in an Oxford instruments variable temperature liquid nitrogen cryostat or sample holder for room temperature measurements were optically excited by (a) A Photophysics 250 W Xenon arc lamp which was focused into a 1/4 meter Spex minimate monochromator or (b) A Coherent model 52 argon ion laser which pumped a coherent CR-599 Dye

laser (Rhodamine 6G dye). The emission from the sample was dispersed through a Jobin Yvon 1 meter focal length monochromator with a 1200 grooves\mm diffraction grating. Light emerging from the exit slit was detected using a Hamamatsu (R928) photomultiplier tube with a Hamamatsu (E717) base. The output was fed to a current measuring device which gave a voltage output. The resultant signal was plotted on paper using a x-y recorder or fed to a B.B.C. micro computer and stored on disc.

3.5 PHASE SENSITIVE DETECTION.

As luminescence from inequivalent centres will have different decay rates, it is possible using the phase sensitive technique to "null" unwanted signals. [40]

The exciting light is square wave modulated at some frequency ω_m and we look for a component of this frequency in the luminescence signal V_{sig} . A reference voltage V_{ref} modulating at frequency ω_m is obtained from the chopper. The chopper is in turn switching the signal V_{sig} on and off every half cycle . When the signals V_{sig} and V_{ref} are of the same frequency and phase, the phase sensitive detector acts as a rectifier and gives a d.c. voltage V_{det} proportional to the amplitude of the signal V_{sig} . To obtain the best output voltage V_{det}, the reference voltage V_{ref} is adjusted to be in phase with V_{sig} .

If the signal (as is the case with Cr^{3+} in glass) consists of two components each with a different lifetime then the modulated components of these two signals will be out of phase with each other. When the signal of one of these components and the reference are out of phase by 90^0 the component is said to be "nulled" as the average output is zero. If the phase of the reference is adjusted to "null" one of the components , the other will still give an output signal.

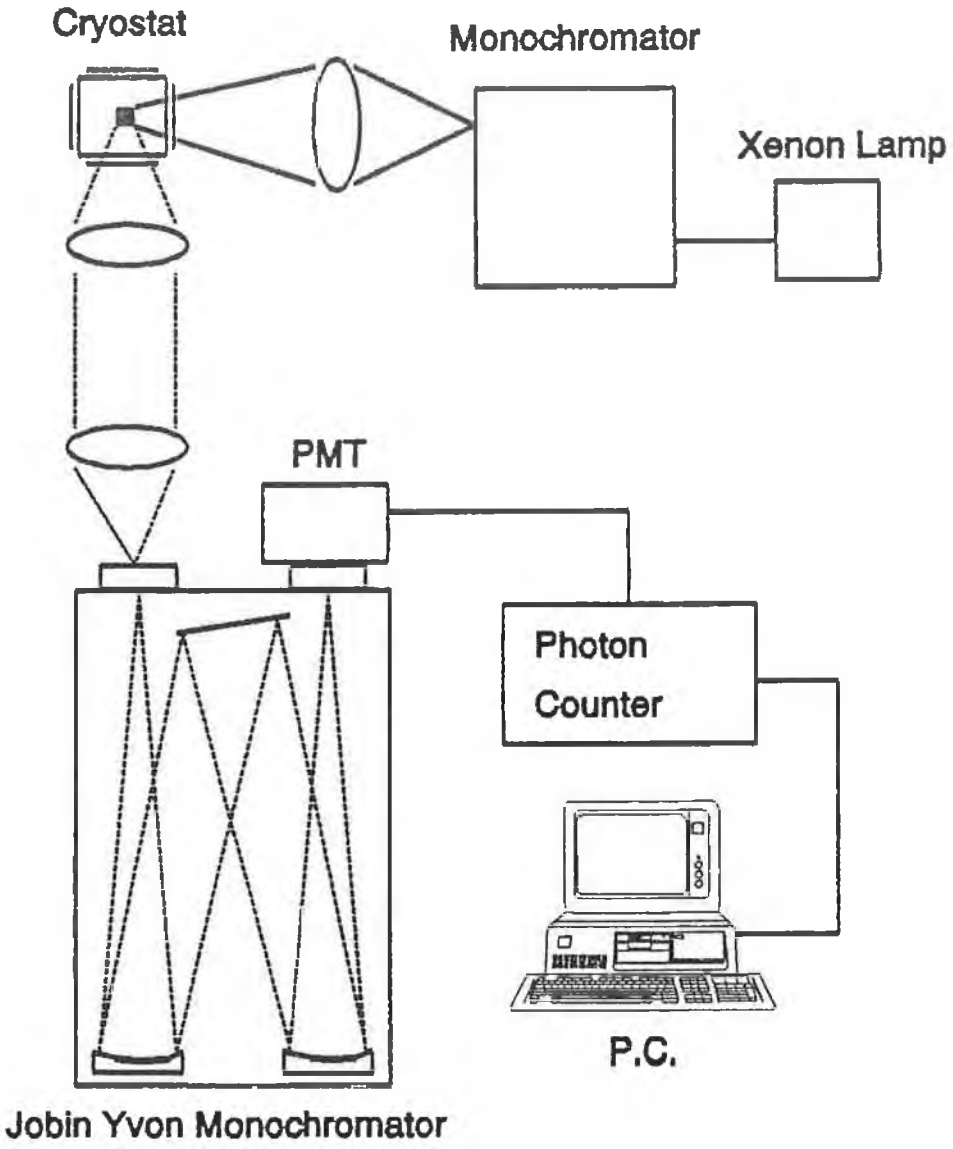

Fig 3.1 Steady state luminescence apparatus.

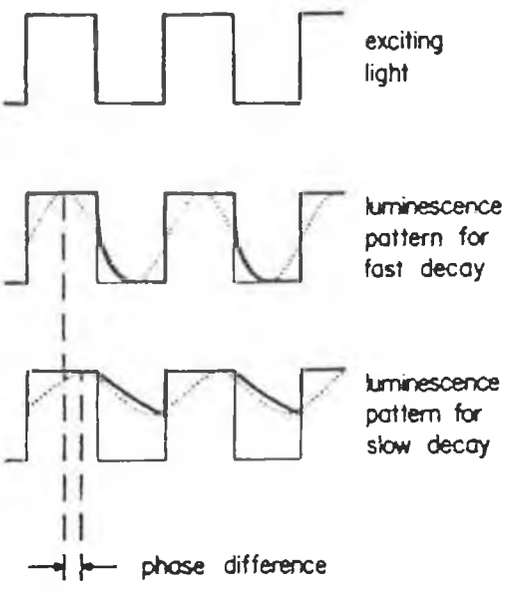

Fig 3.2 Phase sensitive detection.

As the luminescent decay rates from the $^2E \rightarrow {}^4A$ and $^4T_2 \rightarrow {}^4A$ levels in a Cr^{3+}doped glass are quite different it is possible to "null" the broadband $^4T_2 \rightarrow {}^4A$ transition and just look at the ^2E or vice versa.

3.6 FLUORESCENCE LIFETIME MEASUREMENTS.

The experimental arrangement used for measuring fluorescence lifetimes is shown in Fig 3.3. Excitation of the sample was achieved using a [model] Nd :YAG pulsed laser which when used in conjunction with a dye laser and a frequency doubling crystal [KDP], yields a pulse of wavelength 318 nm. The output signal from the photomultiplier tube was measured using a Stanford Research Systems model SR400 gated photon counter. To improve the

signal to noise ratio, the luminescence output of the sample was measured using both channels A and B of the photon counter. Channel B was used as a monitor of the pulse to pulse repeatability of the laser system and was used to take account of any fluctuations in output power. This was achieved by maintaining a set delay on channel B and using the photon count for each point as a measure of output intensity fluctuation. Channel A of the photon counter was used in the normal lifetime measuring mode with the gate being scanned across the time base range. When the scan was complete the signal recorded on channel B was normalised to the maximum signal and each point on channel A was divided by the corresponding value from channel B. This procedure yielded decay plots with a marked improvement in signal to noise as the fluctuation in pulse to pulse power was a major source of noise.

The lifetime of a single component exponential decay can be described as follows,

$$I(t) = K \exp(-t/\tau) \qquad (4.3)$$

$$\tau = 1/k \qquad (4.4)$$

where K is the pre-exponential factor contributing to the signal at zero time, and k is the decay rate constant. In this case a semi-logarithmic plot of ln(I(t)) versus t yields a straight line of slope -k and the lifetime τ is defined as 1/k [41]. A computer program to calculate the lifetime τ of a decay is given in appendix A(3). The program uses a weighted least square fit of the semi-logarithmic plot to yield the lifetime τ [42]. Another computer program is also given to allow the lifetimes of a two component decay to be evaluated. If the experimental decay curve is the sum of a number of emitting components, it can be described as follows,

$$I(t) = \sum_{i=1}^{N} K_i \exp(-t/\tau_i) \qquad (4.5)$$

$$\tau_i = 1/k_i \qquad (4.6)$$

If the experimental decay is the sum of two components, that are quite different, the long lived component will not be effected by the short lived component. Initially a ln(I(t)) versus t plot is made. At long enough times the curve would be linear with a slope of $-1/\tau_1$ and an intercept of ln K_1. Using the K_1 and τ_1, the contribution from the long lived component is subtracted from I(t) to yield,

$$I^{\circ}(t) = I(t) - K_1 \exp(-t/\tau_1) \qquad (4.7)$$

It should be noted that $I^{\circ}(t)$ is not the difference between the calculated and observed semi-logarithmic plots but the difference between the observed decay and the calculated exponential decay of the long lived component.

As has been described earlier, when luminescent ions in a glass substrate are excited by a broadband light source, such as a xenon arc lamp, the emission from these samples is a superposition of contributions from ions in slightly different sites. As each of these ions will have a different lifetime, the experimental decay curve from such a sample can be highly non-exponential. In this case, semi logarithmic plots of I(t) versus t are concave upwards unless the τ_i are nearly equal. When dealing with glasses it is often the case that the decay curves are non-exponential, this makes it difficult using the above techniques to assign a consistent lifetime to a particular sample. In order to be able to make a comparison of the lifetimes of different samples, the average lifetime $\overline{\tau}$ is defined as,

$$\overline{\tau} = \int_0^\infty t\, I(t)\, dt \Big/ \int_0^\infty I(t)\, dt \qquad (4.8)$$

where I(t) is the experimental decay curve. Another method that is often used when dealing with non-exponential decay curves is to quote the e-folding times of the decay curve. This is simply giving the time it takes for the intensity to fall to $1/e$, $1/e^2$ and $1/e^3$ of its initial value.

3.7 EXCITATION MEASUREMENTS.

Excitation spectra were recorded by measuring the luminescence output of the sample at a specific wavelength while scanning the excitation wavelength. If the luminescence output is large for a certain excitation wavelength, the sample absorbs strongly at this wavelength. One advantage of this technique over the straight forward absorption method is that the sample may contain impurities or defects that do not contribute to the luminescence output but may have an absorption band. The excitation spectra only shows absorption bands that yield a luminescence output. The experimental arrangement for taking excitation spectra is the same as that used for the steady state luminescence measurements except that the input monochrometer is scanned while the 1M focal length monochrometer is set at a wavelength of interest. A broad band tungsten lamp was used as the light source.

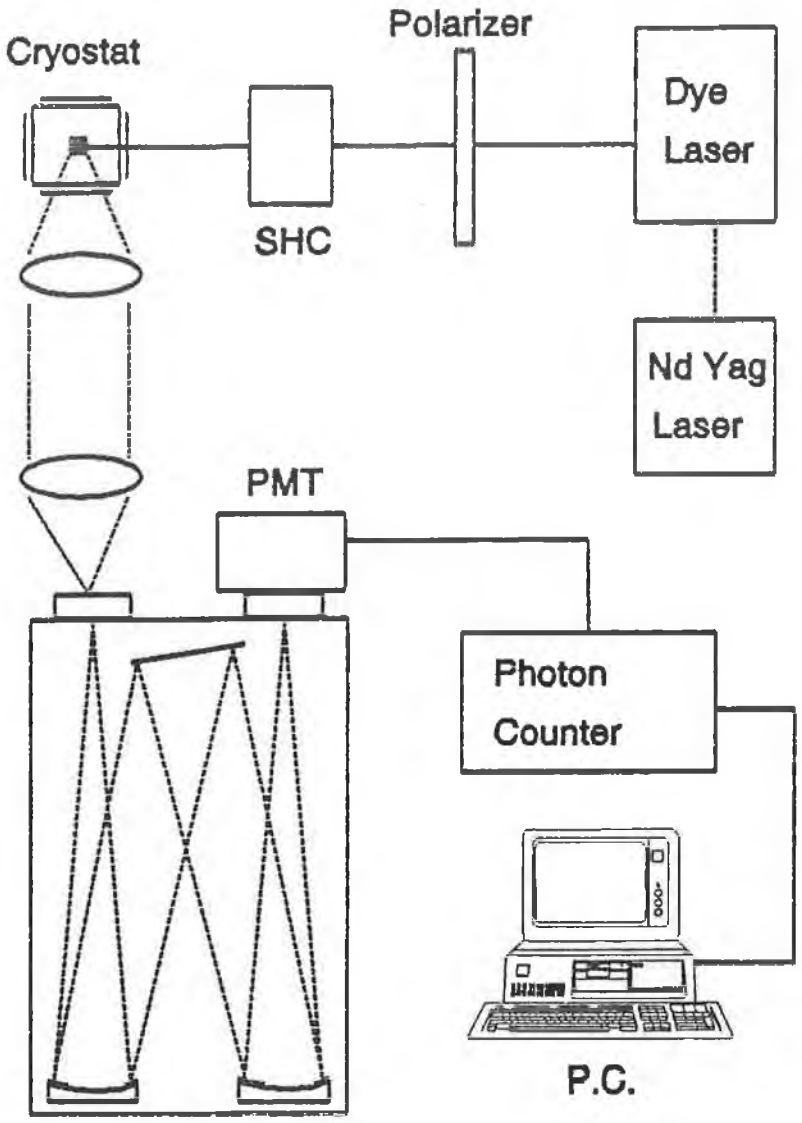

Fig 3.3 Diagram of the apparatus used for measuring lifetimes.

3.8 ABSORPTION MEASUREMENTS.

The absorption spectrum of the glasses was taken using a commercial Shimadzu UV-240 recording spectrophotometer. The glass samples were placed in the sample cavity in a masking frame made for the purpose.

3.9 FLUORESCENCE LINE NARROWING.

Two different experimental arrangements were used to look at the fluorescence line narrowed spectra of the europium doped glasses.

In the first case the excitation source was a PRA model [LN 1000] nitrogen laser, which was used as a pump for a tunable dye laser, PRA model [LN 107]. The dye used was Rhodamine 590 whose emission spectral range matches closely the $^7F_0 \rightarrow ^5D_0$ absorption band of Eu^{3+}. The glass samples were placed in a Oxford instruments liquid nitrogen cryostat and cooled to 77K.

Emission from the samples was analyzed using a 1 meter focal length Jobin Jvon monochromator with a Hamamatsu 928 photomultiplier tube. A Stanford Research SR400 photon counter which was interfaced to a BBC master computer was used to record the data, Fig 3.4.

For the second arrangement a CW Coherent model 52 argon ion laser was used to pump a Coherent model 599 tunable dye laser, again, rhodamine 590 dye was used. In this case the arrangement shown in Fig 3.5 was used. A chopper [43] system that stops any unwanted scattered laser light from entering the monochromator was used.

3.10 DATA AQUISITION AND HANDLING.

A BBC master series computer was used for the data aquisition and subsequent analysis of data. The signal from the photomultiplier tube was measured using a simple current measuring device which gave a voltage output, this

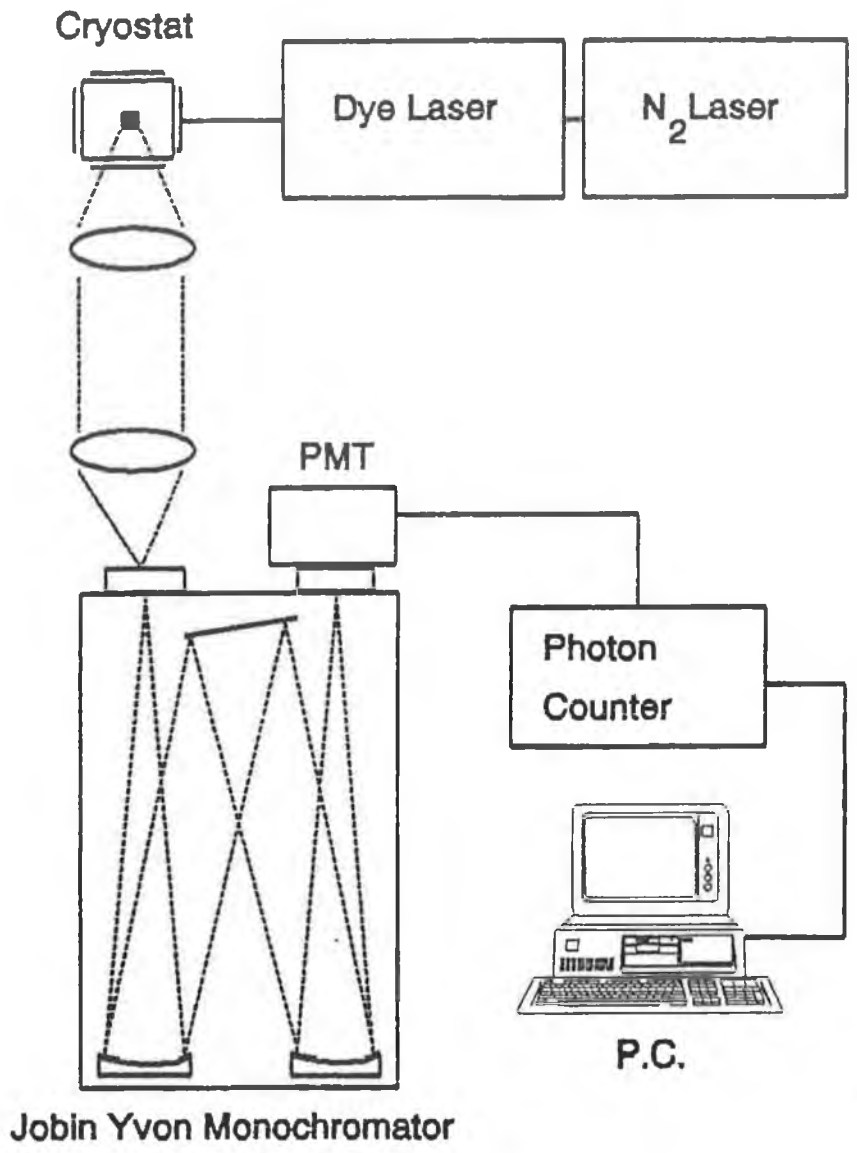

Fig 3.4 Diagram of the experimental arrangement used for FLN experiments with pulsed nitrogen laser.

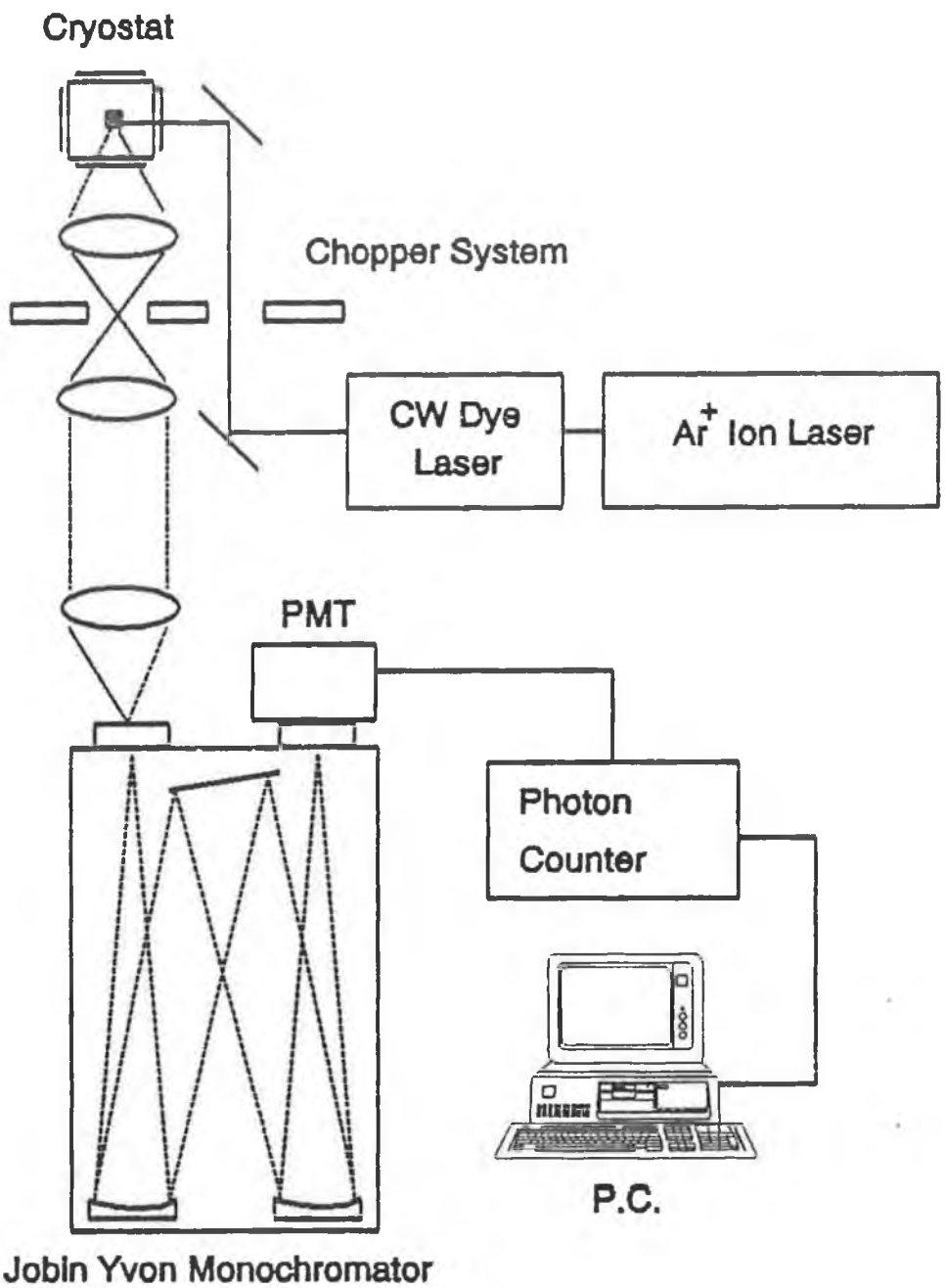

Fig 3.5 Diagram of experimental arrangement used for FLN experiments using a CW dye laser and chopper system.

was fed to a analogue to digital converter. The program used to read the A to D and to move the relevant wavelength scan of the monochromator is given in appendix A(2).

When the photon counter was being used, the BBC was interfaced to the instrument using an IEEE interface adaptor. The program, that reads the photon count and relevant settings of the photon counter is shown in appendix A(1).

3.11 NMR MEASUREMENTS.

All the Magic Angle Spinning ^{29}Si NMR data was taken on a Bruker MSL 300 spectrometer at Dublin University. Further details on this technique are given in appendix B.

CHAPTER 4.

4. TRIVALENT EUROPIUM AS A PROBE OF GLASS ENVIRONMENT.

4.1 INTRODUCTION.

This chapter describes the use of the optically active Eu^{3+} as a probe of the sol-gel process. The Eu^{3+} ion was chosen as it has intense f-f transitions in the visible part of the spectrum which are sensitive to the surrounding ligands, and it is also relatively easy to incorporate it into the sol gel materials. Eu^{3+} has been widely used as a structural probe of both crystalline and glassy materials [44] but very little has been published in the area of sol-gel derived materials [45]. A set of glasses produced by hydrolysis with (1) water and (2) deuterium oxide were investigated using the techniques of fluorescence measurement , fluorescence lifetime measurement and high field NMR. A borate and silicate glass made by the high temperature fusion technique were also investigated for comparison.

4.2 HIGH TEMPERATURE GLASSES.

The fluorescent spectra, excitation spectra and fluorescent lifetimes of a borate and silicate glass doped with trivalent europium were investigated to enable a comparison with glasses made by the sol-gel process. The glasses were made by the high temperature technique described in chapter 3.

The europium atom has a configuration of [Xe] $4f^7$ $6s^2$ and has a ground state $^8S_{7/2}$. In the case of the triply ionised europium atom Eu^{3+} the configuration is as follows, [Xe] $4f^6$ with a ground state $^7F_0$. An energy level diagram for Eu^{3+} can be seen in figure 4.1. The transitions of interest to this investigation are the $^5D_0 \rightarrow {}^7F_J$, where J = 0,1,2, as they exibit the most intense fluorescence. Figure 4.2 shows the absorption spectrum for a 5% europium (borate glass) made by the high temperature technique. The weak

absorptions at approximately 464nm and 525nm are transitions from the $^5D_2$ and $^5D_1$ states respectively [46]. Exact assignments of the line absorptions below 400nm have not been made, but the sharpness and weak intensities indicate that they are 4f-4f transitions. The large absorption from 330nm to shorter wavelengths is due to the absorption of UV by the host glass.

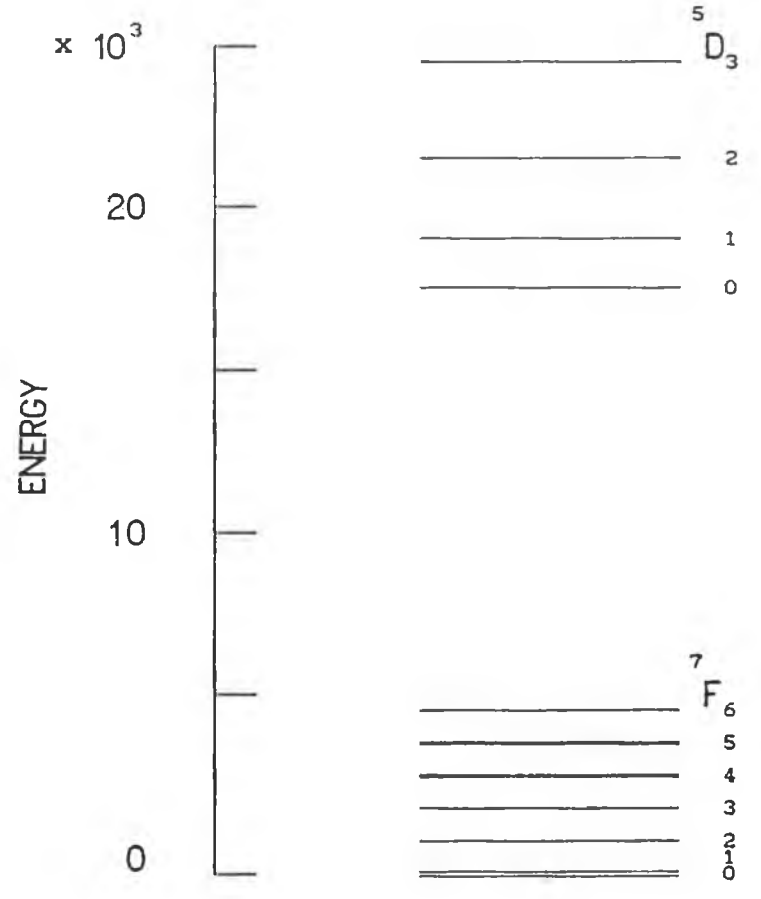

Figure 4.1 Energy level diagram of Eu^{3+} ion.

Examples of the fluorescence spectra from Eu^{3+} doped glasses made by the high temperature method are given in figure 4.4. Fluorescence can occur from any of the levels of the ^5D multiplet to any of the ^7F multiplet. In the two examples given the transitions all originate from the $^5D_0$

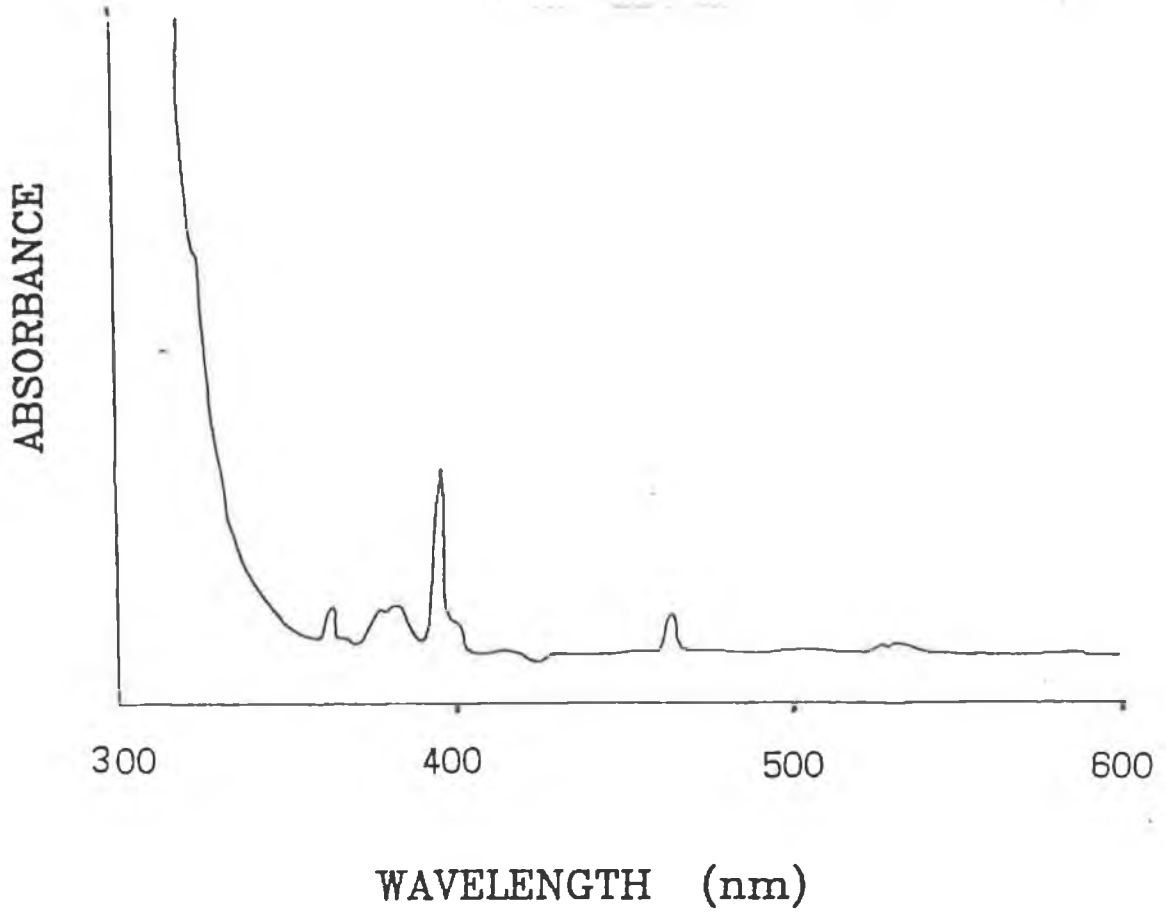

Fig 4.2 Room temperature absorption of borate glass.

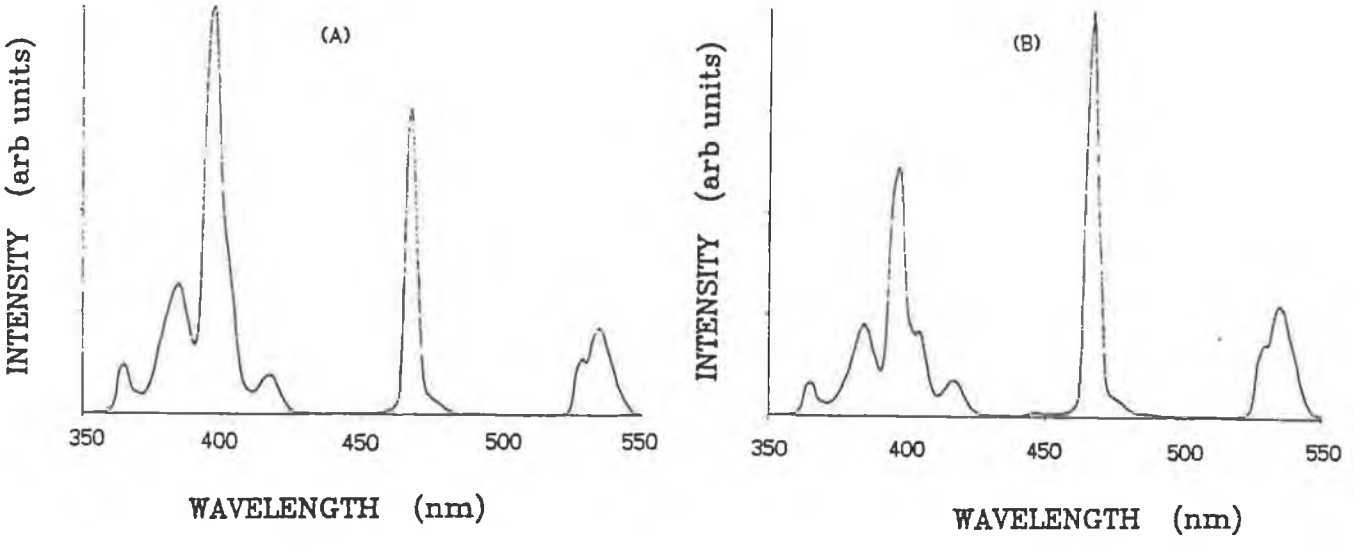

Fig 4.3 Excitation spectra of (a) borate glass and (b) silicate glass. Taken at 611nm. T = 300K.

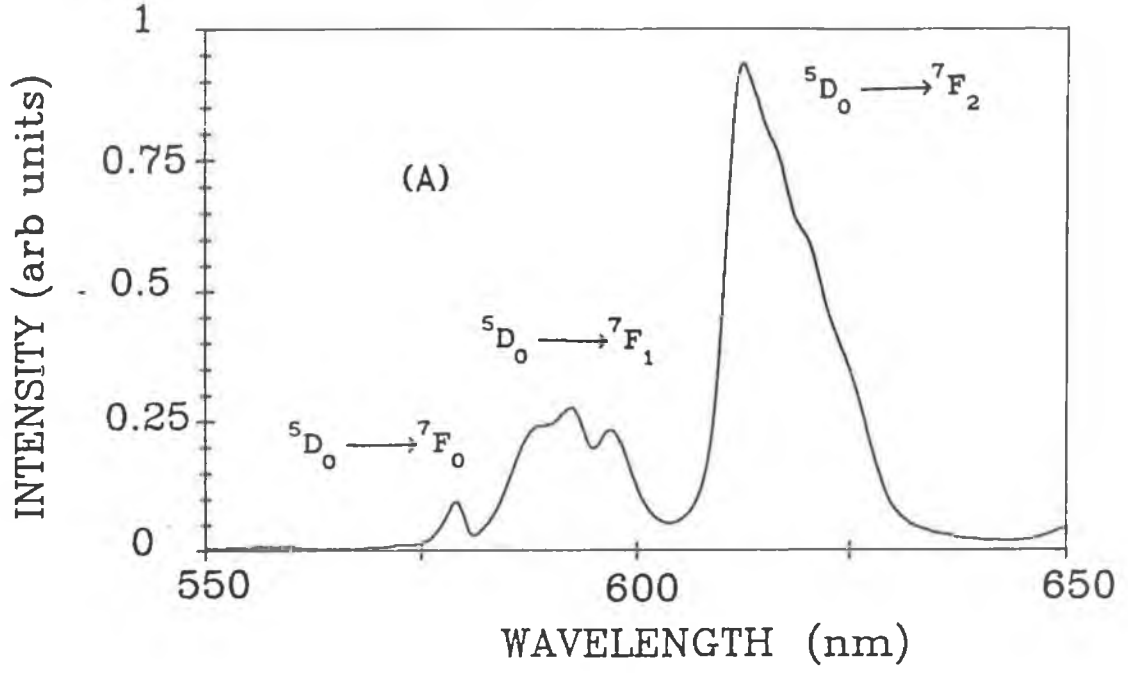

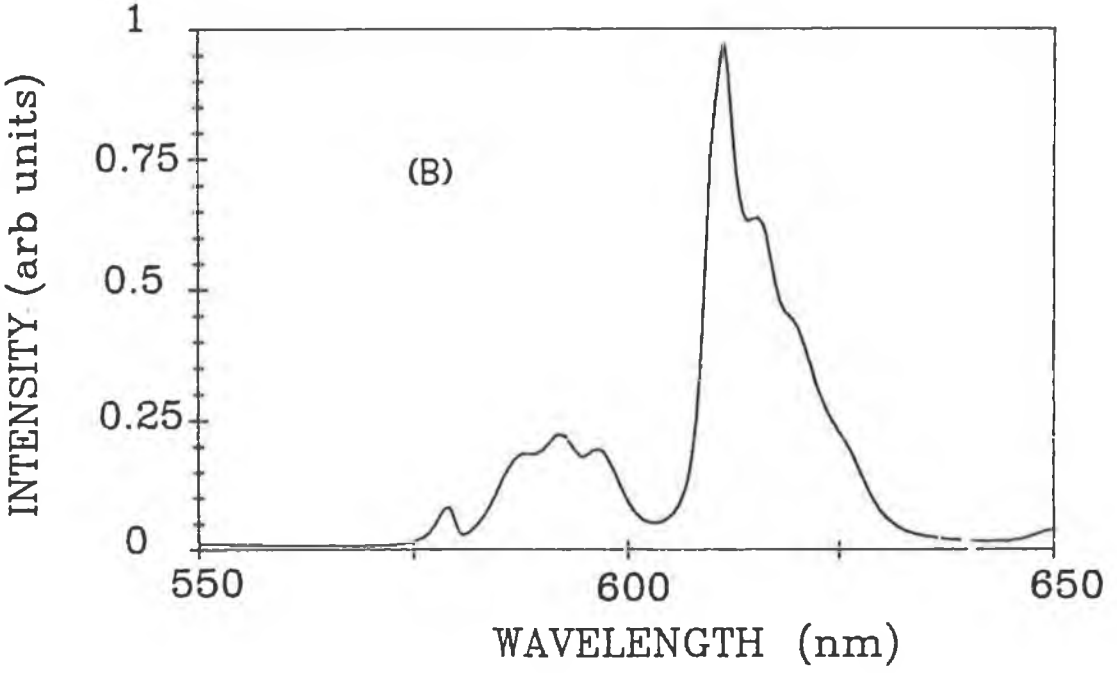

Fig 4.4 Fluorescence spectra of (a) borate glass and (b) silicate glass.

broadening the levels are not always observable, but the splitting is found to be $^5D_0 \longrightarrow {}^7F_0$ = 1, $^5D_0 \longrightarrow {}^7F_1$ = 3, and $^5D_0 \longrightarrow {}^7F_2$ = 5. Figure 4.3 shows the excitation scans of the two glasses and these were used to determine the excitation wavelength that would yield the most intense fluorescence.

The fluorescence lifetimes of the two samples taken at room temperature were also measured and found to be 3 ms for the 2% Europium silicate glass and 2.2 ms for the 5% Europium borate glass.

4.3 PRODUCTION AND HEAT TREATMENTS OF SOL-GEL SAMPLES.

In order to distinguish between the samples that were hydrolysed with water and those hydrolysed with deuterium oxide the notation H_2O and D_2O will be used as appropriate. Both sets of samples went through the same temperature regime. The make-up of the starting materials is the only difference between the two sets of samples. The starting materials for the two series were as follows.

H_2O series.

TEOS hydrolysed with water at a pH of 0.93, Ethanol and 2% Eu on Si.

D_2O series.

The initial solution included TEOS which was hydrolysed by D_2O and was acidified by concentrated Hydrochloric acid, Ethanol and 2% Eu on Si. The final pH was 0.89.

The heat treatments for both sets of samples were as follows, with the (a),(b),(c) and (d) referring to the spectra in Fig 4.5 and 4.6.

(a) This is the solution before any heat treatments.

(b) The solution was cured for 149.5 hours at 73°C then cooled and the container sealed.

(c) The samples in this case were cured for 149.5 hours

at 73°C. At this point any residual free liquid was shaken out of the vials. The samples were then dried at 73°C for 286 hours, heated for 24 hours at 200°C and then cooled and placed in sealed containers.

(d) The samples were put through the same routine as (c) and then furnaced for a further 24 hours at 800°C and finally placed in sealed containers.

4.4 SYMMETRY OF THE EUROPIUM IONS ENVIRONMENT.

The transitions that are considered to give an indication of the symmetry of the europium site are the $^5D_0 \longrightarrow ^7F_2$ and the $^5D_0 \longrightarrow ^7F_1$. The transition $^5D_0 \longrightarrow ^7F_2$ is an electric dipole transition and for an electric dipole transition to occur there must be a change in parity. As the transition is within the 4f shell, it is forbidden by the "Laporte selection rule", so for it to be allowed it needs a mixing of parity to occur. The mixing occurs if the europium ion experiences a field that lacks inversion symmetry, which is the case in glasses. The intensity of this induced electric dipole transition will depend strongly on the degree of assymmetry of the europium ions surroundings.

The case of the $^5D_0 \longrightarrow ^7F_1$ is different as it is an allowed magnetic dipole transition. For a magnetic dipole transition to occur the initial and final states must have the same parity. As the transition is within the 4f shell it is allowed and the symmetry of the europium ions surroundings will have no bearing on the intensity of the transition.

It is for this reason that the ratio of the emission intensities of the $^5D_0 \longrightarrow ^7F_2$ and the $^5D_0 \longrightarrow ^7F_1$ transitions has been used as a measure of the degree of assymmetry of the europium ions surroundings. [36,46,48,49,]

$$R = \frac{^5D_0 \longrightarrow {}^7F_2}{^5D_0 \longrightarrow {}^7F_1} \qquad (4.2)$$

The intensity ratio R is used rather than the peak heights as this removes experimental errors, as the transitions can be quite broad. The larger the value of R, the less symmetry in the surroundings of the europium ion. The value of R has been monitored as the solution gels and then densifies upon further heat treatments. A table of how the ratio changes for the samples both hydrolysed by water and deuterium oxide is shown in table 4.2, again the (a),(b),(c) and (d) refer to the spectra in Fig 4.5.

	H_2O hydrolysed samples.	D_2O hydrolysed samples.
(a)	1.58	1.77
(b)	0.95	1.76
(c)	3.62	3.65
(d)	4.33	4.0

Table 4.2 A table of the ratio R for the samples hydrolysed with H_2O and D_2O.

The most interesting feature of the table of R values for the H_2O hydrolysed material is the reduction in R at the (b) stage, this would imply an increase in the symmetry of the Eu^{3+}ions environment from the (a) stage. The ratio R between the (a) and (b) stages of the D_2O hydrolysis remains constant. This will be discussed in more detail later. For comparison purposes the ratio R for the silicate glass sample made by the high temperature fusion method is 3.25, and this indicates that the Eu^{3+} ions experience a

more symmetrical environment in the high temperature glass than in either the H_2O or D_2O samples.

4.5 LIFETIMES.

A table of the lifetimes for the two sets of samples is given in Table 4.3, the decay curves for both the (a) and (b) curves were found to be exponential. In both cases the (c) and (d) curves were found to be slightly non-exponential.

	τ_{H_2O} (ms)	τ_{D_2O} (ms)	Errors. + or - (ms)
(a)	0.134	0.750	0.002
(b)	0.123	0.760	0.002
(c)	0.380	0.362	0.020
(d)	1.250	1.250	0.020

Table 4.3 The lifetimes of the two sets of samples.

An interesting feature of the lifetime data is the significant difference in decay time between the H_2O and D_2O sols. Also worthy of note is the reduction in lifetime between the (a) and (b) stages of the H_2O series. The value of the 800°C treated materials of 1.25ms is still significantly shorter than the high temperature silicate glass discussed earlier, which was found to be 3ms. A detailed discussion of the above points will follow.

4.6 WATER HYDROLYSED SAMPLES.

The spectra in Figure 4.5 shows how the fluorescence from the Eu^{3+} ion in effected as the environment changes

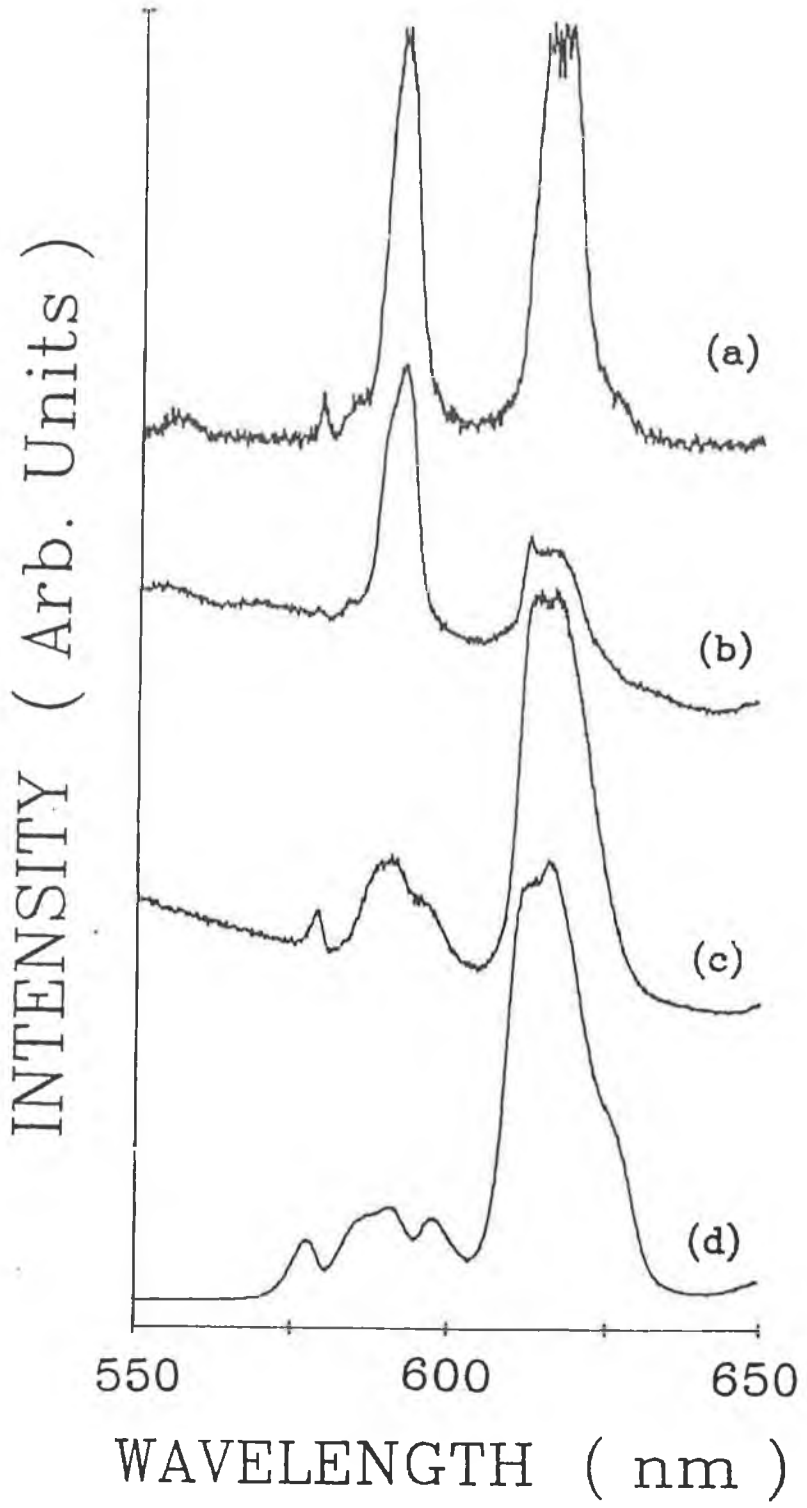

Fig 4.5 Fluorescence from the water hydrolysed samples. (a) solution, (b) gel, (c) 200°C densified and (d) 800°C densified. All spectra taken at room temperature.

from (a) the solution (b) the gel (c) 200°C densified glass and (d) 800°C densified glass. It can be clearly seen that the spectra change to a great extent as the Eu^{3+} ions surroundings change. In the spectrum of the solution or sol, the three transitions $^5D_0 \longrightarrow ^7F_0$, $^5D_0 \longrightarrow ^7F_1$ and $^5D_0 \longrightarrow ^7F_2$ can be seen. The narrow shape and position of these lines suggest that the trivalent europium is surrounded by a symmetric solvation shell as would be expected [50]. As the sample is cured (spectrum (b)) there is a notable change in the relative intensities of the two main transitions and this is verified by the value of R. This change in the intensity ratio suggests an increase in the symmetry of the Eu^{3+}ions surroundings at the gel stage compared to the solution. The increase in the symmetry of the ions surroundings is further suggested by the lifetime of this sample being shorter than that of the solution. This will be discussed in more detail later.

As the gel begins to densify and become more like a glass structure as in spectrum (c), the J-splitting begins to appear, indicating that the degeneracy is being lifted by an asymmetric ligand field. In this case, as the glass-like environment is highly asymmetric, the induced electric dipole transition is considerably more intense than the allowed magnetic dipole transition. The spectrum of the gel densified to 200°C is glass-like, but the degeneracy for both J=1 and J=2 is only partially lifted. In spectrum (d), that of the 800°C partially densified glass, the degeneracy is fully lifted for the $^5D_0 \longrightarrow ^7F_1$ transition and three stark components can be clearly seen. For the $^7F_2$ transition at least three of the five components can be seen. It should be noted that the width of the $^5D_0 \longrightarrow ^7F_0$ line for the sample (c) is narrower than the same transition for (d), this indicates that the Eu^{3+} ions occupy a smaller range of sites in the 200°C sample than in the 800°C sample. As the sample becomes more glass like this line broadens out and is an indication of the multiplicity of europium sites that are present in an amorphous solid matrix. [51]

The fluorescence lifetimes of Eu^{3+} have been found to be very sensitive to structural changes as the material proceeds to a densified glass. A complete table of the lifetimes can be seen in table 4.3. Initially the lifetime in the solution was found to be 0.134(2)ms, where estimated errors in the last figure are given in parentheses. This value compares with a value of 0.1ms for Eu^{3+} in a nitrate solution [52] and 0.12ms in water [53]. The values of the lifetimes for the 200°C sample (c), and the 800°C sample (d), were 0.38(2)ms and 1.25(2)ms respectively. The lifetime of silicate glass made by the conventional fusion method is 2.3ms [54]. This would suggest that the environment of the Eu^{3+} ion is quite different in sample (d) than in the conventional glass.

The width of the $^5D_0 \longrightarrow {}^7F_0$ transition is due mainly to the site to site variations in (a) the electrostatic interaction of the six 4f electrons and this determines the separation of the ^5D and ^7F lines, and (b) the $^7F_0$ position can be changed by crystal-field admixing with other ^7F_J states. In reality it is a combination of (a) and (b) that causes the large inhomogeneous width. (a) and (b) are determined by Racah and crystal field parameters respectively.

A diagram of the widths of the $^5D_0 \longrightarrow {}^7F_0$ transition for the (a) 200°C and (b) 800°C water hydrolysed samples is given in Fig 4.6, the same transition for the high temperature silicate glass (c) is also given. The broadening of the transition from the 200°C to 800°C heat treatments reflects the greater number of sites and more asymmetrical field that the europium ions experience upon densification. This data is in agreement with the intensity ratio R and the lifetime data, which also points towards this. An interesting feature of Fig 4.6 is that the 800°C densified sol-gel glass has a broader $^5D_0 \longrightarrow {}^7F_0$ transition than the high temperature fusion glass. This apparently anomalous feature is due to the unique fields experienced in a unitary glass and will be dealt with in detail in chapter 6. The position of the peak of the $^5D_0 \longrightarrow {}^7F_0$ has

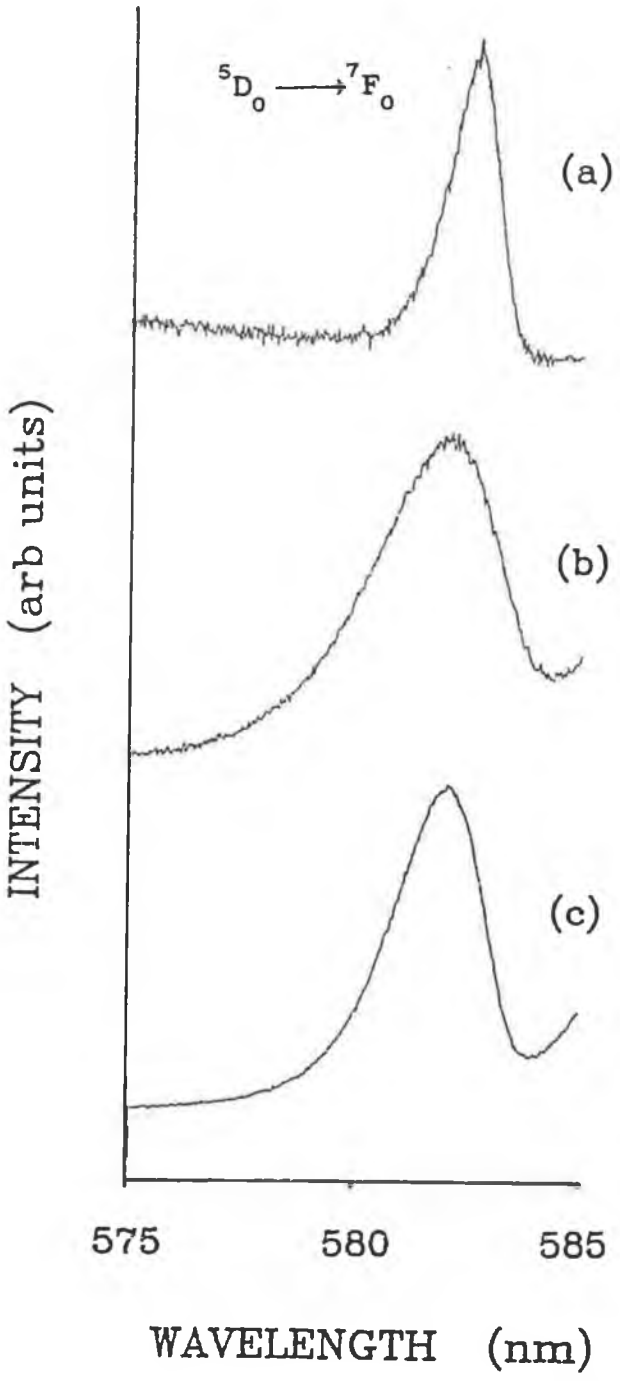

Fig 4.6 Diagram showing the widths of $^5D_0 \longrightarrow {}^7F_0$ for (a) 200°C densified water hydrolysed sol gel material, (b) 800°C densified water hydrolysed sol gel material and (c) the high temperature silicate glass. Taken at room temp.

been used by Gallagher et al [46] as an indication of the interaction of the Eu^{3+} ion with oxygen atoms within the structure. The peak shifts to a shorter wavelength in Fig 4.6 from (a) to (b) and this reflects the coordination of the oxygen atoms to silicon as the densification takes place.

An interesting effect occurs between the samples (a) and (b) in that the lifetime of the gel (0.123(2)ms) is not longer but shorter than the sol (0.134(2)ms), this would suggest an increase in the symmetry of the luminescent ions environment. The shorter lifetime is consistent with the change in intensity ratio R between (a) and (b), which again suggests an increase in symmetry of the europium sites. This change in lifetime can be explained by taking account of the radiative and non-radiative contributions to the total fluorescent decay time τ. From equation 4.3, we have,

$$\frac{1}{\tau} = \frac{1}{\tau_R} + \frac{1}{\tau_{NR}} \qquad (4.3)$$

where τ_R is the radiative decay and τ_{NR} is the non-radiative decay. It has been shown [53] that in solutions the introduction of a single OH group into the environment of europium ions is sufficient to reduce the lifetime to a value of 0.12msec. The OH group has an effective quenching action which increases the non-radiative decay rate shortening the lifetime. This is discussed in more detail in the next section.

4.7 DEUTERATED SAMPLES

Lanthanide ions in solution are surrounded by a coordination shell of solvent molecules in a more or less ordered fashion. This occurs because close to the ion the molecules of solvent are held under compression in a relatively stable configuration [55,56]. It has been found in the investigation of rare earth chelates for use as

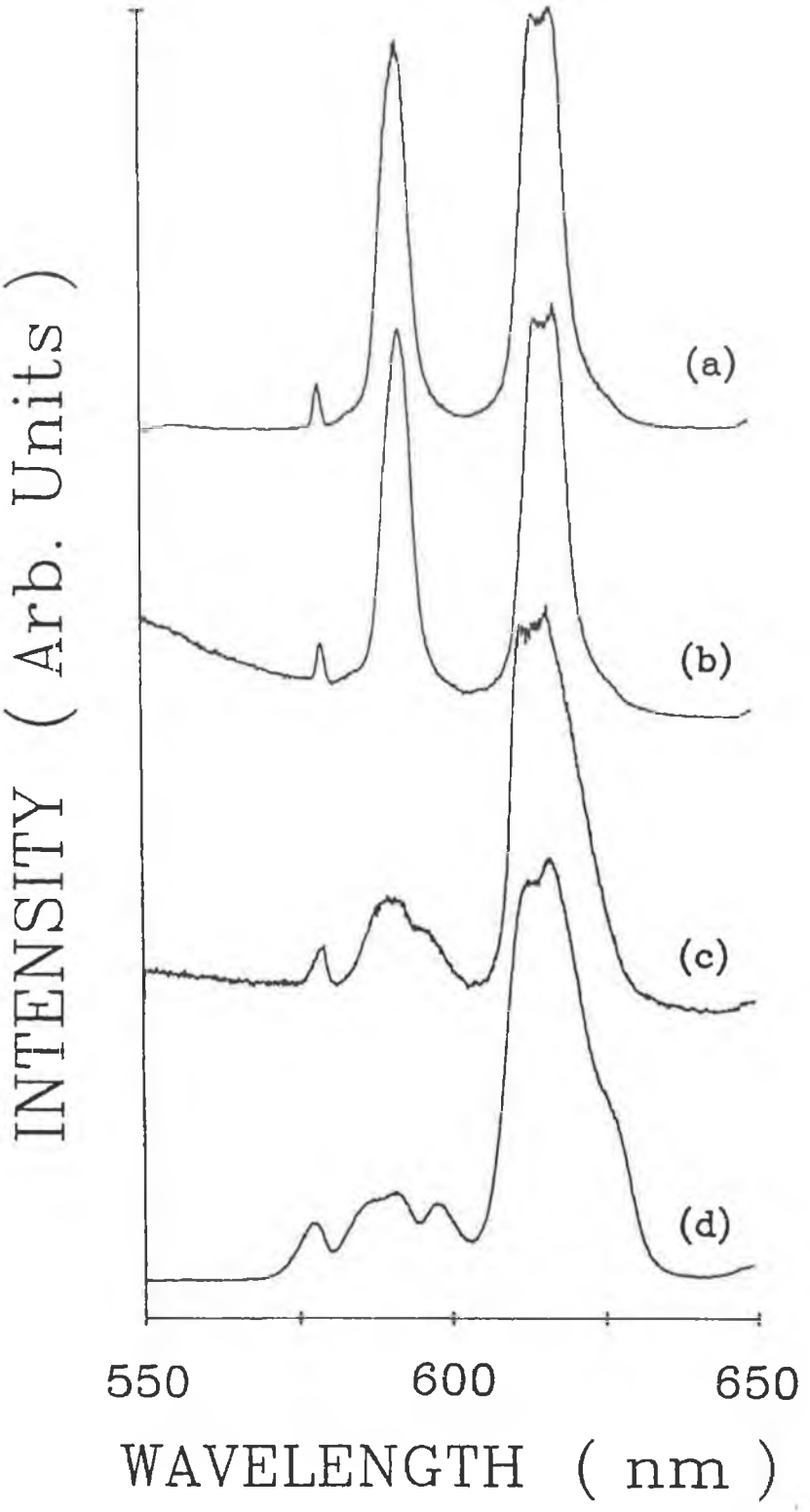

Fig 4.7 Fluorescence from the deuterium oxide hydrolysed samples. (a) solution, (b) gel, (c) 200°C densified and (d) 800°C densified. All spectra taken at room temperature.

liquid lasers that the fluorescence yields and the lifetimes of solutions of europium are greatly enhanced by using deuterated solvents [57,58,59]. The reason that this occurs, is that the dominant mode of radiationless decay of a rare earth ion in solution is by loss of energy to OH stretch vibrations. The deuterium atom is heavier than the hydrogen atom, so the frequency of vibration is smaller in the case of a deuterated solvent. The vibrations are reduced in energy (from 3600 to 2700 cm^{-1} for the O-H stretch) by the substitution of deuterium for hydrogen. Consider the simple harmonic oscillator,

$$\begin{aligned} f &= m\,a \\ &= -k\,x \qquad\qquad k = \text{spring const.} \\ &= -m\,\omega^2\,x \qquad \omega = 2\pi f. \end{aligned}$$

as,

$$k = m\,\omega^2$$

$$\omega = \sqrt{k/m}$$

$$\omega \propto 1/\sqrt{m} \qquad (4.4)$$

It can be seen from equation 4.4 that as the mass is increased by substituting hydrogen for deuterium the frequency of vibration is reduced.

The nonradiative decay is reduced and there is a significant increase in the luminescence output from europium in a deuterium oxide solution compared to a water solution. Also, the difference in decay rates for the H_2O and D_2O solutions can be related to the number of water molecules p associated with the Eu^{3+} ion [60].By monitoring the value of p in the initial stages of the process, reasonable assumptions about the changing environment of the europium ions can be made.

For the samples that were hydrolysed with D_2O there was a notable increase in the intensity of the fluorescence, (approx eight times), and also a marked increase in the lifetime. The fluorescence lifetime for the solution changed from 0.134(2)ms for the H_2O solution to 0.750(5)ms for the D_2O solution as shown in table 4.3. The

value of p was estimated as approximately 6 for the sol and 7 for the gel. Since the coordination number for europium in solution is about 9 [60], it would appear that the ion in the sol is surrounded by 6 water molecules and 3 organic groups, while at the gel stage, the number of water molecules increases to 7. For the H_2O sample the decrease in the lifetime from the sol to gel is consistent with the increase in the number of water molecules. As mentioned earlier, one OH group in the solvation shell of the ion is sufficient to increase the non-radiative rate and hence decrease the decay time. For the D_2O series, no decrease in the decay time or indication from the intensity ratio that the environment is more symmetrical has been observed. This structural change upon deuteration indicates that the hydrolysis and condensation reactions differ in detail for the H_2O and D_2O systems due to a kinetic isotope effect.

4.8 ^{29}SILICON NMR DATA.

Magic Angle Spinning ^{29}Si NMR experiments were conducted on the samples to try and give some further information on the coordination of the europium ion within the structure [39]. ^{29}Si magic angle spinning NMR was measured on a Brüker MSL 300 spectrometer. The data which is given in figure 4.8 shows that the glass treated to 200°C contains silicon coordinated to two, three and four other silicon atoms, via oxygens, while the 800°C glass contains four-fold coordinated silicon only [61]. This data would suggest that the environment of the Eu^{3+} ion at 200°C is still quite different than the further densified 800°C glass, and this is in agreement with the lifetime decay results. It should be noted that although the NMR data indicates that the silicon is fully coordinated at 800°C, the lifetime data suggests that the environment of the dopant Eu^{3+} ions is still not that of a conventional fusion glass. It is possible that the lifetime of the sol gel glasses could be reduced due to residual OH^- still within

the structure, and also due to clustering of the Eu^{3+} ions together into clumps and the resultant concentration quenching. This will be dealt with further in chapter 6.

4.9 STRUCTURAL INFORMATION.

A gel is an extremely porous material before complete densification, when it becomes a monolithic glass. It was important to check that the Eu^{3+} was in fact part of the structure and not just sitting on the pore surface. A series of undoped samples were prepared which were heated to 600°C, and then soaked in a 2% europium solution. The soaked glasses were then (a) dried out at 73°C and (b) dried out at 73°C and then heated to 200°C. The fluorescence decay times measured for the samples are given in table 4.4. The decay time of 0.16(1)ms for sample (a) is quite different than the gel lifetime of 0.123ms (Table 4.3).

	Lifetime τ (ms)
Dried at 73°C	0.16 (1)
Dried at 73°C Heated to 200°C	0.25 (1)

Table 4.4. Lifetimes for sol-gel material heated to 600°C and soaked in 2% europium solution.

It is anticipated that upon soaking the europium ions are incorporated into pores in the partially densified glass structure. The lifetime of 0.16(1)ms is too long to be attributed to Eu^{3+} in a symmetric water solvation shell. It is suggested that the ion is attached to the pore surface and surrounded on the other side by water molecules. Work which has been done on the surface of Vycor

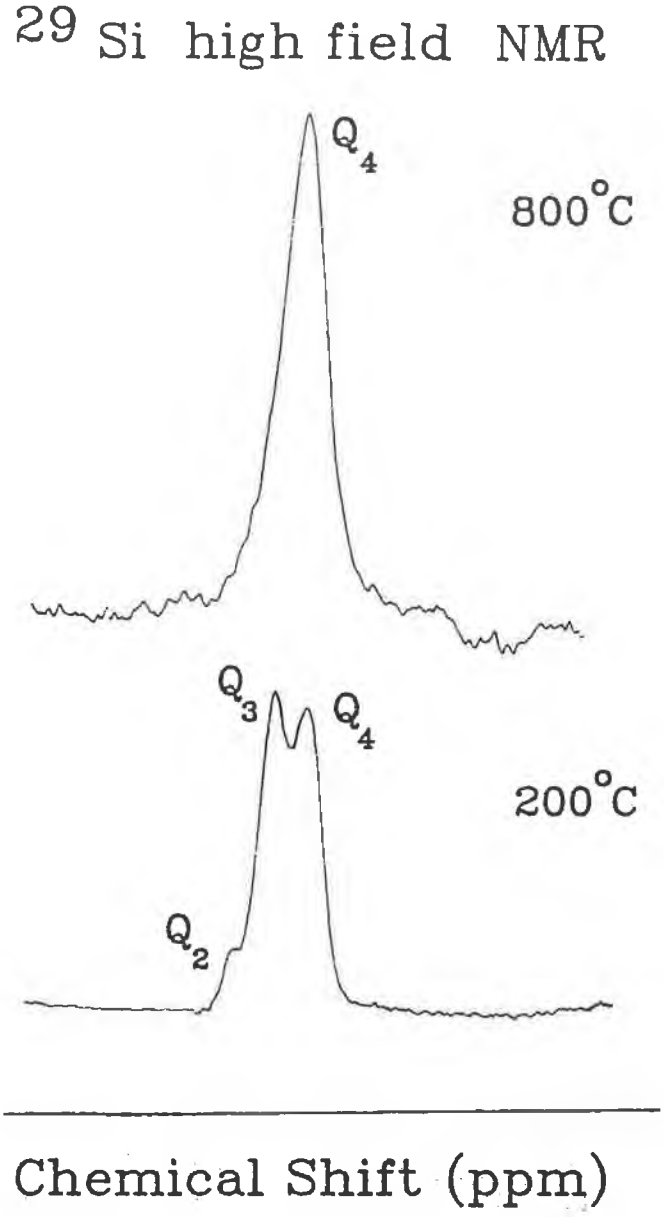

Fig 4.8 NMR data showing the coordination of silicon to other silicon atoms via oxygen.

glass [62,63] quotes a decay time of 0.25ms as corresponding to four water molecules coordinated to the adsorbed Eu^{3+} ion. In this case the sample yields a lifetime of 0.16ms which would give approximately five wafer molecules coordinated to the Eu^{3+} ion. The measured decay time of 0.25(1)ms for the 200°C soaked glass is also quite different to the value of 0.37ms obtained for the 200°C sample where europium was incorporated in the sol. The above results indicate that the environment of the Eu^{3+} ion is quite different from that of the ion in the 200°C partially densified glass. It is concluded from this analysis that the dopant ions when incorporated at the sol stage, become part of the glass skeleton as densification proceeds.

It can be deduced from the data above that the Eu^{3+} ion, when in the solution or "sol" resides in a coordination sphere consisting of approximately three organic groups and six hydroxyl groups. As the solution begins to gel, another organic group is hydrolysed and this allows a further OH into the coordination sphere. The gel structure for the water : silicon ratio and pH used in this study is a stringy polymeric network, and it is expected that the Eu^{3+} ion will be sensitive to structural changes throughout the entire densification process. The similarity of both the 200°C samples lifetimes would suggest that at this temperature hydrolysis is complete and that the free H_2O - D_2O is used up. The reduced lifetime when compared to the further densified material can be attributed to non-radiative pathways due either to residual CH groups [45] or to OH groups which are generated during combustion of the organic species. Most of the organics should be removed upon reaching a temperature of 400°C [64] but hydroxyl groups are known to exist within the structure until at least 800°C [64]. A third possible non-radiative decay route via the thermal population of the $^5D_1$ level is unlikely to have a significant effect on the observed lifetimes. Another possible cause of non-radiative decay is clustering of the ions within the structure and this will

be discussed in chapter six. The large lifetime differences observed throughout the process is evidence of the sensitivity of the Eu^{3+} ion to structural changes and also to the presence of hydroxyls in the materials. When the spectra for the 200°C and the 800°C samples are compared it can be seen that the 200°C sample exhibits more order than the 800°C, as the width of the $^5D_0 \longrightarrow ^7F_0$ transition is used as an indicator of symmetry. This reflects the smaller degree of cross linking in the structure at this temperature and the range of Eu^{3+} sites is correspondingly smaller. The 800°C structure has more cross linking, and therefore more strain, and approximates better to a disordered glass environment. The width of the singlet transition and large fluorescence ratio R, imply a wide range of sites and a highly asymmetric environment for the Eu^{3+} ion. The decay time of 1.25ms is short compared to that of conventional glass and it is evident that some non-radiative paths still exist.

4.10 INTRODUCTION OF A NETWORK MODIFIER.

As the introduction of Eu^{3+} ions into a normal high temperature fusion glass is assisted by the introduction of a network modifier [44], as discussed in chapter 2, it was attempted to introduce a modifier via the sol-gel process. Figure 4.9 shows the spectra of a sol-gel sample containing 5% Na_2O and follows the change in the spectra as the gel is densified.

The spectra of the gel which was cured at 73°C is similar to the spectrum of a solution and suggests that the ion is part of a symmetrical solvation shell as described earlier. Upon further heat treatments the spectrum begins to exhibit the characteristics of a less symmetrical environment.

The spectrum of the sample heated to 800°C is unusual in that there is a distinct narrowing of the $^5D_0 \longrightarrow ^7F_0$ transition, which would indicate that the Eu^{3+} ions are in a more symmetrical environment. The 800°C sample was

checked by X-ray diffraction to see if it was still an amorphous material [39]. It was found that the sample was composed of micro-crystals of α-cristobalite, also the samples were milky white due to hydrolytic attack on the NaO_2. It appears that the introduction of Na_2O into the process encourages the crystallisation of the sample upon reaching higher temperatures.

Various amounts of sodium were added to see if this made any difference to the process. It can be seen in figure 4.10 how the spectra of samples with 0%, 1%, 5%, and 20% Na_2O compare. The narrowing of the $^5D_0 \longrightarrow {}^7F_0$ is an indication that even as little as 1% sodium causes the crystallisation to occur and this can be clearly seen in Fig 4.10.

It appears that the introduction of Na_2O into the sol-gel process is in fact a complicated process. It has been found by Villegas et al [66] that the introduction of Na_2O, which is usual in conventional glasses, results in seggregation of the Na^+ ions in the form of salts (carbonates, bicarbonates, and nitrates). It has also been shown by Villegas et al, that in Na_2O sol-gel prepared glasses heated above 600°C that a large content of α-crystobalite is observed. In an effort to avoid crystallisation and retain monolithic pieces of glass, several authors [67,68,69] have used drying control chemical additives (DCCA's) during sol preparation. The DCCA's that are most commonly used are formamide and triethylorthoformiate, which are both capable of being adsorbed to the gel surface, thus accelerating the drying process. It has been found that [70] Na_2O - SiO_2 gel glasses have higher electrical conductivity values compared with glasses of the same composition prepared from the melt. This is caused by the lack of Na^+ ions incorporated into silica gel structure. Another feature of the Na_2O - SiO_2 gel derived silicate glasses is that they are much less resistant to corrosion or hydrolytic attack than

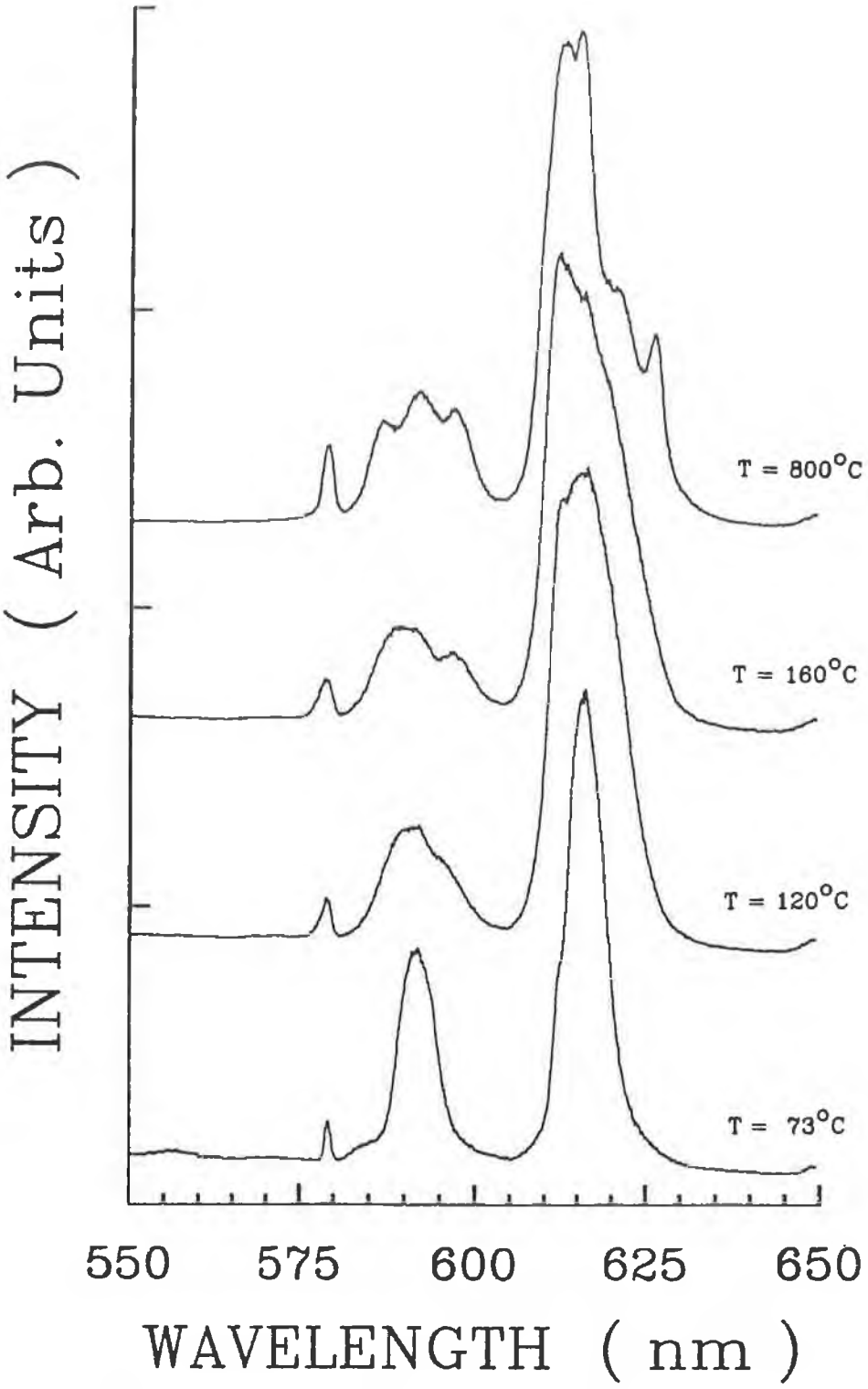

Fig 4.9 Fluorescence spectra of a sol-gel sample containing 5% Na_2O as the process proceeds. All of the spectra were taken at room temperature.

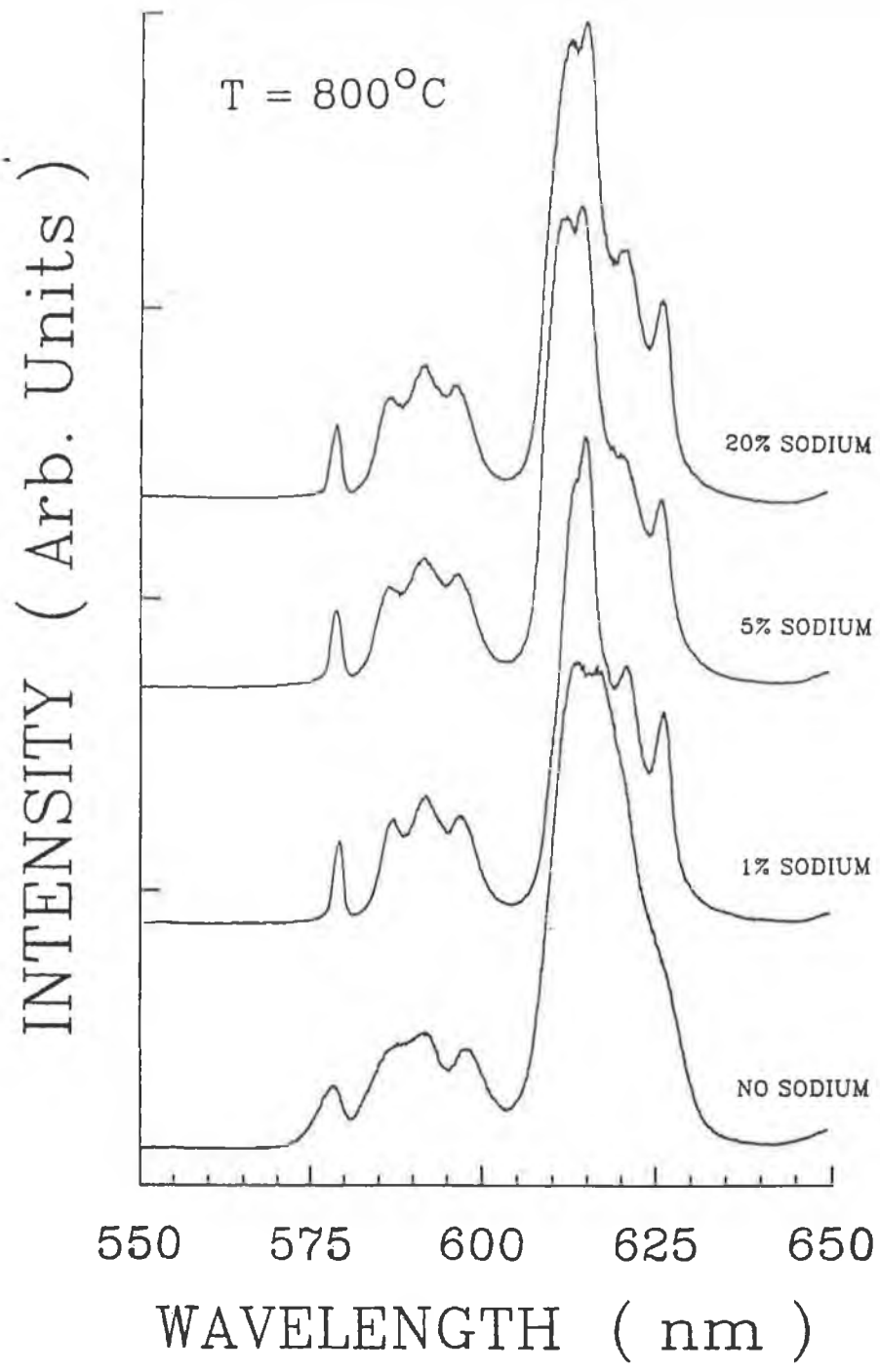

Fig 4.10 Fluorescence spectra of similar samples containing 0%, 1%, 5% and 20% Na_2O. All samples were furnaced to 800°C. The spectra were taken at room temperature.

conventional glasses. This is again due to the Na^+ ions not being incorporated into the gel structure by a strong bond.

CHAPTER 5.

5. OPTICAL SPECTROSCOPY OF Cr^{3+} IONS IN GLASS.

5.1 INTRODUCTION.

Since the development of the ruby laser in the 1950's much work has been carried out using Cr^{3+} ions as an optically active dopant in a variety of host materials. As a result of the use of chromium in the ruby laser, there has been a great deal of interest in Cr^{3+} in different glass environments. Broadband luminescence from chromium doped glasses has been reported by Karapetyan et al [71], Sharp et al [72], Brawer and White [73] and a very comprehensive study of Cr^{3+} ions in a number of glasses has been published by Andrews et al [74]. In this chapter a study of silicate and lithium borate glasses made by the high temperature technique described in chapter 3 is given. A short discussion will also be given on the introduction of Cr^{3+} into sol-gel materials. The two high temperature glasses investigated were both doped with 0.1% Cr^{3+}. The composition of the two glasses were as follows [38],

SILICATE (A).

SiO_2	Na_2	$CaCO_3$	Cr_2O_3
75%	12.9%	12%	0.1%

Melting temperature = 1400°C
Annealing temperature = 700°C

BORATE (B).

$LiBO_2$	SiO_2	Al_2O_3	Cr_2O_3
83%	8.4%	8.5%	0.1%

Melting temperature = 1200°C
Annealing temperature = 700°C

Absorption, fluorescence, excitation, and fluorescence lifetime measurements were made to investigate how the Cr^{3+}

ions environment differs within the two different host glasses.

A transition metal ion when used as a probe ion in a crystal, yields an emission that retains much of the sharpness of the individual ions transitions. When the same dopant ions are used with an amorphous material, such as glass, the transition frequency varies from site to site. In this case, the observed broad transition is a composite of sharp line transitions at different frequencies. The resultant absorption and fluorescence spectra from the doped glass samples are significantly broadened compared to a similarly doped crystal. This inhomogeneous broadening is caused by a variety of crystal fields both in strength and symmetry. This can be indicated using a Tanabe-Sugano diagram, details of which, along with the coordination of optically active ions within a solid are given in chapter 1.

5.2 ABSORPTION.

Absorption spectra of both the borate and silicate high temperature glasses were taken and are shown in Fig 5.1. The absorption peak at approximately 650nm has been identified as the vibronically broadened $^4A_2 \longrightarrow {}^4T_2$ transition. This is consistent with a Cr^{3+} site surrounded by a regular octahedron of nearest neighbour ions as described by Brawer and White [73]. On the broadband absorption spectra in Fig 5.1 there are slight features which are due to the transitions $^4A_2 \longrightarrow {}^2E$ and $^4A_2 \longrightarrow {}^2T_1$. There is a shift in the peak of the $^4A_2 \longrightarrow {}^4T_2$ absorption between the two glasses. The peak for the silicate glass (A) is at 650nm, and for the borate glass (B) it is at 610nm. This indicates that the Cr^{3+} ions within the glass substrates have different local environments. This feature was also observed by van Die et al [75] for another borate glass. The absorption spectra are only shown from 450nm as the higher energy $^4A_2 \longrightarrow {}^4T_1$ absorption is obscured by an intense Cr^{6+} charge transfer band [76,77]. In general when

transition metal ions are introduced into a molten glass they often distribute into more than one oxidation state, each of these states gives rise to optical absorption. [77,78].

5.3 FLUORESCENCE.

The fluorescence spectra of both samples A and B at 300K and 77K are given in Fig 5.2. The narrow peak on the high energy side of the spectra is attributed to the $^2E \longrightarrow {}^4A_2$ transition. In Ruby this is the very efficient transition known as the R line. The broad band which makes up the only other feature in the spectra is identified as the $^4T_2 \longrightarrow {}^4A_2$ transition [74]. It can be clearly seen in the silicate sample (A) that the $^4T_2 \longrightarrow {}^4A_2$ emission is the dominant transition within the spectra, and therefore the majority of Cr^{3+} ions within this glass substrate occupy low field sites. The division of sites into low field and high field sites is shown schematically on the diagram shown in Fig 5.3. The figure shows how the luminescent energy levels in a glass vary against the range of crystal field values. Details on the splitting of energy levels due to crystal field variations are given in chapter 1.

A low field site is indicated in Fig 5.3, where the $^4T_2$ level is below the ^2E level, and hence yields $^4T_2 \longrightarrow {}^4A_2$ luminescence. In the case of sample (B), the ^2E is much more intense than in the silicate sample, and a greater number of Cr^{3+} ions occupy high field sites, with the ^2E level below the $^4T_2$ level. The main point of interest in Fig 5.2 is the difference in relative intensities between the ^2E and $^4T_2$ transitions for both the silicate and borate glasses, A and B. The quite different intensity ratios between the two samples would indicate that there is a different range of crystal field sites experienced by the Cr^{3+} ions within the two samples.

In the case of the sample(A), the $^2E \longrightarrow {}^4A_2$ transition is seen to be very weak and hardly visible at 300K, but when the sample was cooled to 77K a small peak was observed.

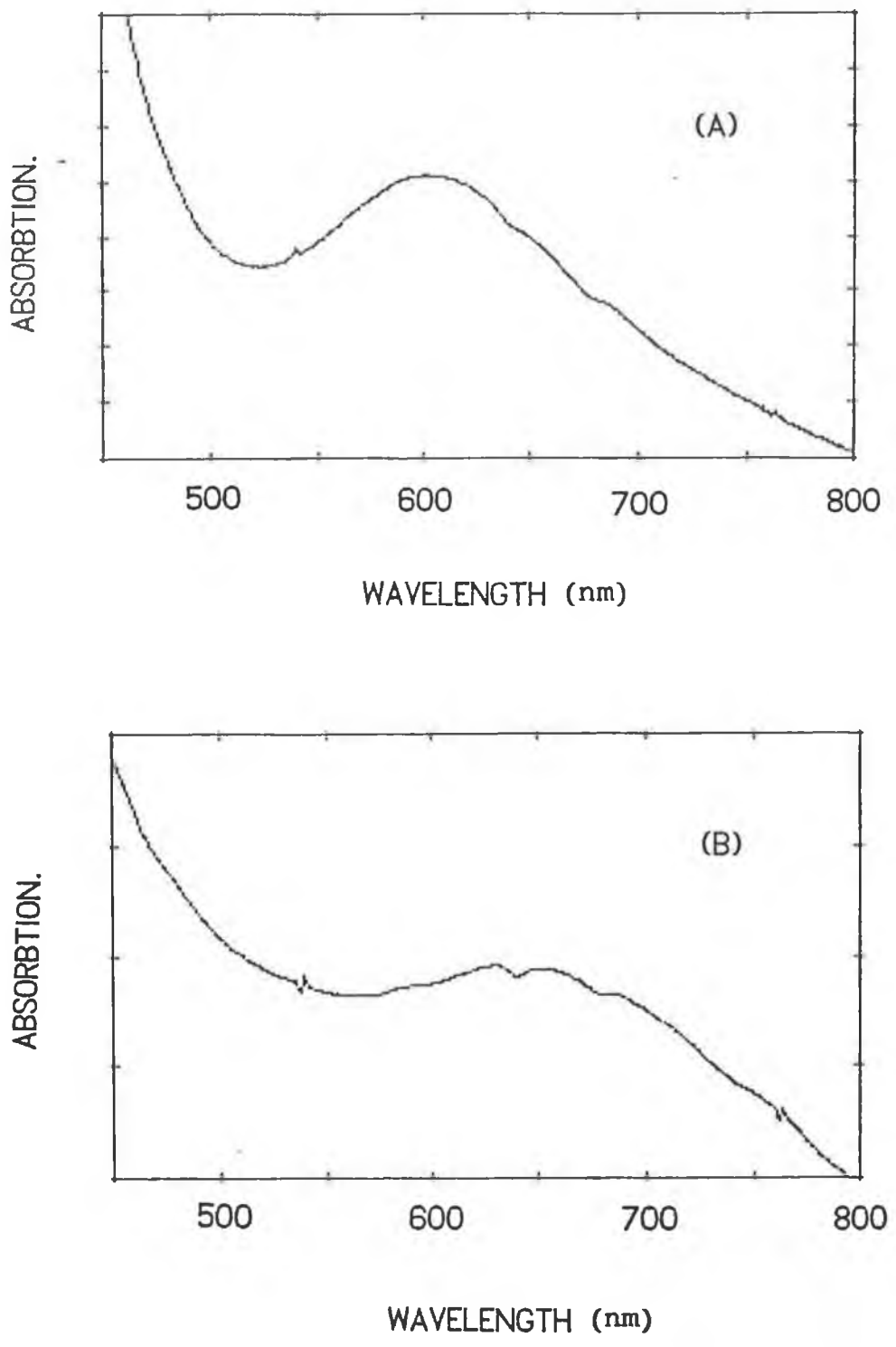

Fig 5.1 Room temperature absorption spectra of Cr^{3+} doped (a) borate and (b) silicate glasses.

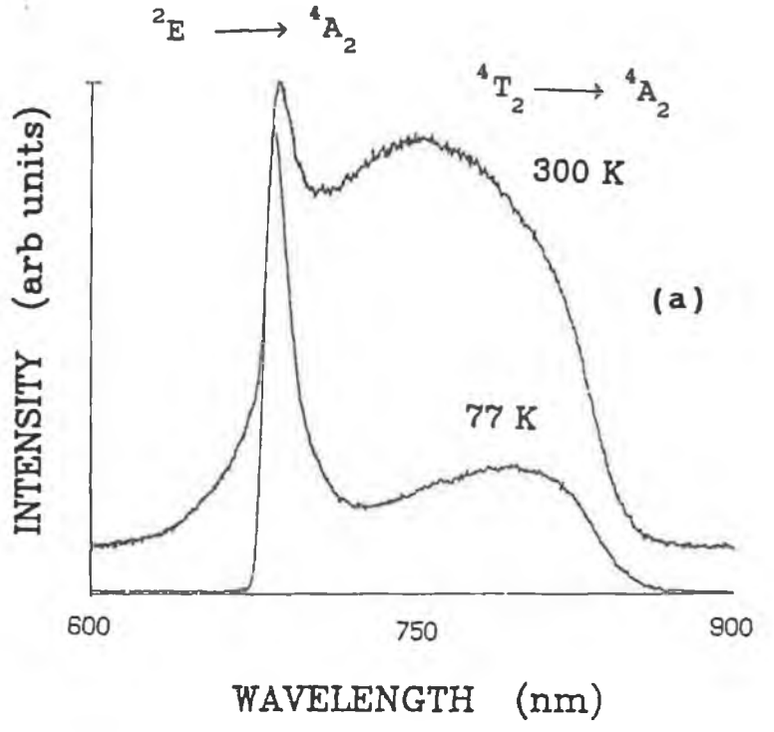

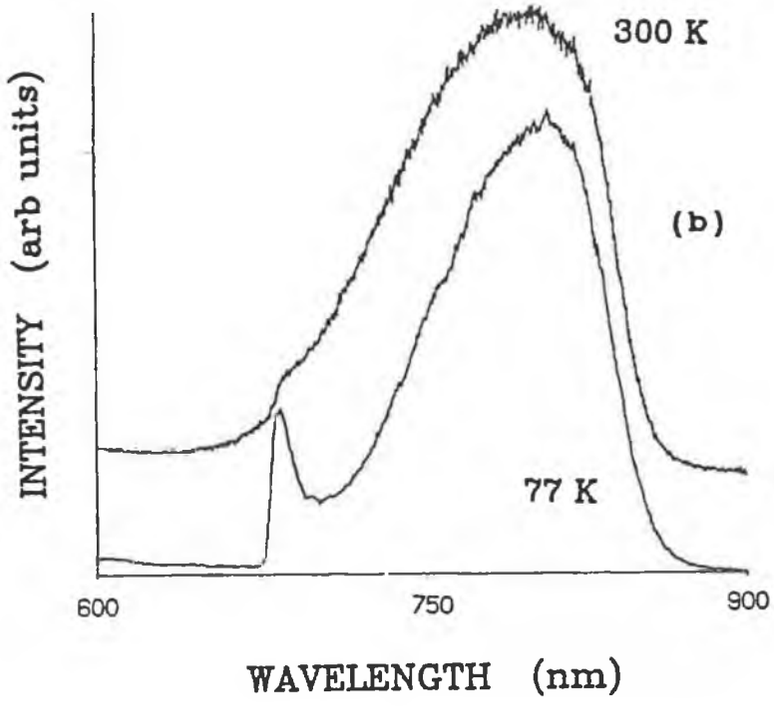

Fig 5.2 Fluorescence spectra of Cr^{3+} doped (a) borate and (b) silicate glasses at 77K and 300K.

For sample (B), (borate) the $^2E \longrightarrow {}^4A_2$ transition is more intense than the $^4T_2 \longrightarrow {}^4A_2$ transition at 300K, and significantly more intense at 77K.

It can be clearly seen that a greater number of Cr^{3+} ions occupy high field sites in the lithium borate glass than in the silicate glass, as the ^2E fluorescence is significantly more intense.

As the luminescence from the Cr^{3+} doped glasses is composed of luminescence from two different energy levels with two different decay times, it was possible using a technique called phase resolved spectroscopy to separate the two contributions. The technique used was described by M.O. Henry [40] and is given in section 3.4. It can be clearly seen in figure 5.4 that the spectrum is composed of two separate contributions, which arise from the ^2E and $^4T_2$ energy levels. Each of these transitions has a quite different decay time and this will be discussed in more detail in the next section.

5.4 FLUORESCENT DECAY TIMES.

The fluorescent decay curves for the two glasses were measured and as expected were found to be non-exponential in nature, due to the broad range of sites occupied by the optically active ions. The technique that was used to measure the fluorescent decay curves is given in section 3.6. The various analytical methods that can be used to give a value for the non-exponential decay times of doped glasses have been discussed in chapter 3. The technique that seemed to give the most reproducible data for the non-exponential decay curves was calculating the time required for the fluorescence to decay to $1/e$,$1/e^2$ and $1/e^3$ of its initial intensity. Table 5.1 shows the experimental values for both glasses. The non-exponential nature of the decay can be clearly seen in Fig 5.6, as the semi-log plot curves upwards.(see section 3.6)

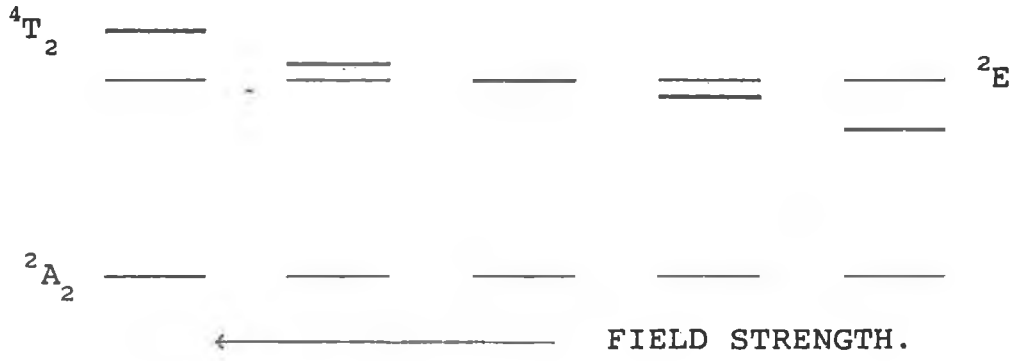

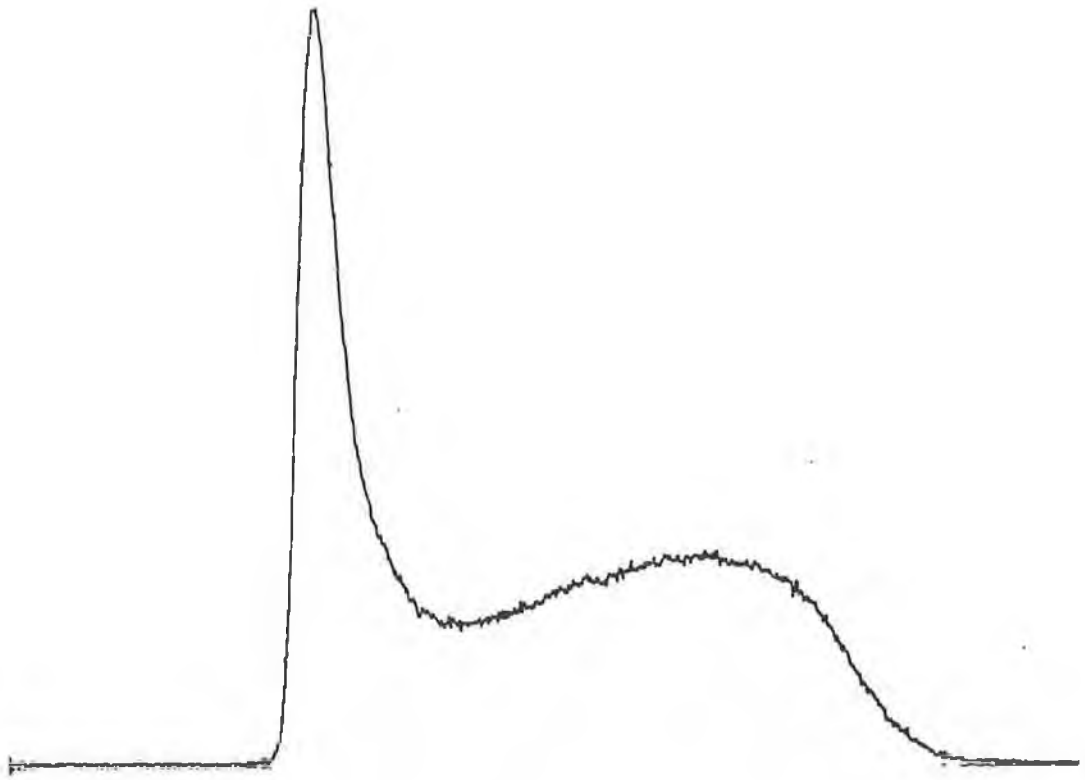

Fig 5.3 Division of ions into low field and high field sites shown against the spectra of the borate glass. Temp = 77 K.

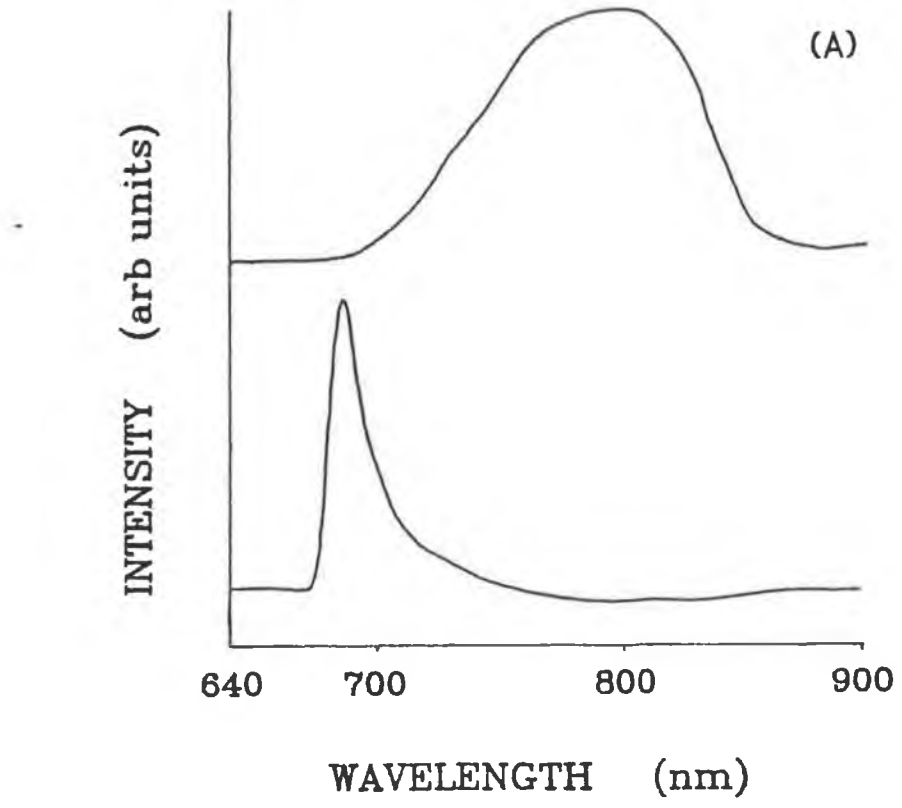

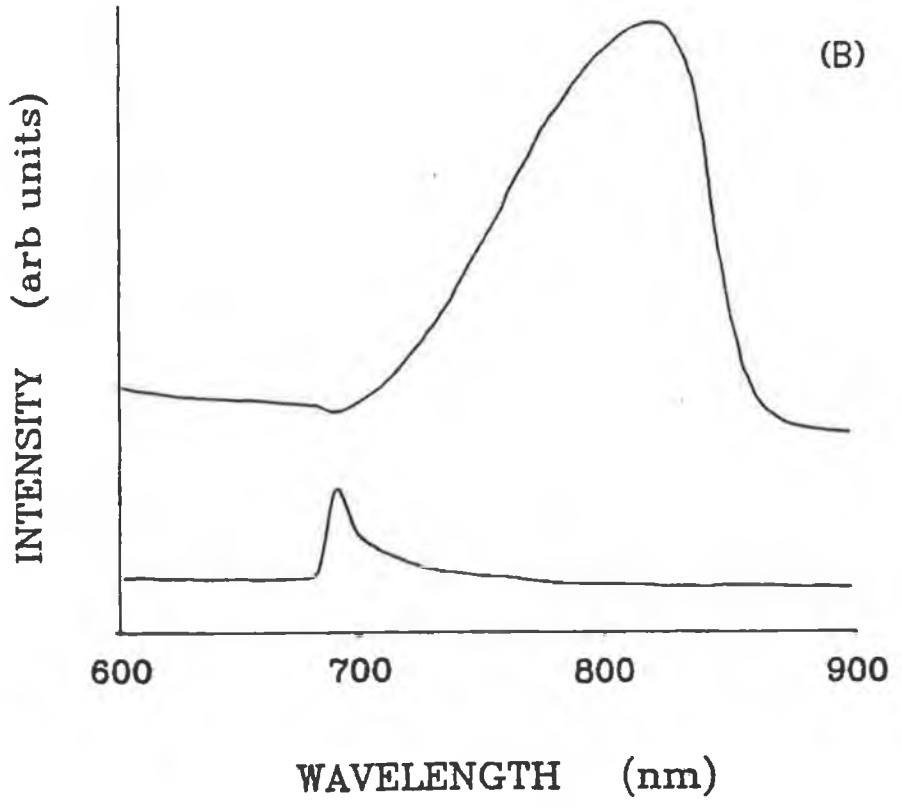

Fig 5.4 Spectra of (a) borate and (b) silicate glasses taken using the phase resolved technique. Temp = 77 K.

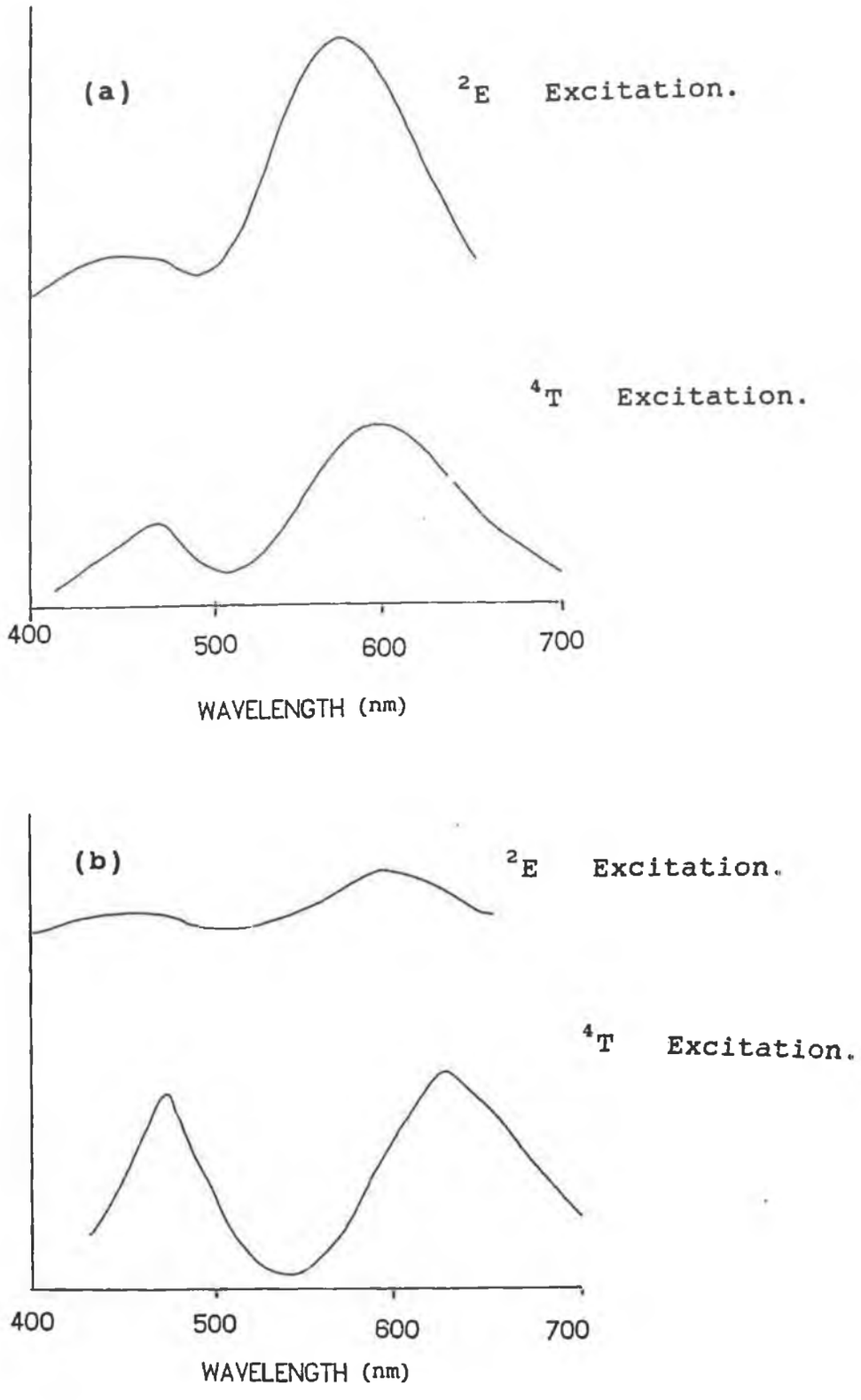

Fig 5.5. Excitation scans for the ^2E and ^4T fluorescence peaks for (a) borate and (b) silicate glasses. T = 77 K.

SAMPLE A (Silicate)	1/e	$1/e^2$	$1/e^3$
$^2E \longrightarrow {}^4A_2$ (msec)	0.8 ± 0.1	2 ± 0.3	3.8 ± 0.4
$^4T_2 \longrightarrow {}^4A_2$ (μsec)	52 ± 2	122 ± 5	213 ± 7

SAMPLE B (Borate)	1/e	$1/e^2$	$1/e^3$
$^2E \longrightarrow {}^4A_2$ (msec)	1.2 ± 0.05	2.8 ± 0.1	4.9 ± 0.2
$^4T_2 \longrightarrow {}^4A_2$ (μsec)	39 ± 2	93 ± 4	179 ± 6

Table 5.1 shows the characteristics of the fluorescent decay curves for the Cr^{3+} doped glasses. All lifetime measurements were taken at 77K.

The shorter value for the borate ($^4T_2$) lifetime is consistent with previous ambient temperature values for borate and silicate glasses, given in ref [75] and reflects the higher probability for non-radiative decay in the borate glass. The longer borate (^2E) value of 1.2 msecs is consistent with this spin forbidden transition. The value of 0.8 msecs for the silicate may be partly due to the overlapping $^4T_2$ band, as the ^2E transition in this glass is very weak.

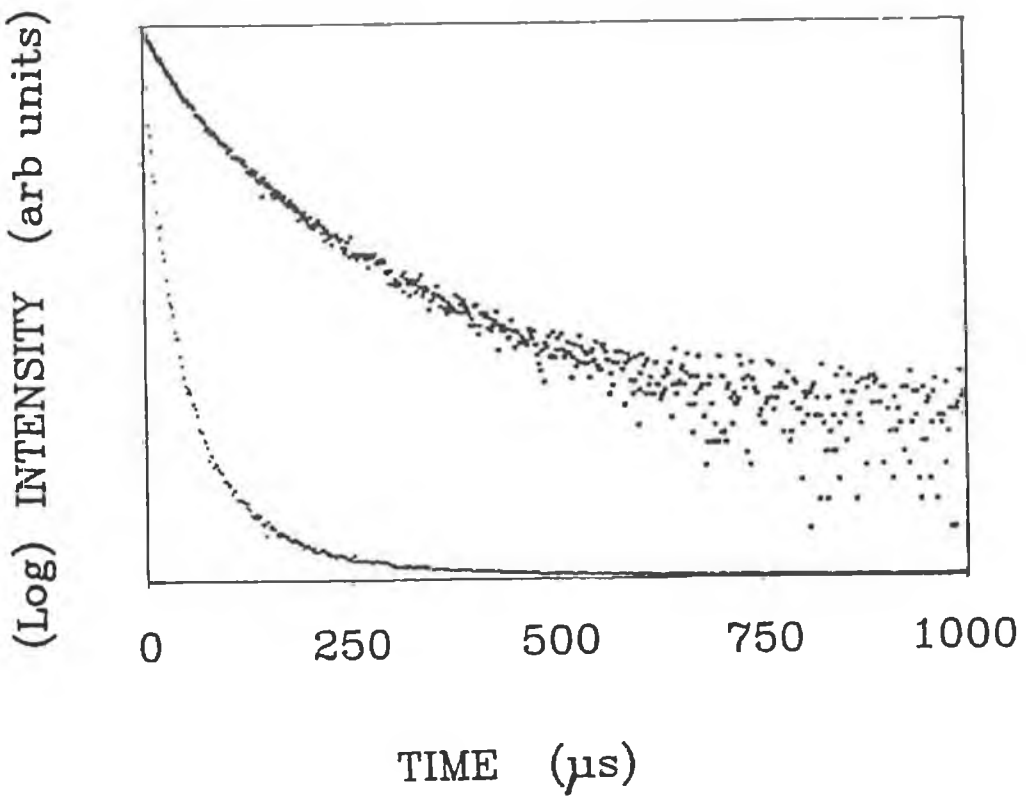

Fig 5.6. An example of a decay curve from the high temperature silicate sample. The curve shows the decay of the $^4T_2 \longrightarrow {}^4A_2$ fluorescence, and the non-exponential nature can be seen by the curve of the semi-log plot. Temp = 77 K.

5.5 Cr^{3+} IN SOL - GEL MATERIALS.

A series of sol-gel materials with chromium introduced into the starting solution were prepared and furnaced to allow for densification to take place. A solution of $Cr(NO_3)_3.9H_2O$ in ethanol was used as a "stock solution" to prepare precursor mixes containing various percentage weights of Cr on Si. The sol-gel preparation was as described in chapter 3. Three different series of samples, each with a different chromium concentration were made. The samples were studied at the sol, gel and partially densified glass stages of the process. Some of the samples were prepared under flowing hydrogen to try to minimise oxidation effects.

SERIES.	% Cr (on Si).	"pH" OF MIX.
1	0.11	0.84
2	0.52	0.66
3	1.02	0.76

Table 5.2 Table of the Chromium content and pH of the mix for the Chromium sol-gel samples.

The starting solutions were subdivided into three parts to allow for different heat treatments. Each of the above solutions were subjected to one of the following heat treatments.

(a) The solutions were mixed and placed in sealed containers in a fridge to avoid evaporation. They were then placed in a furnace at 76°C for 188 hours.

(b) These samples were dried as above and heated for another 2 hours at 200°C in flowing hydrogen.

(c) These samples were treated as (b) except they were heated in air.

Optical absorption measurements were made of all the samples. The absorption spectra for each of the solutions (sols), before any heat treatments can be seen in figure 5.7. In figure 5.7, the chromium concentration of the samples was as follows, (a) 0.1%, (b) 0.5%, (c) 1%, and (d) is of a 0.1% $Cr(NO_3)_3$ solution for comparison purposes.

The absorption spectra shown in figure 5.8 (a) and (b) are from materials that were heated for 2 hours at 400°C. (a) was heated in a flowing hydrogen environment and (b) was heated in air. Reference should also be made to figure 5.1 which shows the absorption spectra of Cr in the conventional high temperature borate and silicate glasses discussed earlier.

The samples that were heated to 400°C were glass-like in appearance and were a yellow/brown colour. Neither of the samples exhibit the familiar green colour that would be expected for Cr^{3+} in glass. The samples that were heated to 200°C were pale green in colour as also were the sols.

It is clear from the absorption spectra that trivalent chromium is predominant in all samples up to the 200°C heat treatment and this was also evident from the pale green colour. The yellow/brown colour of the 400°C is characteristic of Cr^{6+}, which has been shown to occur in many conventional glasses [79]. Cr^{6+} is known to absorb at 270nm and 370nm [77]. In acid conditions, dichromate (CrO_4^{2-}) and trichromate complexes have a tendency to form [76], and this has the effect of shifting the absorption band further into the visible. In figure 5.9 a band appears at about 450nm which would indicate the presence of Cr^{6+} and some dichromate in the 400°C samples. The yellow colour and absorbtion edge at approx 450nm is widely used as an indicator of the presence of Cr^{6+}[78]. It is postulated from the absorption spectra and colour of the samples that the samples with heat treatments below 200°C contain Cr mainly in the trivalent state. It is also clear from the spectra of the samples heated to 400°C that most of the

Cr^{3+} has been oxidised to Cr^{6+}. In an attempt to reduce the oxidation of the Cr^{3+}, hydrogen gas was flowed over the samples as they were dried and densified.

It can be seen in Fig 5.8 that the spectra of the samples that were heated to 200°C with and without the flowing hydrogen are similar. In the case of the 400°C samples shown in Fig 5.9, the sample that had flowing hydrogen over it during heat treatments shows some evidence of the $^4T_2$ transition from Cr^{3+} within the sample, but the absorption edge from Cr^{6+} is still dominant. The 400°C sample that was heated in air does not appear to show any evidence of Cr^{3+} absorption.

It would appear that the $Cr^{3+} \longrightarrow Cr^{6+}$ conversion is minimal at 200°C, but upon further heat treatments to 400°C, even in a reducing atmosphere, a larger proportion of Cr^{6+} exists. The sol-gel material at the gel stage consists of a porous network of loosely branched polymer chains containing Si-O, methyl groups, hydroxyls and water molecules (see chapter 3). As the glass is further densified, the water molecules and organic groups gradually burn off and the degree of cross linking of the Si-O groups gradually increases. At 200°C most of the loosely bound water will have been removed from the material [80], and as the temperature approaches 400°C most of the organic groups are removed. It has been shown however that some hydroxyl groups can remain within the structure up to much higher temperatures [80,33]. It is proposed that the radicals produced as byproducts of the organic group removal facilitate the oxidation of Cr^{3+} to Cr^{6+}. This would explain the small role played by the hydrogen atmosphere in preventing oxidation.

The samples were also scanned through various excitation wavelengths to see if there was any fluorescence present, but no output was observed from any of the samples. Even for the samples that show some Cr^{3+} absorption, no fluorescence was observed. This is interpreted tentatively to be due to quenching by hydroxyl ions.

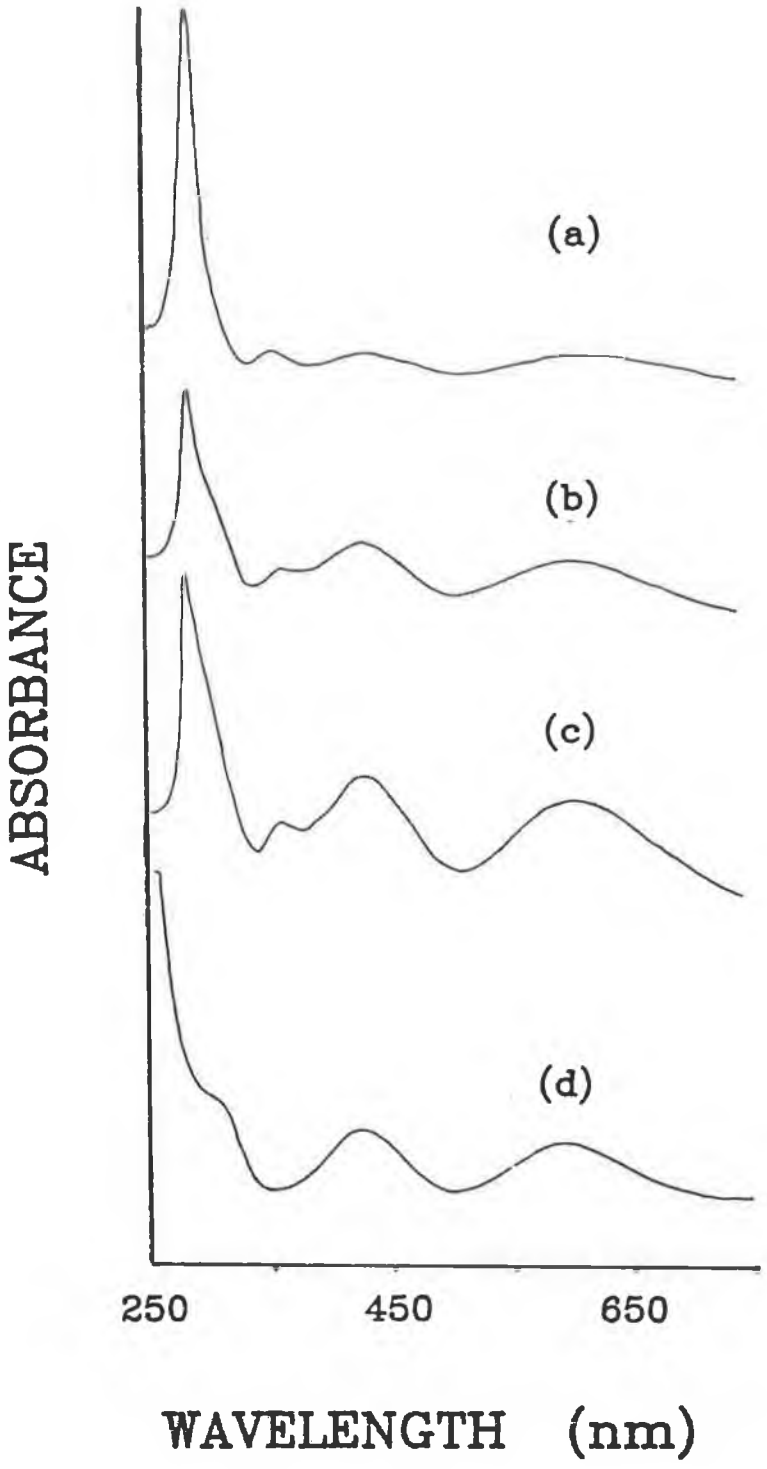

Fig 5.7. Room temperature absorption spectra of solutions with Chromium concentrations of (a) 0.1%, (b) 0.5%, (c) 1% and (d) is a 0.1% $Cr(NO_3)_3$ solution.

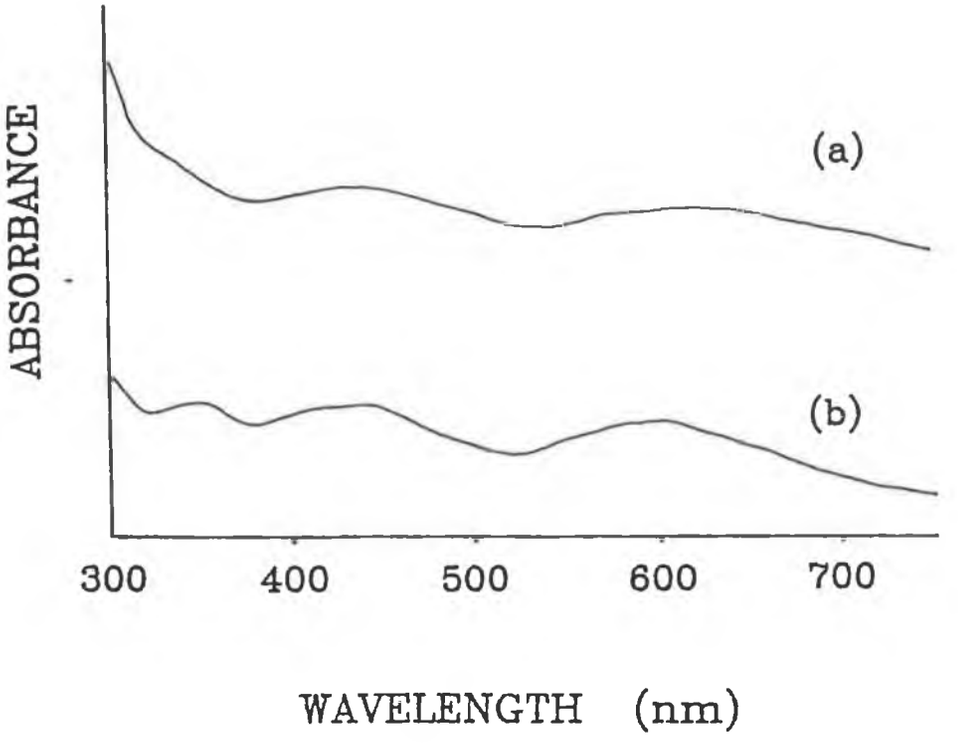

Fig 5.8. Room temperature absorption spectra of samples heated to 200°C. (a) Heated in flowing hydrogen and (b) heated in air.

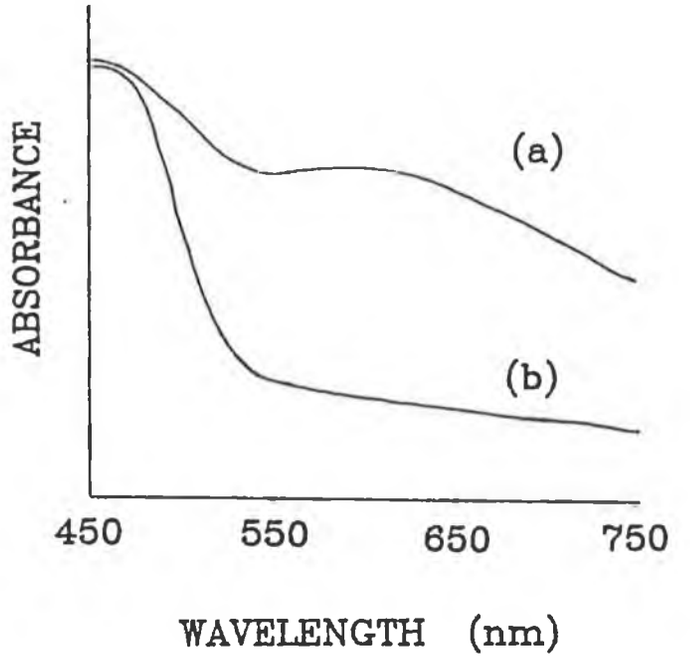

Fig 5.9 Room temperature absorbtion spectra of Cr^{3+} doped sol-gel samples heated to 400°C. (a) Heated in flowing hydrogen and (b) heated in Air.

5.6 CONCLUSION.

A comparison has been made between the spectroscopic properties of Cr^{3+} in a borate and silicate glass. The borate glass host is shown to have a greater proportion of high field sites than the silicate host. The shift in wavelength between the absorption and excitation peaks for both glasses, like the lifetime data reflect the higher probability of non-radiative decay of Cr^{3+} in glasses and particularly for low field sites. The intense $^2E \longrightarrow {}^4A_2$ luminescence from the borate glass is of particular interest. The ambient temperature luminescence from this transition is significantly more intense than other borate glasses reported [75,74], and points to this composition as a good candidate for a more detailed study of ^2E fluorescence from Cr^{3+} in glass hosts.

The introduction of Cr^{3+} into densified sol-gel materials has proved extremely difficult to date, as the the Cr appears to enter the densified glass in the Cr^{6+} state. Heating the material in a reducing atmosphere produced materials with some evidence of trivalent chromium, but hexavalent chromium was still dominant. No fluorescence output could be obtained from any of the densified materials, and this possibly due to quenching of the fluorescence due to the presence of residual OH still within the structure. Further work on the processing of these materials is being carried out in this laboratory at present.

CHAPTER 6.

6. FLUORESCENCE LINE NARROWING STUDIES.

6.1 INTRODUCTION.

As glass is an amorphous medium, the environment of each dopant ion is not identical as is the case with a crystal. In a glass host, the photoluminescence emission from transition metal or rare-earth ions consists of a superposition of contributions from individual ions distributed among the entire range of local environments. If a broadband light source (e.g. Arc lamp.) is used, it excites the ions in different environments with an equal probability and the luminescence output exhibits the inhomogeneous broadening of the material. When a narrow band source, such as a tunable dye laser is used, it excites ions in a small subset of sites where the absorption frequencies are within the narrow laser linewidth. The luminescence output in this case will have greatly reduced inhomogeneous broadening and a line narrowed fluorescence is obtained. This phenomenon is called Fluorescence Line Narrowing (FLN).

The technique of FLN in glass was first reported in 1967 by Denisov and Kitzel [81], while laser induced FLN was demonstrated initially by Szabo [82] and later for rare earth ions in glass by Riseberg [83]. The use of FLN is in fact a relatively simple method of overcoming inhomogeneous broadening and can provide valuable information about ions and molecules in solids.

A borate and a silicate glass made by the high temperature techniques described in sections 3.1.1 and 3.1.2 and doped with Eu^{3+} were investigated by the technique of fluorescence line narrowing. The resultant spectra are similar to those reported by others [84,85,86,87,88] for borate and silicate glasses.

Investigations into the two sol-gel glass samples, described in chapter 4, that were furnaced at 800°C, show

many of the characteristics of the high temperature glasses, but under narrow band laser excitation into the $^5D_0 \longrightarrow {}^7F_0$ band, the emission did not show any obvious narrowing. This chapter gives the results of the FLN for the two conventional glasses for comparison purposes and suggests reasons why the Eu^{3+} doped sol-gel glasses do not show any evidence of narrowing.

6.2 BACKGROUND.

The degree of narrowing observed depends on the pumping and de-excitation paths, hence FLN may be categorized into resonant fluorescence line narrowing (RFLN) and nonresonant fluorescence line narrowing (NRFLN), see Fig 6.1.

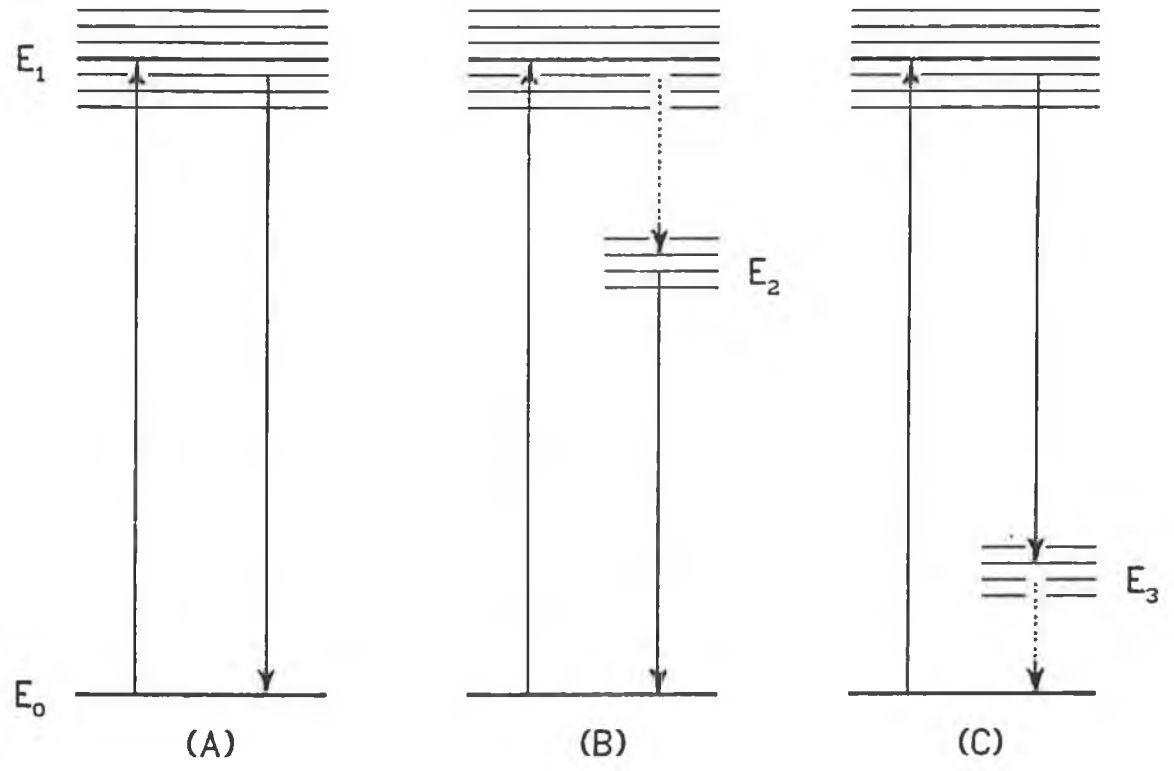

Fig 6.1 (a) is an example of resonant fluorescence line narrowing (RFLN) and (b) and (c) are examples of nonresonant fluorescence line narrowing (NRFLN).

If as is illustrated in (a) the excited ions decay radiatively directly to the ground state this is called resonant fluorescence line narrowing (RFLN). The width of the observed luminescence output $\Delta\nu_0$ is determined by the laser bandwidth $\Delta\nu_L$,the homogeneous broadening of the absorption transition $\Delta\nu_H$,and the instrumental width of the system $\Delta\nu_{INS}$. In this case the luminescence output is emitted at the same wavelength as the exciting laser light and this can cause some experimental difficulties to which there are several different solutions. [43,90]

If the excited ions decay radiatively to a level lower than the excited state, but not the ground state, or decay nonradiatively to a lower level, and then decay radiatively to the ground state, this is called nonresonant fluorescence line narrowing (NRFLN). The luminescence output from NRFLN will be of lower energy than the laser light and it is therefore easier to perform experimentally.

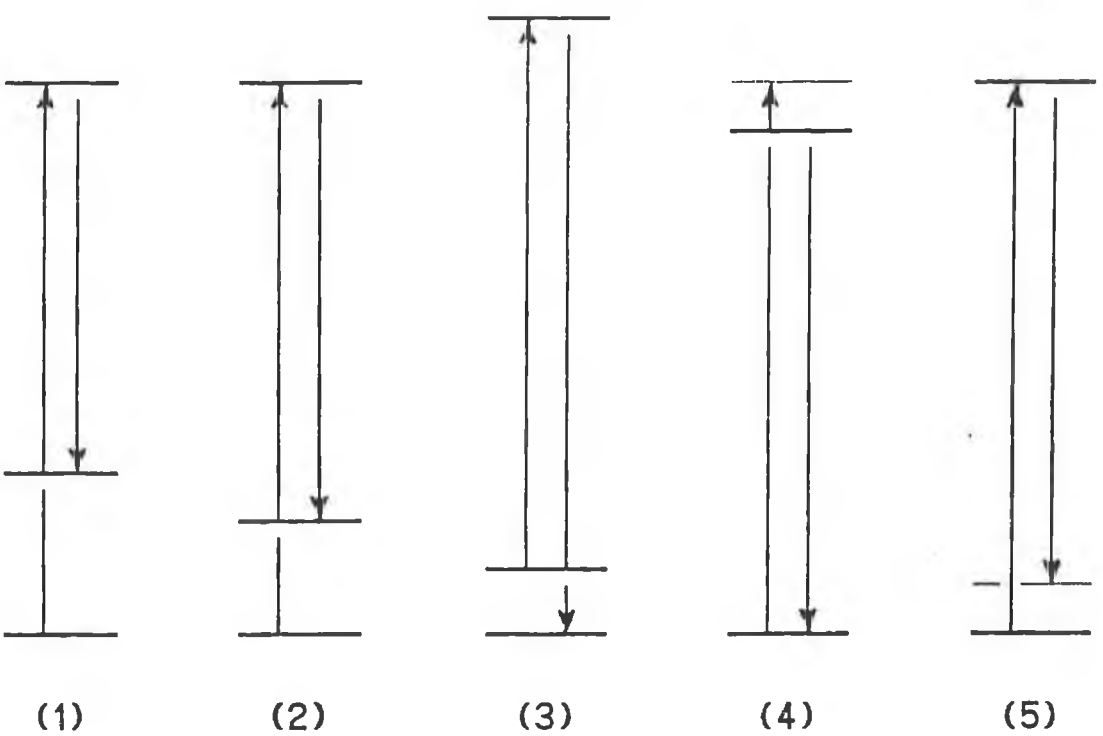

Fig 6.2 An example of fluorescence sites all excited with the same frequency which fluoresce non-resonantly at different frequencies.

A difficulty that is encountered as well as some of the experimental difficulties is that of accidental coincidences of excitation levels of ions in [89,44] different sites. As can be seen in fig 6.2 ions in sites 1,2,3,4 and 5 are all excited by the same wavelength but they all de-excite to different levels and hence emit at different wavelengths. In the diagram examples 1 and 2 show how broadening occurs due to spectral accidental coincidences, while 4 and 5 show examples of transitions originating or terminating on vibronic energy levels. 3 is an example of excitation from a thermally populated level [89].

6.3 HIGH TEMPERATURE GLASSES.

The two high temperature glasses, (a) silicate and (b) borate described in chapters 3 and 4 were both investigated using the technique of non-resonant fluorescence line narrowing (NRFLN).

The samples were cooled to 77K to reduce the homogeneous linewidths. It should be pointed out that the spectral widths of the emission lines were not significantly reduced, upon further reduction of the temperature to 10K. This would suggest that the widths of the emission lines in Fig 6.3 are determined mainly by the site to site variation of the crystal field acting on the Eu^{3+} ions. In each of the examples given in figures 6.3 and 6.4, a nitrogen pumped dye laser (Rhodamine 6G dye) was used to selectively excite the inhomogeneously broadened $^5D_0$ levels by using laser excitation within the range of the inhomogeneous linewidth of the $^7F_0 \longrightarrow {}^5D_0$ transition. The fact that the $^5D_0$ and $^7F_0$ states are non-degenerate helps to simplify the interpretation of the results. In the transition $^5D_0 \longrightarrow {}^7F_1$, three lines which overlap with each

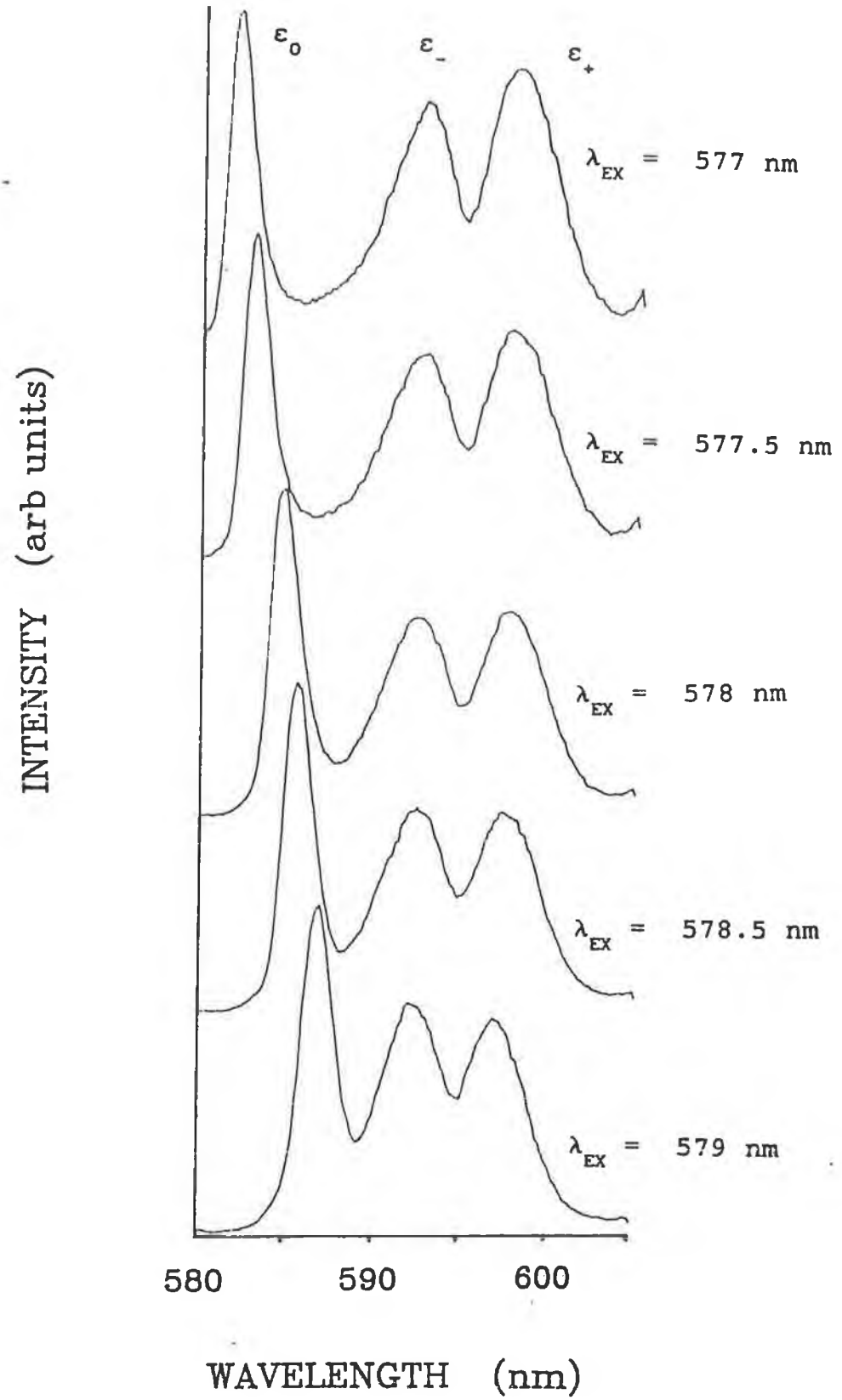

Fig 6.3 Fluorescence line narrowed spectra of the high temperature borate glass. Spectra taken at 77 K.

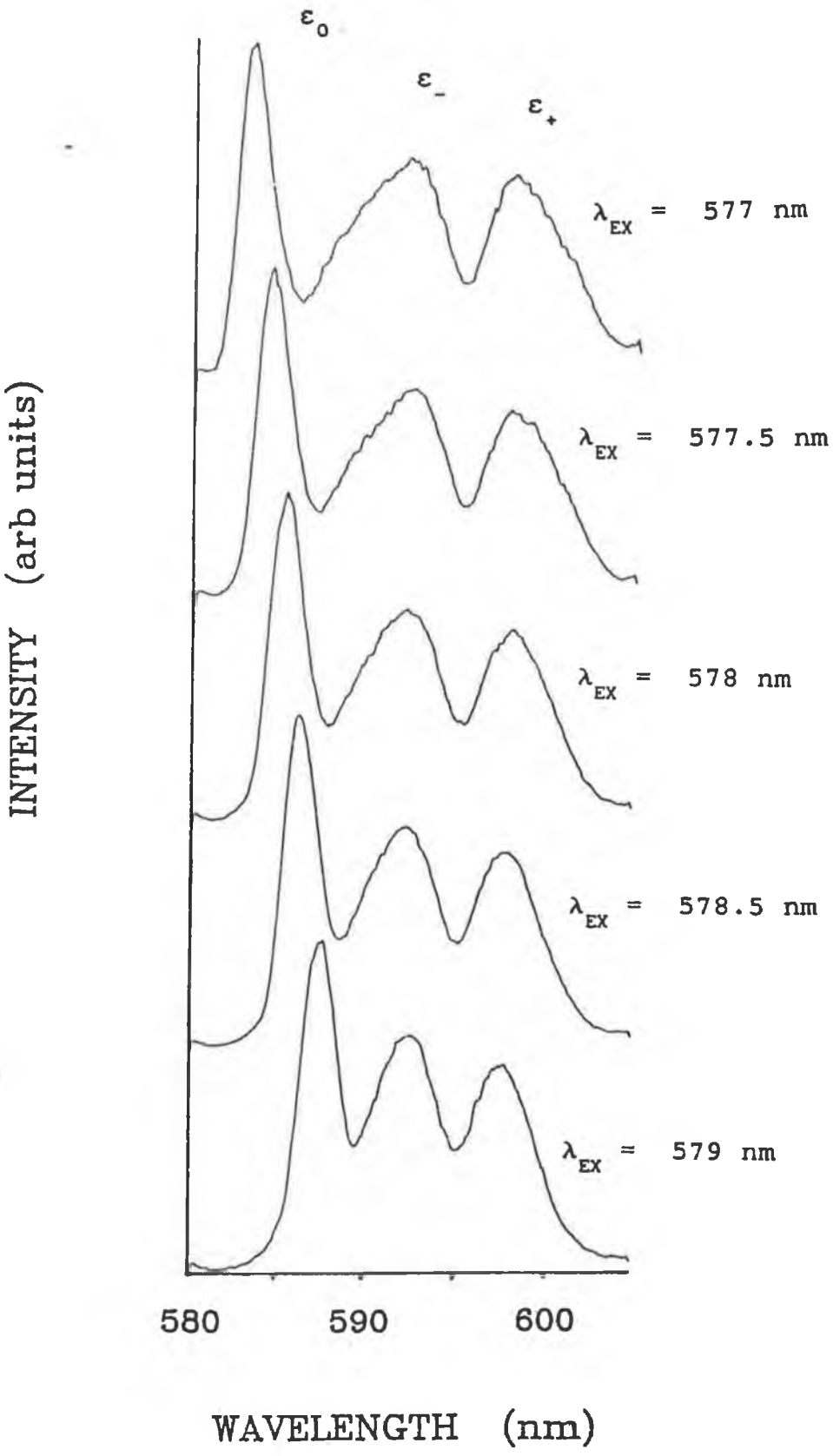

Fig 6.4 Fluorescence line narrowed spectra of the high temperature silicate glass. Spectra taken at 77 K.

other are observed corresponding to the three Stark components of the $^7F_1$ state. The three components have been conventionally [88] labelled ε_0, ε_- and ε_+ in the order of decreasing energy.

The spectra in figures 6.3 and 6.4 were measured at a delay of 100μs after the laser pulse. It can be clearly seen that the emission lines of the $^5D_0 \longrightarrow {}^7F_1$ under narrow band laser excitation are quite different from the broadband excited spectra i.e. Fig 6.5. The widths of the emission lines from ε_0, ε_- and ε_+ are much narrower and the positions of the peaks are also shifted. It can be seen that by changing the excitation across the inhomogeneously broadened absorption, it becomes possible to map the variations of the crystal field across the entire range of microscopic environments in a doped glass.

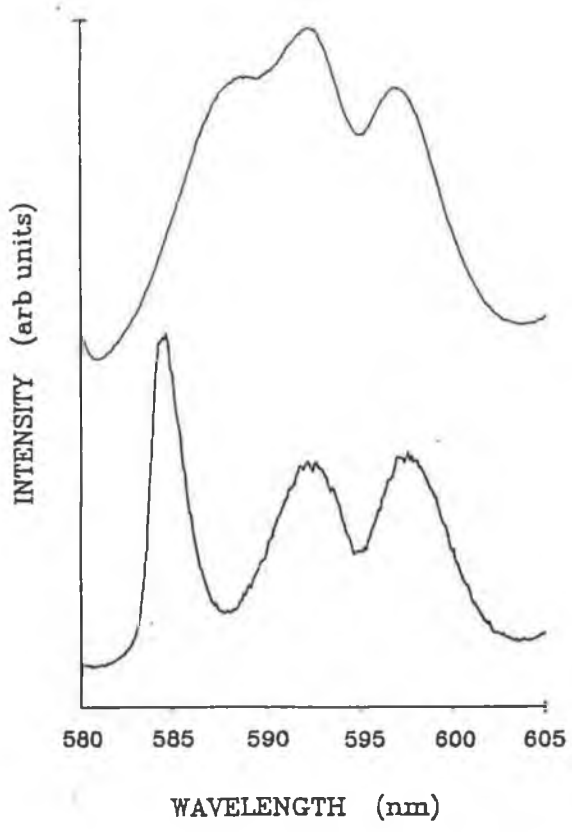

Fig 6.5 Shows comparison of broadband excited glass and narrow laser excited glass. Both were taken at 77 K.

The position of the peak ε_0 is most sensitive to the

excitation wavelength. The fluorescence spectra show a marked degree of narrowing, but the widths of the lines are much greater than the homogeneous or the instrumentation widths. The line narrowing is clearly evident, and the most noticeable feature is the sharpness and excitation dependent shift of ε_0, the lowest wavelength component of the $^5D_0 \longrightarrow {}^7F_1$ transition. The spectra of the Eu^{3+} doped borate and silicate glasses would suggest that despite the amorphous nature of glass that some local order exists at the Eu^{3+} ions themselves. Brecher and Reisberg [84] have shown that the best approximation to the symmetry of the local environment of the dopant ion in a silicate glass is C_{2v}. This is the highest symmetry in which full splitting of the $^7F_1$ and $^7F_2$ levels is allowed while maintaining symmetry based distinctions between almost all the components. C_{2v} is also the lowest symmetry for which simple crystal field calculations can be easily performed. Brecher and Reisberg [84,85] found that all tetrahedral oxidic network formers yield similar spectra, consistent with a common structural model involving a gradual transition from eightfold to ninefold coordination at the Eu^{3+} ion. This structural model for the coordination of Eu^{3+} in oxide glasses involves eight coordinators initially equidistant from the Eu^{3+} ion, arranged in a distorted Archimedes antiprism with C_{2v} symmetry, and a ninth coordinator introduced along the C_2 axis at a variable distance from the central ion. This model is illustrated in Fig 6.6 [85]. It was also found that by adjusting the ions positions, that agreement could be obtained between the calculated crystal field parameters and the experimental values from the splitting of the $^7F_1$ and $^7F_2$ states.

The fact that the peak positions and the linewidths of ε_- and ε_+ are not significantly changed from those excited by broadband excitation would indicate that there exist few correlations between the terms of the crystal field potential and those dominating the $^5D_0$ and $^7F_0$ states. The above is not true of the ε_0 line of the $^5D_0 \longrightarrow {}^7F_1$ transition as the peak shifts and becomes significantly

narrower under laser excitation compared with under broadband excitation. This indicates that there is a strong correlation among the terms of the crystal field potential dominating the $^5D_0$ and $^7F_0$ states and ε_0 [88]. The fact that the ε_0 line is broader than the laser excitation line indicates that some of the terms are not the same.

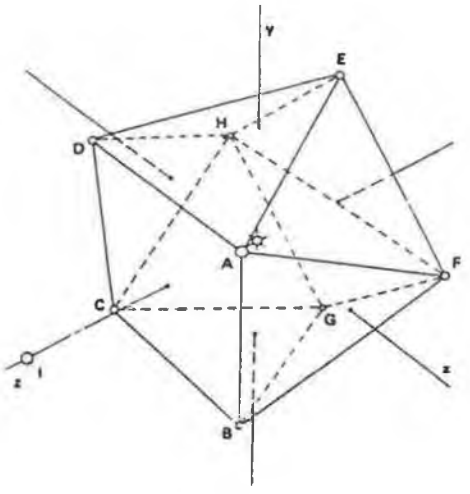

Fig 6.6. Structure for a silicate glass is derived from the square Archimedean antiprism with the Eu^{3+} ion at the origin and eight equidistant oxygens at the vertices. A 9th coordinating oxygen (I) is introduced along the z direction. After Brecher and Riseberg [88].

The energies of the $^5D_0$ and $^7F_1$ states were taken from the plots in Fig 6.3 and 6.4 which were obtained by pumping the $^5D_0$ directly, and these are plotted as a function of the $^5D_0$ excitation energy in Fig 6.7 and 6.8. This technique is generally regarded as a measure of the local crystal field strength at the Eu site [88]. The ions which have larger energy separations between the $^5D_0$ and $^7F_0$ states are exposed to stronger crystal fields. As can be seen in the FLN spectra of both glasses the three lines of the $^5D_0 \longrightarrow {}^7F_1$ are clearly resolved and the symmetry at the Eu^{3+} site is low enough to remove the (2J+1)-fold

degeneracy of the free ion states.

When the splitting of the $^7F_1$ for both the borate and silicate glasses are compared with each other and with other glasses [86,84], they are found to be very similar, although not identical. The oxygen ligand coordination and bonding appear to determine the general spectroscopic properties and not the network forming or modifying ions.

The splitting of the $^5D_0 \longrightarrow {}^7F_1$ plotted against crystal field strength can be seen in figures 6.7 and 6.8 for the borate and silicate glasses respectively.

6.4 SOL-GEL DOPED GLASSES.

The two 800°C treated sol-gel glasses were both cooled to 77K and were excited with the narrow band tunable dye laser to see if they exhibited FLN.

A delay of 100μs was initially set and the fluorescence output resembled that of the broadband excited samples. The laser was tuned across the entire range of the $^5D_0 \longrightarrow {}^7F_0$ transition and no recognizable line narrowing was produced. The temperature of the samples was further reduced to 10K, and again the spectra resembled the broadband excited spectra, as shown in Fig 6.9. Initially this experiment was carried out using the cw dye laser and chopper system described in chapter 3, but as this system was limited in the delays that could be used, the pulsed nitrogen - dye system was used subsequently. The delay was increased from 100μs up to 5ms with no significant change in the spectra. The delay was reduced in an effort to see a narrowed spectra perhaps broaden as energy transfer takes place. No change was noticed as the delay was reduced, but as the delay approached 20μs an intense background fluorescence from the untuned rhodamine 6G dye masked any fluorescence from the sample.

A close investigation of the lifetime decay curve from the sol-gel prepared glasses revealed a fast decay component (FDC) in the 5μs region of the curve. The high temperature melt glasses were investigated and no evidence

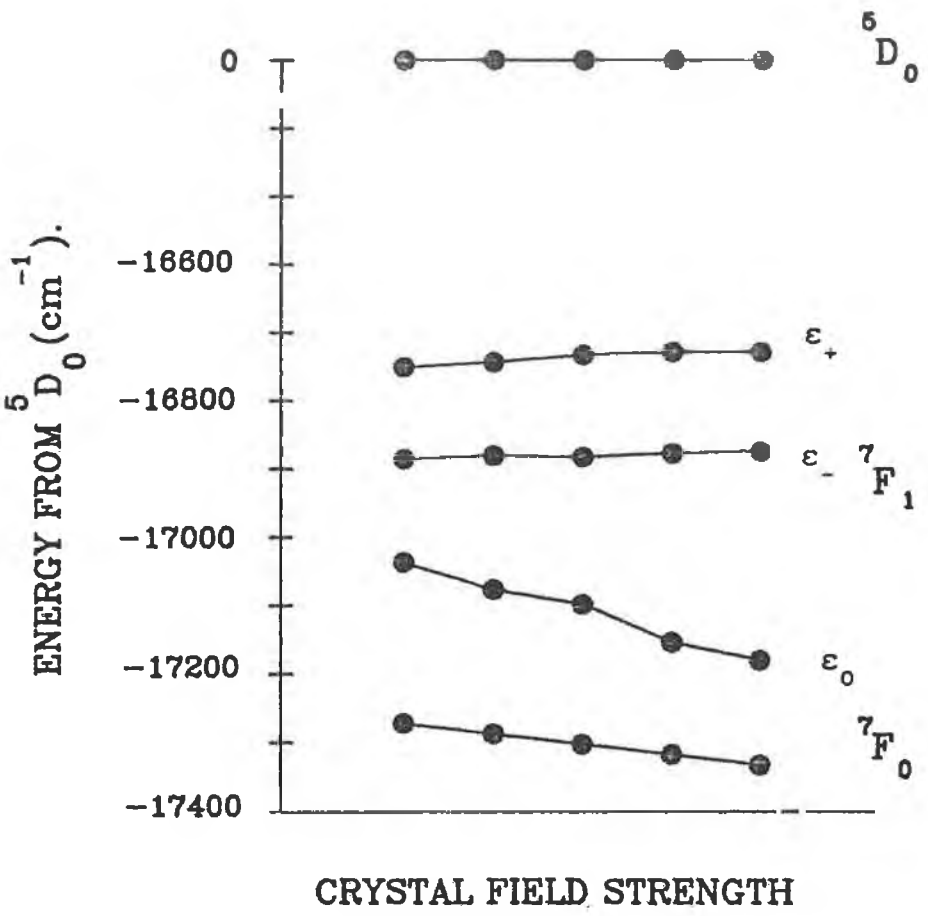

Fig 6.7 Crystal field strength versus splitting. (Borate glass.)

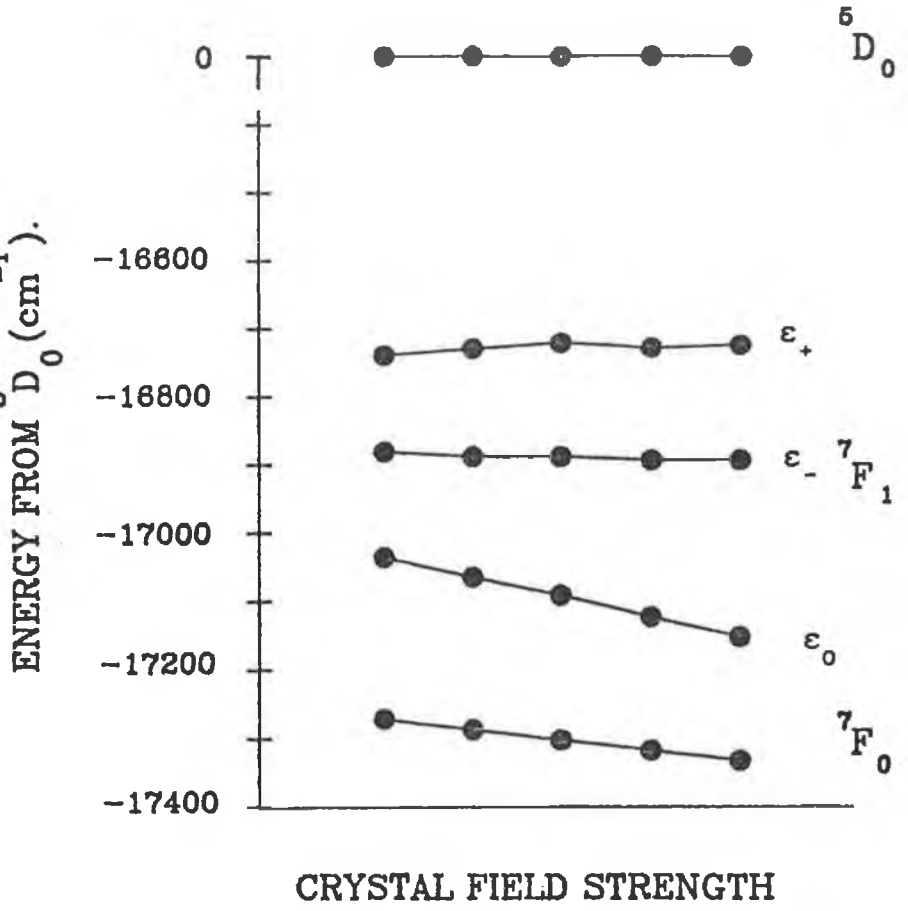

Fig 6.8 Crystal field strength versus splitting. (Silicate glass.)

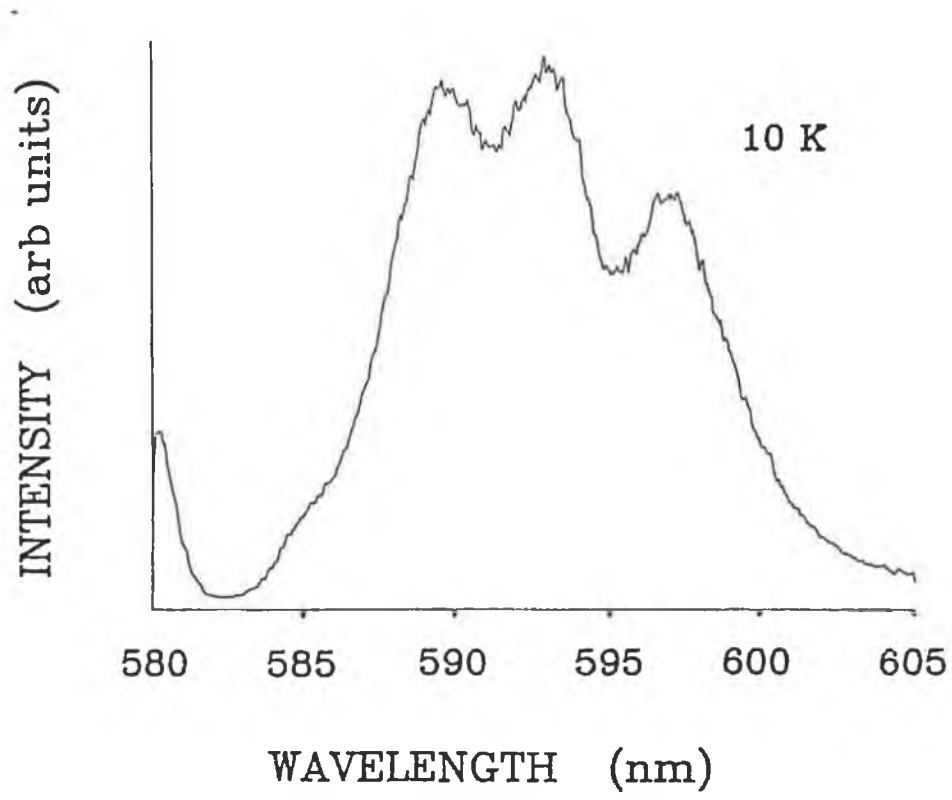

Fig 6.9 Spectrum of sol-gel glass under narrow excitation at 10K. Delay = 100μs.

of this FDC was seen. A plot showing the shape of the decay curve and the clear evidence of the fast decay component can be seen in Fig 6.10.

Attempts to achieve a fluorescence line narrowed spectra at a delay within the FDC ran into experimental difficulties. Intense background fluorescence from the Rhodamine 6G dye with a lifetime longer than the FDC, masked the FDC of the output fluorescence and subsequently no FLN data at this delay could be taken.

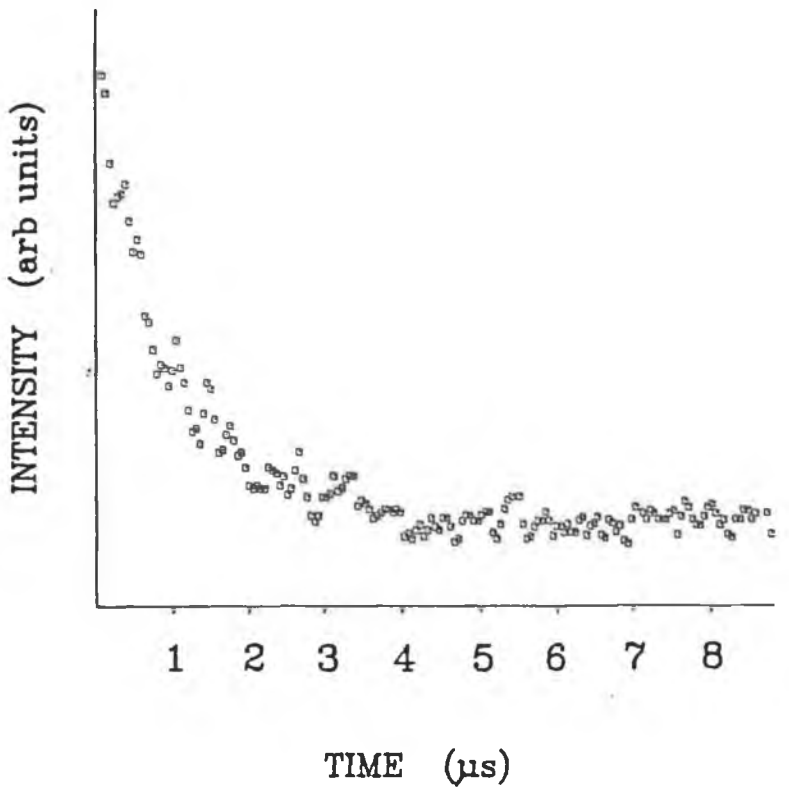

Fig 6.10 Decay curve of sol-gel glass, showing the FDC at short times. Temp = 77 K.

6.5 DISCUSSION.

The site selectivity of the narrow band laser used for fluorescence line narrowing can be degraded in a number of ways. The presence of a untuned broad band emission from the Rhodamine 6G dye that is used in the dye laser can be significant. However, the fact that no narrowed spectra are recorded at all for the sol gel doped glasses at a 100μs delay, would suggest that this could not be the only reason why this occurs.

Energy migration could also be a cause of the degradation of the site selectivity during FLN experiments and this will be investigated in more detail.

A problem that seems to be inherent in the use of lanthanide doped SiO_2 glasses is the clustering of the optically active ions into clumps within the glass matrix [91]. It has been shown that for Nd^{3+} doped sol-gel

glasses, that the Nd ions are not dispersed throughout the gel-silica matrix but are clumped together [35,92,93]. It seems that rare earth ions have such large cationic field strengths Z/r, where Z is the valence of the cation and r is the ionic radius, that dopant ions require coordination of a high number of non-bridging oxygens for screening the electric charge of the cation. When the host environment for the dopant rare earth ion is a rigid network such as SiO_2 , it cannot coordinate to enough non-bridging oxygens and it finds itself in a higher enthalpy state. The ions have a tendency to gather together and form a cation rich phase so as to reduce the excess enthalpy by sharing non-bridging oxygen amongst the clustering cations. It has been reported that the addition of a codopant such as Al or P dissolves clustering Nd^{3+} ions and disperses them throughout the SiO_2 glass matrix [35]. An investigation into the use of codopants such as Al in Eu doped glasses is underway at the moment in this laboratory.

A unitary glass is a single constituent glassy network without any modifying ions. It has been shown by Brecher and Reisberg [84,85] that there are many difficulties associated with FLN experiments on doped unitary glasses. In their experiments they found that the resulting FLN spectra were broader and more complex than from multicomponent glasses. It would seem that when network modifier ions are present in a glass matrix they allow a latitude in free energy which allows the rare earth ions to settle in a single energetically favoured coordination. When a single constituent glass is used this latitude is removed and the rare earth ions take up positions that they would not if modifier ions were present. The resultant spectra are broader due to a greater distribution of sites.

It has been found in investigations of silica glasses prepared by melting that it is very difficult to incorporate large quantities of lanthanide ions uniformly into the rigid covalently bonded silica network [84,85]. In this case crystallization tends to occur at concentrations

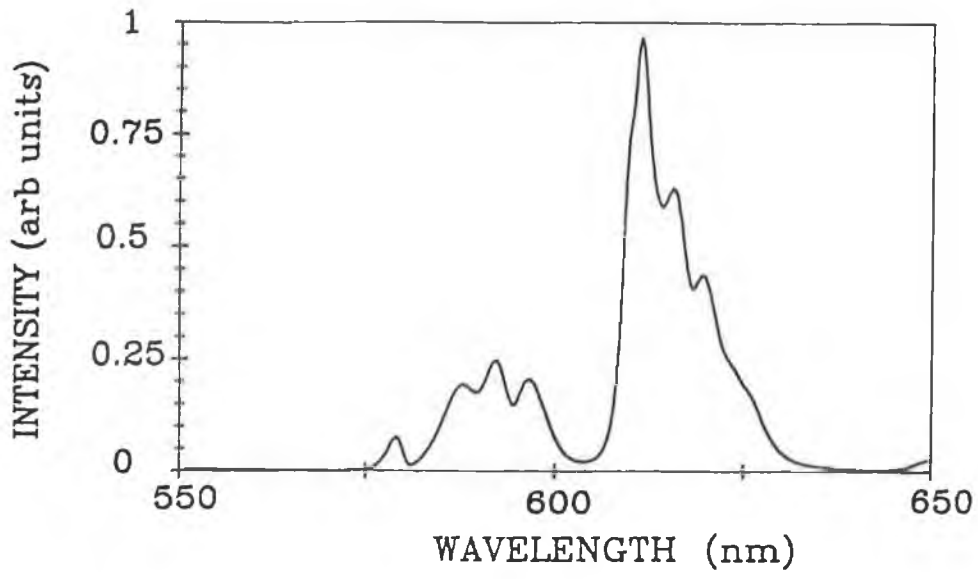

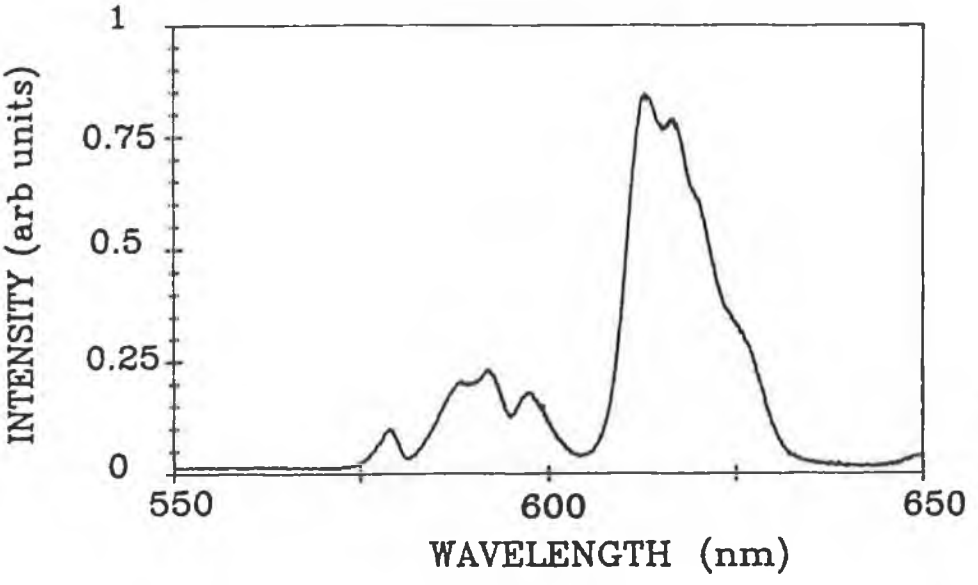

Fig 6.11 A comparison of fluorescence between the high temperature fusion glass and the sol-gel glass. Temp = 77 K.

of ≥ 0.1 mol%, and also at higher concentrations the lanthanide ions are not distributed uniformly throughout the matrix but group together in a cluster embedded in the matrix.

Investigations into the lack of FLN for the sol-gel produced glasses revealed the presence of a very fast lifetime component. The observation of a fast decay component and then a slower decay component for a similar material doped with Nd^{3+} has been reported by Arai et al [91]. It is suggested that the fast component of the Eu^{3+} doped sol-gel glass (≅ 0.5 μs) is due to the concentration quenching of the Eu^{3+} ions within a clustered structure. When the Eu^{3+} ions are excited by the narrow laser line from the dye laser, a rapid energy transfer takes place between the ions. This can occur as the clustering ions are in such close proximity. When two lanthanide ions are close together, they can interact by a multipole process resulting in pairs of nonradiative transitions that reduce the radiative lifetime. This concentration quenching due to clustering would partly explain the lack of FLN, the shorter lifetime and less intense fluorescence emitted from the 800°C treated sol-gel glass compared to the conventional high temperature melt glass. Attempts to increase the temperature of the processing to 1100°C resulted in foaming of the glasses. Foaming is the release of residual OH still within the glass structure at higher temperatures and results in the glass losing its clearness and becoming white. That this occurred for the samples under investigation is evidence that at 800°C, there is still a significant amount of OH present within the structure.

The fact that the general luminescence features are very similar to the multi-component high temperature glasses can be seen in Fig 6.11. This would suggest that the environment of the Eu^{3+} ions is similar to that experienced by ions in a high temperature glass. As the fluorescence features of a multicomponent glass are a collection of contributions from many sites it would appear

that the Eu^{3+} ions in the sol-gel glass also have a multiplicity of sites. These sites contribute to the slow decay component (SDC) which is due to isolated Eu^{3+} ions within the glass structure and also, ions at the outside of the clustering group. The isolated ions experience a crystal field that is unique to a pure SiO_2 glass without any network modifier added. This is an unusual feature of dopants in a unitary glass, as described earlier, and would account for the broader $^5D_0 \longrightarrow {}^7F_0$ transition of the sol-gel prepared glass compared with the high temperature glass discussed in chapter 4. The broader width of this transition is an indication of the greater number of site to site variations in the field experienced by the dopant ions within a pure unitary glass compared to a multicomponent glass. Another indication that the Eu^{3+} ions are situated in a more assymetrical environment than in the high temperature glass is the intensity ratio R of two of the transitions which was described in chapter 4. The value of R for the sol-gel prepared glass that was hydrolysed with water was 4.33 compared with a value of 3.25 for the high temperature silicate glass. The higher the value of R the more assymmetrical the environment of the Eu^{3+} ions.

6.6 CONCLUSION.

In this chapter FLN experiments were carried out on Eu^{3+} high temperature borate and silicate glasses. It has been shown that for these two glasses the fluorescence and the splitting of the $^5D_0 \longrightarrow {}^7F_1$ transition are both similar. It is suggested for these glasses that the oxygen ligand coordination and bonding determine the general spectroscopic properties and not the network forming ion.

Eu^{3+} doped sol-gel glasses were also investigated using FLN techniques. In this case no narrowing of the $^5D_0 \longrightarrow {}^7F_0$ was observed unlike the high temperature glasses. It is proposed in this case that clustering of the dopant Eu^{3+} ions into clumps within the glass structure causes concentration quenching. This occurs as the optically

active ions are clumped together and are therefore in close proximity. It is also clear that even at heat treatments of 800°C that there is still a significant amount of OH^- within the structure and this is responsible for non-radiative decay. Further studies need to be done on the FDC, and the introduction of modifier ions to disperse the Eu^{3+} ions. The use of supercritical drying to remove the OH^- within the glass needs to be investigsted also.

BIBLIOGRAPHY

[1] Henderson, B., Imbusch, G.F. (1989), Optical Spectroscopy of Inorganic Solids. Clarendon Press.
[2] Di Bartolo, B., Optical Interactions in Solids (1967), Wiley and sons.
[3] Imbusch, G.F. (1978), in Luminescence Spectroscopy, Ed' by M. Lumb. Academic Press.
[4] Hufner, S. (1978), Optical Spectra of Transparent Rare Earth Compounds. Academic Press.
[5] Imbusch, G.F. (1978), Luminescence of Inorganic Solids, Ed' by B Di Bartolo, Plenum Press, p 115-133.
[6] Imbusch, G.F. (1987), Spectroscopy of Solid State Laser Type Materials. Ed' by B. Di Bartolo. Plenum Press.
[7] Tanabe, Y., Sugano, S. (1954), J. Phys. Soc. Japan. Vol 9, No 5, 766.
[8] Elliot, J.P., Dawber, P.G., (1979), Symmetry in Physics, Macmillan Press.
[9] Weber, M.J. (1979), in Handbook on the Physics and Chemistry of Rare Earths, Ed' by K.A Gschneider and L. Eyring. North-Holland Publishing Company.
[10] Dieke, G.H. (1968), Spectra and Energy Levels of Rare Earth Ions in Crystals, Interscience Publishers.
[11] Imbusch, G.F. and Kopelmann, R. (1981), in Laser Spectroscopy of Solids, Ed' by W.M. Yen and P.M. Selzer. Topics in Applied Physics Series Vol 49. Springer-Verlag.
[12] Atkins, P.W. (1984), Physical Chemistry, Oxford University Press.
[13] Harris, E.A., Yngyesson, K.S., (1968), J. Phys C. 1,990.
[14] Förster, T., Ann Physik, (1948), 2,55.
[15] Dexter, D.L., J Chem Phys, (1953), 21,236.
[16] Morgan, G.P., Yen, W.M. (1989), in Laser Spectroscopy of Solids II. Topics in Applied Physics Vol 65. Ed' W.M. Yen. Springer-Verlag.
[17] Inokuti, M. and Hirayama, F., (1965), J. Chem. Phys., Vol 43, no 6.
8 [18] Yakota, M., Tanimoto, I. (1967) J. Phys Soc. Jpn. 22, 779.
[19] Holstein, T., Lyo, S.K., Orbach, R., (1981), in Laser

Spectroscopy of Solids, Ed' by W.M. Yen and P.M. Selzer. Topics in Applied Physics Series Vol 49. Springer-Verlag.
[20] Huber, D.L. (1981), in Laser Spectroscopy of Solids, Ed' by W.M. Yen and P.M. Selzer. Topics in Applied Physics Series Vol 49. Springer-Verlag.
[21] Zachariasen, W.H. (1932), J. Am. Chem. Soc. 54, 3841.
[22] Warren, B.E. (1941), J. Am. Ceram. Soc. 24, 256.
[23] Paul, A. (1982), Chemistry of Glasses, Chapman and Hall.
[24] Dietzel, A. (1941), Naturwissenschaften. 23, 537.
[25] Iler, R.K., (1979), The Chemistry Of Silica. Wiley Interscience.
[26] Kawaguchi, T., Hishikura, H., Iura, J., Kokubu, Y. (1984), Jour. Non-Cryst. Solids. 63, 61.
[27] Sakka, S., Kamiyu, K., Makita, K., Yamamoto, Y. (1984), Jour. Non-Cryst. Solids. 63, 223.
[28] Orgaz-Orgaz, F. (1988), Jour. Non-Cryst. Solids. 100, 115.
[29] Dislich, H. (1971), Angew. Chem. Int. Ed. 10, 363.
[30] Roy, R. (1964), J. Amer. Ceram. Soc. 52, 344.
[31] Dislich, H. (1971), Angew. Chem. 83, 428.
[32] Mukherjee, S.P. (1980), Jour. Non-Cryst. Solids. 42, 477.
[33] Mackenzie, J.D. (1988), Jour. Non-Cryst. Solids. 100, 162.
[34] Pope, E.J.A., Mackenzie, J.D. (1988), Jour. Non-Cryst. Solids. 106, 236.
[35] Berry, A.J., King, T.A. (1989) J.Phys.D : Appl.Phys. 22, 1419.
[36] Reisfeld, R. (1973), Structural Bonding, 13,53.
[37] Reisfeld, R. (1976), Structural Bonding, 30,65.
[38] Mc Kernan, D. (1990) MSc Thesis. Dublin City University.
[39] O'Kelly, B. Unpublished. University of Dublin.
[40] Henry, M.O., Larkin, J.P., Imbusch, G.P. (1976), Phys. Rev. B. Vol 13, No 5, 1893.
[41] Demas, J.N. (1983), Excited State Lifetime Measurements. Academic Press.

[42] Bevington. P.R., Data Reduction and Error Analysis for the Physical Sciences. Mc Graw Hill.
[43] Basso, H.C., Aegerter, M.A. (1981), Applied Optics. Vol 20, No 1.
[44] Weber, M.J., (1981), in Laser Spectroscopy of Solids, Ed' by W.M. Yen and P.M. Selzer. Topics in Applied Physics Series Vol 49. Springer-Verlag.
[45] Levy, D., Reisfeld, R. and Avnir, D. (1984), Chem. Phys. Letts. 109, no 6, 595.
[46] Gallagher, P.K., Kurkjian, C.R. and Bridenbaugh, P.M. (1965), Phys. Chem. of Glasses. 6, no 3, 95-103.
[47] Bethe, H. (1929), Ann. Phys. Ser. 5, 3, 153.
[48] Takushi, E., Hirata, K. (1984) Bull.College of Science, Univ. of the Ryukyus. 38, 47.
[49] Zahir, M., Parent, C., Olazcuaga, R., Le Flem, G., Hagenmuller, P. (1986), Jour. Non-Cryst. Solids. 81, 53.
[50] Gallagher, P.K. (1964), Jour. of Chem. Phys. 41, 10, 3061.
[51] Rindone, G.E. Luminescence in the Glassey State. 419-464
[52] Carnell, W.T. (1979), in Handbook on the Physics Chemistry of Rare-Earths, Vol 3,171. Ed's Gschneider, K.A., Eyring, L. (North-Holland Amsterdam)
[53] Gallagher, P.K. (1965), J. Chem. Phys. Vol43, No5, 1742.
[54] Brecher, C., Riseberg, L.A. (1976), Vol 13, no 1, 81.
[55] Sayre, E.V., Miller, D.G., Freed, S. (1957), J. Chem. Phys. Vol 26, No 1, 109.
[56] Kroop, J.L., Windsor, M.W. (1963), J. Chem. Phys. 39, 2769.
[57] Kroop, J.L., Windsor, M.W. (1965), J. Chem. Phys. 42, 1599.
[58] Kroop, J.L., Windsor, M.W. (1966), J. Chem. Phys. 45, 2419.
[59] Kroop, J.L., Windsor, M.W. (1967), J. Chem. Phys. 71, 477.
[60] Albin, M., Whittle, R. and Horrocks, W. (1985), Inorgan. Chem. 24, 4591.

[61] Albin, M, Whittle, R. and Horrocks, M. (1985), Inorgan. Chem. 24,4591.
[62] Mack, H., Reisfeld, R., Avnir, D. (1983), Chem. Phys. Letts. Vol 99, No 3, 238.
[63] Hazenkamp, M.F. and Blasse, G. (1990), Abstract Book, Int. Conf. on Luminescence. Lisbon. p 423.
[64] James, P.F. (1988), J. Non-Cryst. Solids. 100, 93.
[65] Kroop, J. and Dawson, W. (1966), J. Chem. Phys. 45, 2419.
[66] Villegas, M.A. and Fernández Navarro, J.M. (1988), Jour. of Material Science. 23, 4503-4512.
[67] Villegas, M.A. and Fernández Navarro, J.M. (1987), Bol. Soc. Esp. Ceram. Vidr. 26, 99.
[68] Wang, S.H. and Hench, L.L. (1984), Mater. Res. Soc. Symp. Proc. 32, 71.
[69] Hench, L.L. (1984), Mater. Res. Soc. Symp. Proc. 32, 101.
[70] Villegas Broncano, M.A. and Fernández Navarro, J.M. (1986), Proceedings of First International Workshop on Non-crystalline Solids.
[71] Karapetyan, G.O., Lunter, S.G., Yudin, D.M. (1963), Opt. Spectrosc. 14, 370.
[72] Sharp, E.J., Miller, J.E., Weber, M.J. (1973), J. Appl. Phys. 44, 4098.
[73] Brawer, S.A., White, W.B. (1977), J. Chem. Phys. 67, 2043.
[74] Andrews, L.J., Lempicki, A., McCollum, B.J. (1981), J. Chem. Phys. 74, 5526.
[75] van Die, A., Blasse, G., van der Weg, W.F. (1985), J. Phys. C : Solid State Phys. 18, 3379.
[76] Nath, P., Douglas, R.W. (1965) Phys. Chem. Glasses. 6, 197.
[77] Nath, P., Paul, , Douglas, R.W. (1965), Phys. Chem. Glasses. Vol 6, no 6, 203-206.
[78] Weyl Coloured Glasses. ?????
[79] Weber, M.J. (1973), Phys. Rev. B8. 54.
[80] Makishima, A., Mackenzie, J.D. (1975), Jour. Non-Cryst. Solids. 17, 147.[81].....

[81] Denisov, Y.V., Kizel, V.A. (1967), Opt. Spectrosc. 23, 251.
[82] Szabo. A (1970), Phys. Rev. Letts. Vol 23, No 5, 924.
[83] Riseberg, L.A. (1970), Phys. Rev. Lett. 28, 789.
[84] Brecher, C., Riseberg, L.A. (1976), Vol 13, no 1, 81-93.
[85] Brecher, C., Riseberg, L.A. (1980), Jour. of Non-Cryst. Solids., Vol 40, 469-480.
[86] Weber, M.J., Hegarty, J., Blackburn, D.H. (1978) in Borate Glasses, Structure, Properties and Applications. Edited by Pye, L.D., Frechette, V.D., Kreidl, N.J., Plenum Publishing Press.
[87] Kushida, T., Takushi, E. (1975), Phys. Rev. B., Vol 12, no 3, 824.
[88] Motegi, N., Shionoya. S. (1973), Jour. Luminescence. 8, 1.
[89] Weber, M.J., Paisner, J.A., Sussman, S.S., Yen, W.M., Riseberg, L.A. et al (1976), Jour of Luminescence. Vol 12-13, 729-735.
[90] Erickson, L.E. (1975), Opt. Comm. 15, 246.
[91] Arai, K., Namikawa, H.,Kumata, K., Honda, T., Ishii, Y. and Handa, T. (1986), J. Appl. Phys. 59, 3430.
[92] Moreshead, M.V., Nogues, J-L. R., Krabill, R.H., (1990) J. Non. Cryst. Solids. 121, 267-272.
[93] Fujiyama, T., Hori, M., Sasaki,M. (1990), 121, 273-278.
[94] Hegarty, J., Yen, W.M., Weber, M.J. (1978), Phys. Rev. B., Vol 18, no 10, 5816-19.
[95] Imbusch, G.F. (1987), Physica Scripta. T19, 354.
[96] Weber, M.J. (1990), Jour. Non-Cryst. Solids. 123, 208.
[97] Weber, M.J. (1971), Phys. Rev. B4, 2932.
[98] Hegarty, J., Huber, D.L., Yen, W.M., (1982), Phys. Rev. B25, 5683.

APPENDIX A

APPENDIX (A1)

```
10
20 REM                  DATA ACQUISITION PROGRAM
30
40 REM                  FOR SR400 PHOTON COUNTER.
50
60 REM                 Kevin Devlin 1/2/90 D.C.U.
70
80 REM               Luminescence Wavelength Scan.
90 MODE7
100 DIM Q(2000)
110 CLS:*SHADOW
120 PRINT TAB(5)"*****************************"
130 PRINT TAB(5)"**DATA ACQUISITION PROGRAM**"
140 PRINT TAB(5)"**FOR SR400 PHOTON COUNTER**"
150 PRINT TAB(5)"*****************************":PRINT
155 REM ON ERROR GOTO 1055
160 PRINT "PRESS C TO CONTINUE":X$=GET$:PRINT
170 IF X$="C" ELSE GOTO 110
180 INPUT"STARTING WAVELENGTH  (Angs) ";SW$ :PRINT
190 INPUT"ENDING WAVELENGTH    (Angs) ";EW$ :PRINT
200 INPUT"WAVELENGTH INCREMENT (Angs) ";WI$ :PRINT
210 INPUT"SLIT WIDTH           (mm)   ";SL$ :PRINT
220   INPUT"INPUT   DATAFILE   NAME   TO   BE   STORED   ON
DISC";F$:PRINT
230 X=OPENIN(":2."+F$)
240    IF    X<>0    THEN    PRINT"**DATA    FILE    ALREADY
EXISTS**":CLOSE#0:PRINT ELSE 270
250 PRINT"PRESS C TO CONTINUE OR ANY KEY TO RENAME":X$=GET$
260 IF X$="C" THEN 270 ELSE 110
270 *IEEE
280 cmd%=OPENIN("COMMAND")
290 data%=OPENIN("DATA")
300 ESTR$=CHR$(13)+CHR$(10)
310 PRINT#cmd%,"END OF STRING",ESTR$
320 PRINT#cmd%,"BBC DEVICE NO",0
330 PRINT#cmd%,"CLEAR"
340 PRINT#cmd%,"REMOTE ENABLE"
350 PRINT#cmd%,"UNLISTEN"
360 photon%=OPENIN("23")
370
380 REM *********INPUT OF INITIAL SETUP PARAMETERS********
390
400 PRINT#cmd%,"LISTEN",photon%,"EXECUTE"
410 PRINT#data%,"CM;CI0;GD0;NP;DL0;GW0;GY0;CP2;SS;SI"
420 PRINT#cmd%,"UNLISTEN"
430 PRINT#cmd%,"TALK",photon%
440
INPUT#data%,CCM$,CCI0$,GGD0$,NNP$,DDL0$,GGW0$,GGY0$,CCP2$,S
SS$,SSI$
450 PRINT#cmd%,"UNTALK"
460 NNP=VAL(NNP$)
470
480   REM   Display   of   parameters   of   significance   to
measurement of lifetimes.
490
```

```
500 CLS
510 PRINT TAB(5)"**DATA ACQUISITION PROGRAM**"
520 PRINT TAB(5)"**FOR SR400 PHOTON COUNTER**":PRINT
530 PRINT "DATA FILE "TAB(20);F$:PRINT
540 REM PRINT"COUNTING MODE"TAB(20);CCM$:PRINT
550 PRINT"NO OF TRIGGERS"TAB(20);CCP2$:PRINT
560 PRINT "NO OF POINTS"TAB(20);NNP$:PRINT
570 PRINT "A DISC LEVEL"TAB(20);DDL0$:PRINT
580 PRINT "GATE A SCAN STEP"TAB(20);GGY0$:PRINT
590 PRINT "GATE A WIDTH"TAB(20);GGW0$:PRINT
600 PRINT "GATE A DELAY"TAB(20);GGD0$:PRINT
605 PRINT"Press ESCAPE to stop scan & save file":PRINT
610 TIME=0:REPEAT:UNTIL TIME =500
620 PRINT:PRINT "AT POINT NUMBER"  :PRINT
630 PRINT"""COUNTER READING""" :PRINT
640
REM*************************************************************
*********
650
660 REM *********START OF DATA ACQUISITION *********
670
680
REM*************************************************************
*********
690
700       REM*******************Clear       counters,Start
scan.******************
710
720 PRINT#cmd%,"LISTEN",photon%,"EXECUTE"
730 PRINT#data%,"CR;CS"
740 PRINT#cmd%,"UNLISTEN"
750
760       REM*******************Poll       for       data
ready.************************
770 SSS1=0:QQA=0
780 PRINT#cmd%,"LISTEN",photon%,"EXECUTE"
790 PRINT#data%,"SS1"
800 PRINT#cmd%,"UNLISTEN"
810 PRINT#cmd%,"TALK",photon%
820 INPUT#data%,SSS1$
830 PRINT#cmd%,"UNTALK"
840 SSS1=VAL(SSS1$)
850 IF SSS1=0 THEN 780
860 SW=VAL(SW$)
870 WI=VAL(WI$)
880
890       REM       ************************Read       data
value.*********************
900 FOR I=1 TO NNP
910 PRINT#cmd%,"LISTEN",photon%,"EXECUTE"
920 PRINT#data%,"QA"+STR$(I)
930 PRINT#cmd%,"UNLISTEN"
940 PRINT#cmd%,"TALK",photon%
950 INPUT#data%,QQA$
960 PRINT#cmd%,"UNTALK"
970 LO=(I*WI)+SW :LO=(LO-WI)
980 PRINTTAB(20,20); LO
990 QQA=VAL(QQA$)
1000 IF QQA=-1 THEN GOTO 910
```

```
1010 K=I+11:Q(K)=QQA
1020 PRINT:PRINT:PRINT QQA
1030 D=1
1040 PROCSTEP
1050 NEXT I
1055 REM IF ERR=17 THEN NNP=I :PROCLEAR ELSE REPORT
1060 PRINT#cmd%,"REMOTE DISABLE"
1070 CLOSE#photon%
1080 CLOSE#data%
1090 CLOSE#cmd%
1100 CLOSE#0
1110 PROCSAVE
1120 CLS:PRINT:PRINT:PRINT
1130 PRINT "PRESS R IF YOU WISH TO REPEAT SCAN":R$=GET$
1140 IF R$="R" THEN 1150 ELSE 1160
1150 SW=VAL(SW$):EW=VAL(EW$):WI=VAL(WI$)
1155 PROCSTEP
1160 PROCDRAW:PROCBOX
1170 END
1180
1190        REM***************Save        data        to
disk.************************
1200
1210 DEF PROCSAVE
1220 *DISK
1230 Q(0)=VAL(CCM$)
1240 Q(1)=VAL(CCI0$)
1250 Q(2)=VAL(GGD0$)
1260 Q(3)=VAL(NNP$)
1270 Q(4)=VAL(DDL0$)
1280 Q(5)=VAL(GGW0$)
1290 Q(6)=VAL(GGY0$)
1300 Q(7)=VAL(SW$)
1310 Q(8)=VAL(EW$)
1320 Q(9)=VAL(WI$)
1330 Q(10)=VAL(SL$)
1340 Q(11)=VAL(CCP2$)
1350 PRINT:PRINT:PRINT
1360 X=OPENOUT(":2."+F$)
1370 FOR I= 0 TO (NNP+11)
1380 PRINT#X,Q(I)
1390 NEXTI
1400 CLOSE#0
1410 ENDPROC
1420
1430    REM**************Move    wavelength    scan    one
nanometer.**********
1440
1450 DEF PROCSTEP
1480 ?&FE62=&03
1490 FOR L=1 TO WI*100
1500 ?&FE60=1
1510 ?&FE60=0
1520 NEXT
1570 ENDPROC
1580
1590        REM**************Draw        points        on
screen.*********************
1600
```

```
1610 DEF PROCDRAW
1620 CLS
1630 YMAX=-100:YMIN=100
1640 FOR I=12 TO (NNP+11)
1650 IF Q(I)>YMAX THEN YMAX=Q(I)
1660 IF Q(I)<YMIN THEN YMIN=Q(I)
1670 NEXT I
1680 X=0
1690 FOR I=12 TO (NNP+11)
1700 MOVE X,(Q(I)*900/YMAX):DRAW X,(Q(I)*900/YMAX)
1710 X=X+1200/NNP:NEXT
1720 ENDPROC
1730
1740 DEF PROCBOX
1745 MODE0
1750 MOVE 0,0:DRAW 0,900
1760 DRAW 1200,900:DRAW 1200,0
1770 DRAW 0,0
1780 VDU5
1790 MOVE 350,1000:PRINT"Intensity Vs Wavelength  "
1800   MOVE   -10,910:PRINT"|":MOVE   590,910:PRINT"|":MOVE
1190,910:PRINT"|"
1810 MOVE -150,950:PRINT SW
1820 MOVE 900,950:PRINT EW
1830 VDU4
1840 ENDPROC
1845
1846                                  REM***************Stop
scan.*****************************
1847
1849 DEF PROCCLEAR
1850 PRINT#cmd%,"LISTEN",photon%,"EXECUTE"
1860 PRINT#data%,"CH;NE0;ET"
1870 PRINT#cmd%,"UNLISTEN"
1880 FOR I=1 TO 1000
1900 ENDPROC
```

APPENDIX (A2)

```
10 REM ******************************
20 REM **                            **
30 REM **       LUMINESCENCE         **
40 REM **                            **
50 REM **       SIGNAL AVERAGED      **
60 REM **                            **
70 REM ******************************
75 CLS
77 MODE0
80 PRINT:PRINT:PRINT
90 PRINTTAB(5,5)"**************************************"
100 PRINTTAB(5,6)"*                                    *"
110 PRINTTAB(5,7)"*      DATA ACQUISITION PROGRAM      *"
120 PRINTTAB(5,8)"*                                    *"
130 PRINTTAB(5,9)"**************************************"
132 PRINTTAB(5,12)"OPTIONS AVAILABLE"
133 PRINTTAB(5,14)"(A) Scanning Emission Spectrometer"
134 PRINTTAB(5,16)"(B) Scanning Excitation Spectrometer"
136 INPUTTAB(5,18)"CHOICE=    ";CH$
140 CLS
150 CLOSE#0
160 MODE0
170 A=&FCF0
180 ?(A+11)=&C0:?(A+2)=&70:?(A+4)=6:?(A+5)=0
190  C=0
200 INPUTTAB(5,5)" NUMBER OF SAMPLES PER POINT";AV
210 PRINTTAB(5,15)" CHECK TO SEE IF SLIT IS CLOSED"
220 K=GET
230 FOR T=1 TO 10
240 ?A=16:?(A+12)=&0C:?(A+12)=&0E
250 a=(?(A+1))*16+(?(A))MOD16
260
270 C=C+a
280 PRINTa
290 NEXT
300 B=C DIV 10
310 PRINTTAB(5,15)"BACKGROUND D.C. SIGNAL ="B
320 K=GET
330 CLS
340
350 PRINTTAB(5,5) "ADJUST FOR MAX SIGNAL"
360 PRINTTAB(5,10)"TYPE R TO CONTINUE"
370 K=GET
380 ?(A+12)=&0C:?(A+12)=&0E
390 IN=?(A+1)*16+?(A)MOD16
400 PRINTTAB(5,15)"MAX SIGNAL ="B-IN
410 IF K<>69 AND K<>82 THEN 370
420 IF K=69 THEN 380
430 PRINT
440 PRINT
450 CLS
460 *DRIVE0
470 PRINT
480 PRINT"SAMPLE SPECTRUM"
490 PRINT
```

```
500 a=OPENIN"START":INPUT#a,Start
510 b=OPENIN"END":INPUT#b,End
520 c=OPENIN"Inc":INPUT#c,Inc
530 CLOSE#0
540 PRINT"Starting  wavelength "Start
550 PRINT
560 PRINT"Finishing wavelength "End
570 PRINT
580 PRINT"Incremental rate     "Inc
590 P=(End-Start)/Inc+1
600 PRINT
610 INPUT"Do you want to change wavelength range      y/n"
620 IF GET$="Y" THEN PROCINITIAL
630 MODE4
640 DIM Y(2505):DIM K(1)
650 PROCwave
660 PROCADC
670 PROCDATA
680 PROCSAVE
690  INPUT TAB(0,8)" Do you want a copy on chart recorder
y/n"
700 IF GET$="Y" THEN PROCDAC
710 PROCDRAW
720 PROCLABLE
730 *DRIVE0
740 END
750 DEF PROCINITIAL
760 PRINT:PRINT:PRINT
770 INPUT"Starting wavelength ",Start
780 PRINT
790 INPUT"Finish wavelength   ",End
800 PRINT
810 INPUT"Incremental rate ",Inc
820 P=(End-Start)/Inc+1
830 ENDPROC
840
850 DEF PROCDATA
860 X=0
870 A1=Start:b=1 :d=&FCC0:?(d+3)=128
880 CLS:M=1
890 FOR D=1 TO P
900 PROCAVERAGE
903  IF CH$="A" THEN GOTO 910
905 IF CH$="B" THEN PROCSTEP2
906 GOTO 920
910 PROCSTEP
920 PRINTTAB(5,5)A1
930 MOVE X,Y(D)/2:DRAW X,Y(D)/2
940 X=X+1200/P
950 A1=A1+Inc
960 NEXT
970 ENDPROC
980 DEF PROCDRAW
990 MOVE  0,0:DRAW 0,900
1000 DRAW 1200,900:DRAW 1200,0
1010 DRAW 0,0
1020 VDU5
1030  MOVE 250,1000:PRINT"Intensity vs Wavelength  "
1040   MOVE   -10,910:PRINT"|":MOVE   590,910:PRINT"|":MOVE
```

```
1190,910:PRINT"|"
1050  ENDPROC
1060 DEF PROCLABLE
1070 MOVE -150,950:PRINTStart
1080 MOVE 900,950:PRINTEnd
1090 VDU4
1100 ENDPROC
1110 DEF PROCDAC
1120 A1=Start
1130 FOR D=1 TO P
1140 V=2048-(Y(D))
1150 d?b=(V)DIV16
1160 d?2=((V)MOD16)*(1+16*b)
1170 PRINTTAB(5,5)A1
1180 A1=A1+Inc
1190 FOR I=1 TO 200 :NEXT
1200 NEXTD
1210 ENDPROC
1240 DEF PROCADC
1250 A=&FCF0
1260 ?(A+11)=&C0
1270 ?(A+2)=&70
1280 ?(A+4)=6
1290 ?(A+5)=0
1300 ENDPROC
1310 DEF PROCSAVE
1320 INPUT TAB(0,6)" Do you want to save y/n"
1330 IF GET$="N"  THEN ENDPROC
1340 INPUT TAB(5,8)"Name of file  " B$
1350 Y=OPENOUT(B$)
1360 PRINT#Y,Start,End,Inc
1370 FOR D=1 TO P
1380 PRINT#Y,Y(D)
1390 NEXT
1400 CLOSE#0
1410 ENDPROC
1420 DEF PROCwave
1430 a=OPENOUT"START":PRINT#a,Start
1440 b=OPENOUT"END":PRINT#b,End
1450 c=OPENOUT"INC":PRINT#c,Inc
1460 CLOSE#0
1470 ENDPROC
1480 DEF PROCAVERAGE
1490 YD1=0:YD=0
1500 FOR Q=1 TO AV
1510 ?A=16
1520 ?(A+12)=&EC
1530 ?(A+12)=&CE
1540 YD=B-(?(A+1)*16+?(A)MOD16)
1550 YD1=YD1+YD
1560 NEXT
1570 Y(D)=YD1/AV
1580 Y(D)=ABS Y(D)
1590 ENDPROC
1600 DEF PROCSTEP
1610 ?&FE62=&03
1620 FOR L=1 TO Inc*100
1630 ?&FE60=1
1640 ?&FE60=0
```

```
1650  NEXT
1660 ENDPROC
1670 DEF PROCSTEP2
1680 ?&FE62=&07
f1690 FOR L= 1 TO Inc*6
1700 XR=254:YR=250
1710 ?&FE60=XR
1720 FOR K=1 TO 50 :NEXT K
1730 ?&FE60=YR
1740 FOR K=1 TO 50 :NEXT K
1750 NEXT L
1760 ENDPROC
```

APPENDIX (A3)

```
 10 REM ************************************************************
 20 REM ****                                                      ****
 30 REM **** 1. Weighted  Least  square  fit of decay curve      ****
 40 REM ****              semi-log  plot.                         ****
 50 REM ****                                                      ****
 55 REM **** 2. Component stripping for two component            ****
 56 REM ****                 lifetimes.                           ****
 57 REM ****                                                      ****
 60 REM ************************************************************
 80 CLEAR
 90 *DRIVE2
100 MODE0
110 DIM V(12)
120 *.
130 PRINT:PRINT:PRINT:
140 INPUT"Name of data file" ,B$
150 L=OPENIN(B$)
160 FOR I=0 TO 9
170 INPUT#L,V(I)
180 NEXT
190 CLS
200 CM=V(0):CI=V(1):GD=V(2):NP=V(3):DL=V(4):GW=V(5):GY=V(6)
210 N=NP :time=GY
220 DIM Y(N),Y1(N),Y2(N)
230 FOR i=1 TO N-1:INPUT#L,Y(i):NEXT :CLOSE#0
240 B=0
250 PROCCALCULATE:PROCDRAW:PROCINTENSITY:PROCRESET:PROCDUMP
260 END
270
280 DEF PROCCALCULATE                    :REM  Calculates max
290 YMAX=0:YMIN=100                      :REM  & min values of
300 FOR i=1 TO N-1                       :REM  decay curve.
310 IF Y(i)>YMAX THEN YMAX=Y(i)
320 IF Y(i)<=YMIN THEN YMIN=Y(i)
330 NEXT i
340 ENDPROC
350
360 DEF PROCDRAW                          :REM Plots decay
370 X=100                                 :REM curve on
380 FOR I=1  TO N-1                       :REM monitor.
390 REM Y(I)=Y(I)-YMIN
400 MOVE X,(Y(I)*900/YMAX):DRAW X,(Y(I)*900/YMAX)
410 X=X+1200/N:NEXT
430 ENDPROC
440
450 DEF PROCINTENSITY
460 VDU4:VDU 29,50;950;:X=50
470 Y1max=-100:Y1min=100
480 PROCCALC2
490 FOR I=1  TO N-1
500 Y=Y1(I)*-900/Y1min
510 MOVE X+2,Y+2:DRAW X-2,Y-2
520 MOVE X-2,Y+2:DRAW X+2,Y-2
530 X=X+1200/N:NEXT I
540 PROCZOOM
```

```
 550 STA=S:FIN=F
 560 T=STA*time:P=FIN -STA:P=P+1
 570 w=0:w1=0:w2=0:w3=0:w4=0
 580 REM SLOPE OF SLOW COMPONENT
 590 FOR O=STA TO FIN
 600 PROCSUM :T=T+time:NEXT O
 610 PROCSLOPE:PROCEQ
 620 w=0:w1=0:w2=0:w3=0:w4=0
 630 PROCCALCULATE2
 640 T=0:X=50:FOR O=2 TO N
 650 Y1(O)=LN(Y2(O)/Imax)
 660 Y=Y1(O)*-900/Y1min:MOVEX,Y:DRAW X,Y
 670 P=N:PROCSUM:T=T+time
 680 X=X+1200/N:NEXT O:PROCSLOPE
 690 w=0:w1=0:w2=0:w3=0:w4=0
 700 PROCZOOM
 710 STA=S:FIN=F:T=(time)*STA
 720 FOR O= STA TO FIN
 730 Y1(O)=(Y(O)-Y2(O))
 740 IF Y1(O)<=0 THEN GOTO 770
 750 Y1(O)=LN(Y1(O)/(YMAX-Imax))
 760 PROCSUM
 770 T=T+time:NEXT O
 780 PROCSLOPE:PROCEQ:ENDPROC
 790
 800 DEF PROCSUM
 805 WEIGHT=(1/(Y1(O)*(-1)))
 860 w=w+WEIGHT            :REM  sum w
 870 w1=w1+WEIGHT*T*Y1(O) :REM  sum t*y
 880 w2=w2+WEIGHT*T        :REM  sum t
 890 w3=w3+WEIGHT*Y1(O)    :REM  sum y
 895 w4=w4+WEIGHT*T*T      :REM  sum sqr t
 900 ENDPROC
 910
 920 DEF PROCSLOPE
 935 Slope=((w*w1)-(w2*w3))/((w*w4)-(w2*w2))
 940 Intercept=((w4*w3)-(w2*w1))/((w*w4)-(w2*w2))
 950 PRINTTAB(0,20)Slope
 960 LIFT=-1/Slope
 970 PRINTTAB(0,25)LIFT
 980 ENDPROC
 990
1000 DEF PROCEQ
1010 T1=0:X=50:FOR p=1 TO N
1020 Y1(p)=T1*Slope+Intercept:Y=Y1(p)*-900/Y1min
1030 MOVE X,Y:DRAW X,Y :X=X+1200/N :Y2(p)=EXP(Y1(p))*YMAX
1040 T1=T1+time:NEXT p
1050 ENDPROC
1060
1070 DEF PROCZOOM
1080 *FX4,1
1090 C=400:hold=0 :M=0 :UZ=0
1100 MOVE C,50:PLOT 6,C,-900
1110 PRINT TAB(0,0);"
1120 PRINT TAB(0,0);"Slow [";CHR$(200);" "CHR$(201);"]
     Fast[<>] HOLD(H) EXPAND (E)  REMOVE (R)";
1130 X$=GET$
1140 IF X$=CHR$(136) THEN PROCBAR(-1200/N)
1150 IF X$=CHR$(137) THEN PROCBAR(1200/N)
```

```
1160 IF X$="H" THEN PROCHOLD
1170 IF X$=">" ORX$="." THEN PROCBAR(10*1200/N)
1180 IF X$="<" ORX$="," THEN PROCBAR(-10*1200/N)
1190 IF X$="R" THEN PROCREMOVE
1200 IF X$="E" THEN PROCEXPAND
1210 IF M=1 THEN GOTO1230
1220 GOTO 1130
1230 ENDPROC
1240
1250 DEF PROCBAR(I)
1260 MOVE C,50:PLOT 6,C,-900
1270 C=C+I
1280 IF C>1250 THEN C=50
1290 IF C<50 THEN C=1250
1300 MOVE C,50:PLOT 6,C,-900
1310 ENDPROC
1320
1330 DEF PROCHOLD
1340 PRINTTAB(0,0)"                                                    "
1350 IF hold =1 THEN PRINT TAB(0,0);
    "Point already held press R to remove  ":X$=GET$:GOTO 1450
1360 UZ=1200/N:POINT=((C-50)/UZ)
1370 F=POINT
1380 VDU5
1390 PLOT 4,C,-900
1400 PLOT0,2,-4
1410 PRINT CHR$(202);
1420 VDU4
1430 hold=1
1440 C=C+UZ:MOVE C,50:PLOT 6,C,-900
1450 ENDPROC
1460
1470 DEF PROCREMOVE
1480 IF hold=0 THEN GOTO 1570
1490 J=C
1500 C=INT(POINT)
1510 hold=0
1520 GCOL4,1:PROCHOLD
1530 MOVE C,50:PLOT 6,C,-900:C=C+UZ:MOVE C,50:PLOT 6,C,-900
1540 hold=0
1550 C=J
1560 GCOL0,1
1570 ENDPROC
1580
1590 DEF PROCEXPAND
1600 PRINTTAB(0,0);"
 "
1610 D=((C-50)/UZ)
1620 S=D
1630 IFS>F THEN TEMP=S:S=F:F=TEMP
1640 PRINT S,F
1650 M=1
1660 W=1
1670 ENDPROC
1680
1690 DEF PROCRESET
1700 *FX4,0
1710 ENDPROC
1720
```

```
1730 DEF PROCCALC2
1740 FOR I=1 TO N-1
1750 IF Y(I)<=0 THEN 1790
1760 Y1(I)=LN((Y(I))/YMAX)
1770 IF Y1(I)>Y1max THEN Y1max=Y1(I)
1780 IF Y1(I)<=Y1min THEN Y1min=Y1(I)
1790 NEXT I
1800 ENDPROC
1810
1820 DEF PROCDUMP
1830 D$=GET$:IF D$="D" THEN CALL D%
1840 ENDPROC
1850
1860 DEF PROCCALCULATE2
1870 Imax=-100:Imin=100
1880 FOR i=1 TO N
1890 IF Y2(i) > Imax THEN Imax=Y2(i)
1900 IF Y2(i) <= Imin THEN Imin=Y2(i)
1910 NEXT i:ENDPROC
```

APPENDIX B.

NUCLEAR MAGNETIC RESONANCE.

This is the absorbtion of electromagnetic radiation at a precise frequency by a nucleus with a nonzero magnetic field. This occurs if the nucleus has nonzero spin, in which case it acts as a small magnet. If an external magnetic field is present, the nucleus's magnetic moment precesses about the field direction but only certain orientations are allowed by quantum rules. NMR is the absorbtion of radiation at an energy equal to the difference between allowed levels. The difference between energy levels is small and the radiation is in the radiofrequency region of the electromagnetic spectrum. NMR spectroscopy depends on the fact that the electrons in a molecule shield the nucleus to some extent from the field and this causes different atoms to absorb at slightly different frequencies. These effects are known as chemical shifts.

In samples of low viscosity, the molecules are relatively free to move in the matrix so that averaging of molecular alignments, with respect to the applied magnetic field can be accomplished under apropriate circumstances. One of these techniques is the averaging caused by spinning the sample. The spinning of the sample provides motion to the molecules so that one experiences an average magnetic field. Although NMR spectra of liquids can be readily obtained by spinning the sample, the spectra of viscous liquids have poorly resolved spectra. This is mainly due to the nonaveraged dipolar interactions. This effect becomes extreme in the case of solids and a technique called Magic Angle Spinning is used.

The Chemical Shift of a nucleus depends on, among other things, the orientation of the molecule in the applied magnetic field. If nucleus X in a general structure A-X-B is being examined, the magnetic field at X in this molecule will be different when it is aligned with the magnetic field (parallel) than when the molecule is

situated at right angles to the applied field. It will experience a greater field when parallel than at right angles. In a solid the molecules align themselves at the two extremes as well as at all of the possible intermediate angles. This results in a chemical shift of X spread over a wide range. The chemical shift anisotropy (CSA), is defined as the width of this spread i.e. the chemical shift nucleus when the system is parallel to the applied magnetic field minus the chemical shift when it is at right angles to it. It is this value that is added to the isotropic chemical shift to describe the chemical shift of a nuclide in a solid state. The anisotropic part of the chemical shift is 1/3 [CSA] [3 $\cos^1(\theta)$-1]. The angle θ is the angle that the A-X-B axis makes with the applied magnetic field. When this angle is 54.7° and the sample spinning rate is greater than the CSA, the anisotropic contribution to the chemical shift becomes zero and the spectrum that is obtained approximates that of a solution spectrum in terms of resolution.